

THE ROLE OF EDDIES FOR THE
DEEP WATER FORMATION
IN THE LABRADOR SEA

Dissertation
zur Erlangung des Doktorgrades
der Christian-Albrechts-Universität
zu Kiel

vorgelegt von
Lars Czeschel

Kiel
2004

Referent Prof. Dr. Claus W. Böning

Koreferent Priv.-Doz. Dr. Peter Brandt

Tag der mündlichen Prüfung: 27.01.2005

Zum Druck genehmigt: 27.01.2005

gez. Prof. Dr. J. Grotemeyer (Dekan)

Abstract

The Labrador Sea is one of a few sites of the world ocean where open ocean deep convection occurs. Previous ocean general circulation models of the North Atlantic tend to show large deficits in simulating observed characteristics of deep water formation in the Labrador Sea. It is shown that three key processes lead to significant improvements: 1) an adequate representation of the freshwater exchange with the Nordic Seas; 2) an efficient representation of eddy fluxes between the boundary currents and the interior of the Labrador Sea; 3) low (numerical) diapycnal mixing. Based on these results, a refined eddy resolving model of the North Atlantic is developed and analyzed with respect to the important aspects of the deep water formation and its variability in the Labrador Sea.

The dominant eddy kinetic energy signal is associated with the generation of well stratified "Cape Desolation Eddies" which are not a direct result of the deep water formation process. These eddies are able to suppress deep convection in the interior of the Labrador Sea. A second type of rather unstratified "rim current eddies" are formed during the deep convection process. Both types contribute to the restratification after convection and are important for this process to occur on observed timescales.

Beside the well known correlation between surface heat flux changes and Labrador Sea Water formation, the model suggests two novel mechanisms of convection variability related to wind stress: 1) in case of enhanced wind stress the eddy kinetic energy at Cape Desolation increases. The resulting higher generation of well stratified Cape Desolation eddies leads to significantly lower Labrador Sea Water formation; 2) wind stresses parallel to the coast west of Greenland causes Ekman transports of relatively fresh and cold water off the coast towards the interior. This buoyant water at the surface stratifies the water column on the Greenland side of the Labrador Sea and suppresses deep convection.

Zusammenfassung

Die Labradorsee ist eines der wenigen Gebiete im Weltozean, in der tiefreichende Konvektion im offenen Meer vorkommt. Zirkulationsmodelle des Nordatlantiks zeigen enorme Abweichungen von beobachteten Charakteristika der Tiefenwasserbildung in der Labradorsee. In dieser Arbeit wurden drei Schlüsselprozesse identifiziert, die zu einer erheblichen Verbesserung der Modellergebnisse beitragen:

- 1) ein hinreichender Austausch von Frischwasser mit dem Nordmeer; 2) der Effekt der Wirbel beim Austausch zwischen Randströmen und Innerem der Labradorsee; 3) eine geringe (numerische) diapkyknische Vermischung.

Unter Berücksichtigung dieser Prozesse wurde ein wirbelauflösendes Zirkulationsmodell des Nordatlantiks entwickelt und analysiert, um wichtige Aspekte der Tiefenwasserbildung in der Labradorsee und ihrer Variabilität zu untersuchen.

Das dominierende Signal in der kinetischen Wirbelenergie ist eng verknüpft mit der Erzeugung von geschichteten "Cape Desolation Wirbeln", welche nicht im direkten Zusammenhang zur Tiefenwasserbildung stehen. Diese Wirbel unterdrücken Konvektion entlang ihres Hauptpfades ins Innere der Labradorsee. Ein zweiter Typ von eher schwach geschichteten Wirbeln ("rim current eddies") wird während des Konvektionsprozesses erzeugt. Beide Typen von Wirbeln beteiligen sich an der Restratifizierung nach Konvektion und sind erforderlich, damit dieser Prozess auf beobachteten Zeitskalen stattfindet.

Neben dem bereits bekannten Zusammenhang von Wärmeverlust an die Atmosphäre und der Bildungsrate von Labradorseewasser zeigt das Modell zwei neue Mechanismen zur Erzeugung von Konvektionsvariabilität, die mit der Windschubspannung zusammenhängen: 1) bei erhöhter Windschubspannung nimmt die kinetische Energie der Wirbel in der Nähe des "Cape Desolation" zu. Ein vermehrtes Auftreten von geschichteten "Cape Desolation Wirbeln" führt zu geringerer Neubildung von Labradorseewasser; 2) Nordwestlicher Wind, parallel zur Westküste Grönlands, führt zu einem Ekmantransport von relativ frischem und kaltem Wasser von der Schelfregion ins Innere der Labradorsee. Dieses Wasser führt zu einer stärkeren Schichtung in der Wassersäule und unterdrückt Konvektion auf der Grönlandseite der Labradorsee.

Contents

1	Introduction	9
2	The numerical model	17
2.1	Introduction	17
2.2	General features	17
2.3	Survey of experiments	20
2.3.1	Eddy resolving experiments	20
2.3.2	Eddy permitting experiments	22
2.3.3	List of experiments	23
3	Improving the representation of deep convection in the Labrador Sea	24
3.1	Review: Formation of LSW in general circulation models	24
3.1.1	FLAME	24
3.1.2	Other OGCMs	27
3.1.3	Summary of common problems	29
3.2	Freshwater budget in the Labrador Sea	31
3.2.1	Sensitivity to northern boundary formulation	31
3.2.2	The lateral exchange between boundary currents and interior	33
3.3	The role of diapycnal mixing: an idealized process study	37
3.3.1	A simple channel model	37
3.3.2	Restratification in the channel model	38
3.3.3	Applications for the realistic model	41
4	Characteristics of the improved eddy-resolving model	43
4.1	Introduction	43
4.2	General circulation in the Subpolar North Atlantic	43
4.2.1	Upper ocean circulation	43
4.2.2	Deep circulation	46
4.3	Deep convection in the Labrador Sea	48
4.3.1	Mixed layer depths	48
4.3.2	Water mass properties	51
4.4	Export of Labrador Sea Water	54

5	Mechanisms of deep water formation	59
5.1	Introduction	59
5.2	Mesoscale variability	60
5.3	Response to idealized forcing	72
5.4	Hindcasting the "WOCE" period 1989-1997	78
6	Conclusions	83

Chapter 1

Introduction

The North Atlantic Ocean provides an important component of the global thermohaline circulation. The large transfer of heat to the atmosphere from northward-flowing surface waters and the subsequent loss of buoyancy results in convective formation of intermediate- and deep water masses. These water masses play a key role in the oceanic uptake of anthropogenic trace gases.

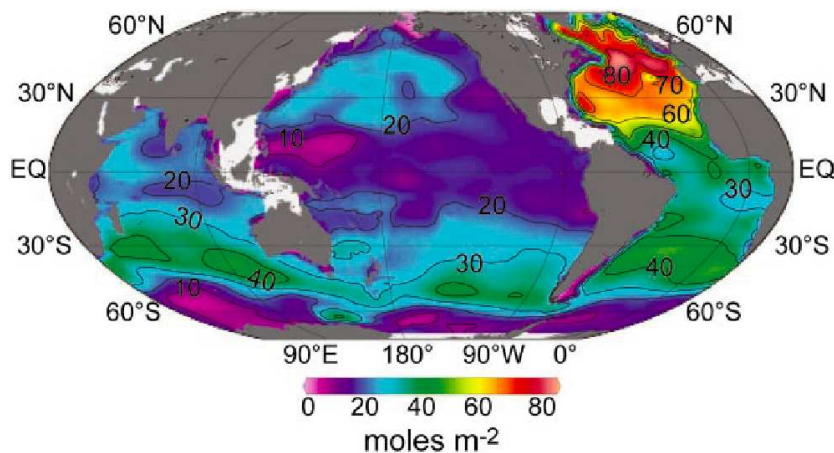


Figure 1.1: Column inventory of anthropogenic CO₂ (mol m^{-2}) in the ocean at the end of the century (SABINE ET AL., 2004).

Since the beginning of the industrial period in the late 18th century humankind has released large quantities of CO₂ into the atmosphere. Recently SABINE ET AL. (2004) show that only about two-thirds of this "anthropogenic CO₂" remains in the atmosphere. Their observational estimate of the total oceanic anthropogenic CO₂ uptake (Fig. 1.1) suggests that the ocean has constituted the only true net sink for anthr. CO₂ over the last 200 years, whereby their total oceanic uptake estimate contains uncertainties of $\sim 20\%$. Earlier studies suggest that the anthr. CO₂ that did not accumulate in the atmosphere must have been taken up by the land biosphere and the ocean in roughly equal shares (IPCC, 2001). However,

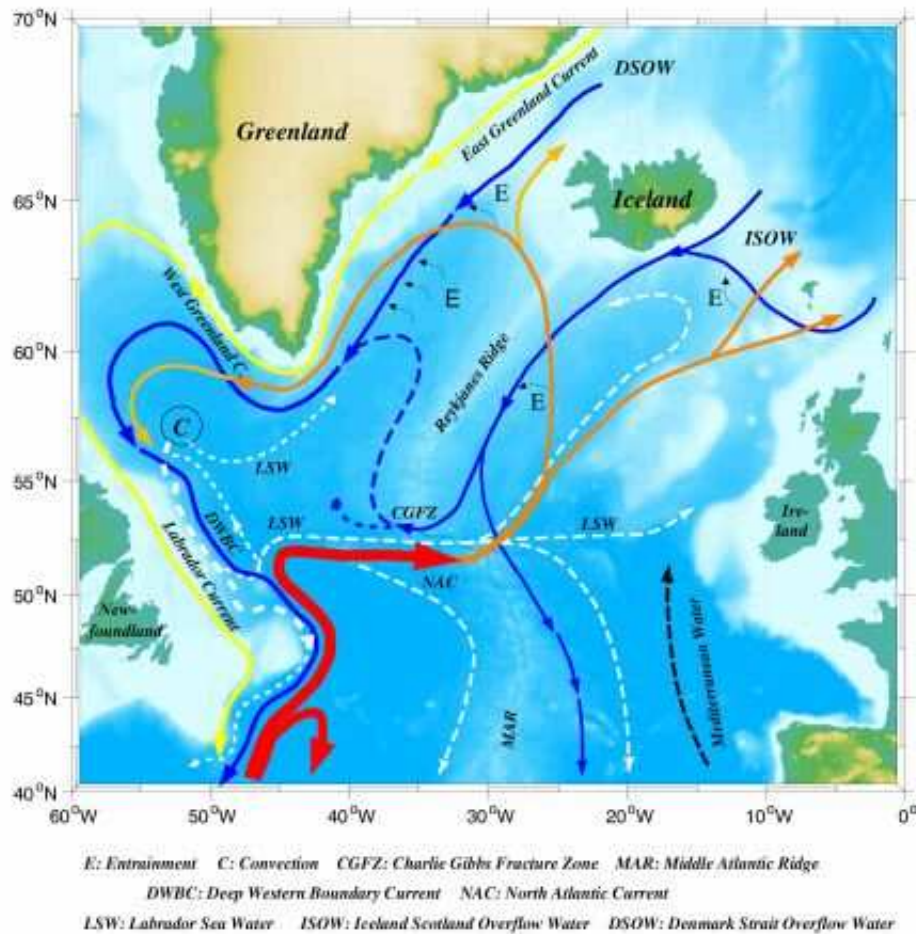


Figure 1.2: Schematic view of surface- and deep circulation in the subpolar North Atlantic. E denotes regions of entrainment and C denotes regions of convection. (SCHOTT ET AL., 2004)

the highest vertical integrated concentrations in the ocean are found in the North Atlantic. As a result, this ocean basin stores 23% of the global inventory, despite covering only 15% of the global ocean area. Globally, only 7% of the total anthr. CO_2 is found deeper than 1500 m. The only place where large concentrations of anthr. CO_2 penetrate to mid and abyssal depths is the North Atlantic, as a result of the formation and downward spreading of Labrador Sea Water and North Atlantic Deep Water (SABINE ET AL. (2004)). Because of the capability of the deep ocean to store large amounts of anthropogenic CO_2 , the deep water formation in the North Atlantic may play a key role in future climate scenarios. It is therefore imperative to obtain a detailed understanding of the deep water formation and its climate sensitivity.

The deep waters formed in the North Atlantic are transported southward via the Deep Western Boundary Current (DWBC) through the subtropics and tropics, and they are eventually advected to other ocean basins. The deep southward flow

is compensated by the near surface northward flow of the North Atlantic Current (NAC) system, together they comprise the Atlantic part of the meridional overturning circulation. Three distinct types of water masses are found within the DWBC south of the Labrador Sea (see also schematic Fig. 1.2):

The Denmark Strait Overflow Water (DSOW) provides the lower portion of the DWBC. DSOW originates north of Iceland and enters the subpolar gyre through the Denmark Strait, being characterized by cold temperatures and low salinities. Above the DSOW lies the Gibbs Fracture Zone Water (GFZW), which enters the western subpolar gyre through the Charlie-Gibbs Fracture Zone. GFZW is closely connected to Iceland Scotland Overflow Water, whose water mass properties are modified due to large entrainment on the eastern side of the Reykjanes Ridge. GFZW is characterized by cold temperatures and relative high salinities compared to the surrounding water masses. Labrador Sea Water (LSW) provides the upper limb of the DWBC. LSW is formed by deep convection in the Labrador Sea and is characterized by a low vertical density gradient, high oxygen content, high anthropogenic tracer concentration, and relative low salinities compared to the surrounding water masses. LSW follows three primary pathways away from the formation region: southward as part of the DWBC, northeastward into the Irminger Basin and eastward near 52°N with several bifurcations east of the Mid-Atlantic Ridge (MAR).

The "classical view" of the open-ocean convection process distinguishes three phases: preconditioning, deep convection, and lateral exchange and spreading (MEDOC-GROUP (1970), MARSHALL AND SCHOTT (1999)). During the preconditioning phase a large-scale cyclonic circulation brings weakly stratified waters of the interior close to the surface (doming). Subsequent cooling events may then initiate deep convection in which a substantial part of the fluid column overturns in numerous sub-mesoscale plumes which distribute the dense surface water in the vertical. The plumes have a horizontal scale of ≤ 1 km. In concert the plumes are thought to rapidly mix properties over the preconditioned site, forming a deep mixed patch ranging from several tens to > 100 km in diameter. With progressing time the horizontal gradient between the dense water in the mixed patch and the less dense surrounding water increases, leading to a "rim current" and development of baroclinic instability. This results in a lateral spreading, associated with geostrophic eddies, of the dense water which causes a break-up of the mixed patch. The vertical and horizontal mixing phases are not necessarily sequential but may occur concurrently.

The Labrador Sea is one of a few sites (besides Mediterranean Sea, Greenland Sea) in the world ocean where open-ocean convection occur. Cold air blowing off the Canadian landmass during winter chills the surface waters, which destabilizes the water column and causes deep convection. The West Greenland Current and the Labrador Current set the large-scale cyclonic circulation, which is a necessary precondition for deep convection. Both boundary currents are characterized by fresh and cold Arctic water on the shelf and warmer and saltier Irminger Water above the continental slope (LAZIER AND WRIGHT (1993), CUNY ET AL. (2002)).

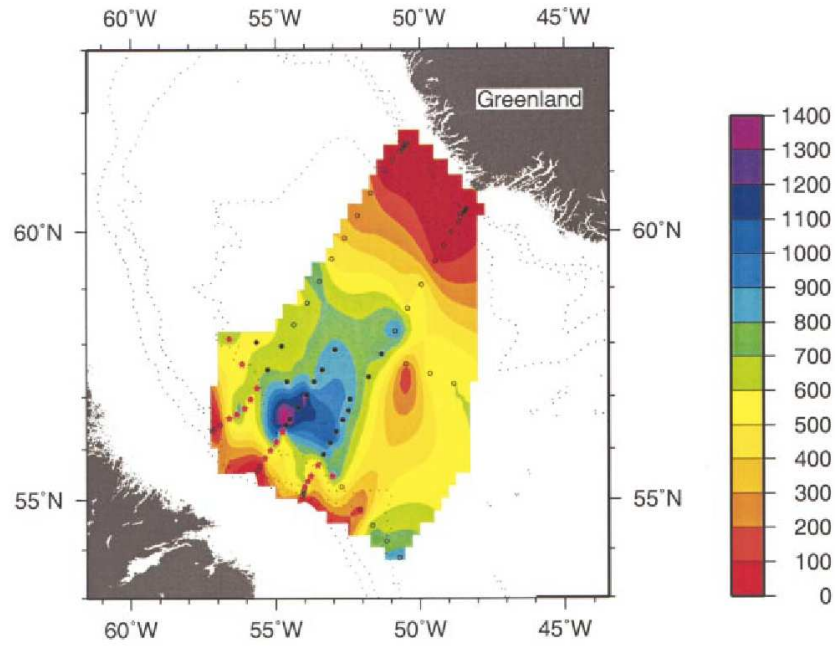


Figure 1.3: Mixed layer depths in March 1997 (PICKART ET AL., 2002)

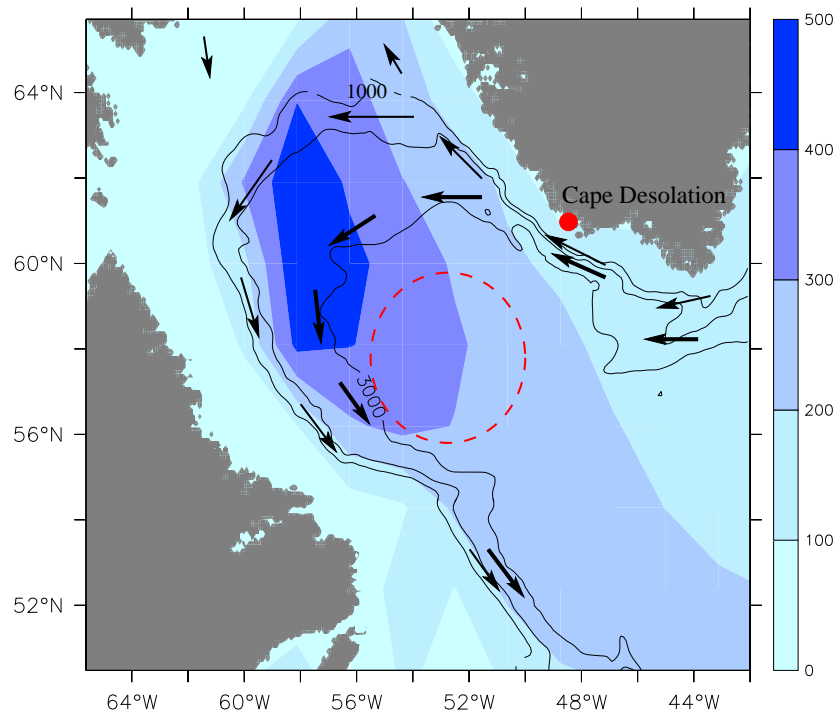


Figure 1.4: Net heat flux (Wm^{-2}) in winter (D/J/F/M) 1996/97 from NCEP/NCAR reanalysis data. The positive values indicate a heat loss to the atmosphere. Also shown are the 1000, 2000, 3000 m isobaths. Currents are schematically indicated by the arrows. The superimposed red-dashed circle marks the location of deep convection shown in Fig. 1.3.

The circulation above the continental slopes is composed of a more baroclinic component flowing between the 1000 m and 2000 m isobaths (Fig. 1.4), and a more barotropic, often denoted as "deep" Labrador Current. The 3000 m isobath is often considered as the offshore limit of the deep Labrador Current. The components are split into two branches in the vicinity of Cape Desolation, where the 3000 m isobath branches off the continental slope. The impact of the preconditioning can be easily seen in the shift towards the interior of the cyclonic circulation of the well mixed convective patch in March 1997 (PICKART ET AL., 2002), compared to the region of maximum heat loss to the atmosphere (Fig. 1.3 and Fig. 1.4).

Deep convection occurs in the region of intense cooling within the cyclonic gyre. Until recently it was thought that the circulation in the interior is very weak compared to the boundary current system (LAZIER AND WRIGHT, 1993). The view of a sluggish interior flow has changed by the study of LAVENDER ET AL. (2000). From an extensive float data set they reveal the presence of a series of sub-basin-scale recirculations. These recirculations might be an important factor for the preconditioning. Moreover, recent observations give evidence that deep convection (up to ~ 1000 m) may also occur within the deep Labrador Current on the Canadian side (PICKART ET AL. (2002), CUNY ET AL. (2004)).

Open-ocean deep convection in the Labrador Sea is not a regular process, with a distinct amount of new deep water formed in every winter, but is subject to considerable interannual variability. There is evidence that the variability of convection intensity is linked to the North Atlantic Oscillation (NAO), the dominant mode of atmospheric variability over the Atlantic sector of the northern hemisphere (DICKSON ET AL., 1996). The NAO is given by the wintertime meridional gradient in atmospheric sea level pressure over the North Atlantic Ocean with strong influences on atmospheric temperatures, precipitation, and storm track activities (HURRELL, 1995). The extent to which this mode is present in a given winter is represented by the NAO index, defined as the normalized wintertime sea level pressure difference, usually taken between Iceland and the Azores (HURRELL, 1995). A high NAO index generally means strengthened winds in the Subpolar North Atlantic. An increase of cold air blowing off the Canadian landmass during winter leads to an increased heat loss over the Labrador Sea, therefore a high NAO state favors deep convection. Observations show that convection in the Labrador Sea in high NAO phases (e.g. late 70's, late 80's/early 90's) reaches depths of more than 2000 m (CLARKE AND GASCARD (1983), LAZIER ET AL. (2002)). Generally, years of intense cooling are accompanied by thickening of the Labrador Sea Water layer. Irrespective of the important role of the NAO for the deep water formation in the Labrador Sea, the notion of a linear NAO-driven convective system is an oversimplification in the light of all the different factors influencing convection (DICKSON ET AL., 1996). For example, the 90's are characterized by an intense convection phase in the beginning followed by a multi-year restratification phase. The absence of a renewal of the deep LSW layers since ~ 1995 (LAZIER ET AL. (2002), STRAMMA ET AL. (2004)) can not be explained by the NAO alone.

Time series of moorings in the Labrador Sea have revealed some important details of the evolution of the restratification process (LILLY ET AL., 1999). After winters

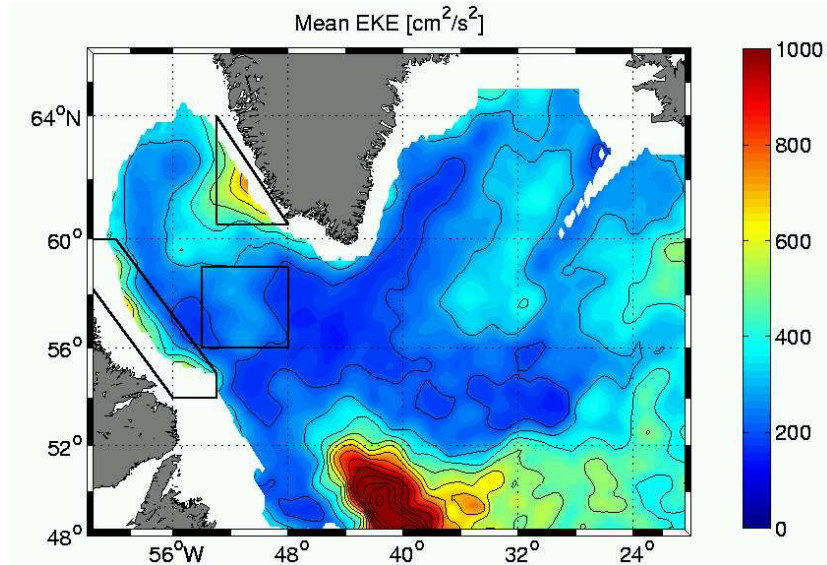


Figure 1.5: Mean eddy kinetic energy (cm^2s^{-2}) from merged T/P and ERS satellite data for the period 1997-2001 (BRANDT ET AL., 2004).

of deep convection, the newly formed LSW is found to be capped by a stratified layer of about 1000 m thickness in summer. The upper part of the water column rapidly becomes warmer and saltier. This generally occurs in late March, while the ocean is still cooled by the atmosphere, indicating that at least part of the restratification is governed by oceanic processes. The fact that the restratification is rapid and deep reaching, points to a mechanism involving lateral eddy fluxes (KATSMAN ET AL., 2004).

Several studies with idealized ocean models show the impact of eddies during the restratification process: JONES AND MARSHALL (1997) put an unstratified cylinder, which represents the well mixed patch after convection, in a stratified environment. A "rim current" arises along the front separating the stratified water from the mixed patch, which is cyclonic down to the depth of the unstratified cylinder and anticyclonic below. Subsequently the rim current becomes unstable and the resulting geostrophic eddies lead to an efficient restratification. These eddies, often referred to as "rim current eddies", appear in comparable quantity as cyclonic and anticyclonic eddies.

The dominant eddy kinetic energy (EKE) signal in the Labrador Sea (Fig. 1.5) is found in the vicinity of Cape Desolation (STAMMER AND WUNSCH (1999), FRATANONI (2001), BRANDT ET AL. (2004)) and is apparently triggered by the local bathymetry (EDEN AND BÖNING (2002), BRACCO AND PEDLOSKY (2004)). The EKE maximum is located in the region where one part of the WGC branches off the continental slope following the ~ 3000 m isobath (Fig. 1.4). In the interior Labrador Sea, the region of observed deep convection, only a small EKE signal is found, which is possibly a combined effect of rim current eddies and eddies advected from the Cape Desolation area. In a five-year observational record from mooring data in the central Labrador Sea, LILLY ET AL. (2003) identify 33 appar-

ent eddies (2 cyclones, 31 anticyclones). 39% of them are classified as "convective lenses" (rim current eddies) with a relatively cold and fresh core. Based on these properties they concluded that these eddies are formed during the convection. 36% are termed as "Irvinger rings" characterized by a warm and salty core of water, originating apparently from the Irvinger Water within the WGC. The remaining eddies are of a different or ambiguous type. In the following, the terms "rim current eddies" and "Cape Desolation eddies" are used.

In an idealized process model KATSMAN ET AL. (2004) demonstrate the importance of Cape Desolation eddies for a restratification in observed timescales. They suggested that the heat transported into the Labrador Sea by the Cape Desolation eddies could be balance the net annual heat loss to the atmosphere. In a further model study, SPALL (2004) shows that the key process determining the water mass transformation and thermohaline circulation in marginal seas (e.g. Labrador Sea) is the interaction between the cyclonic boundary currents and the interior of the marginal seas. This exchange is controlled by baroclinic instabilities in the boundary currents. SPALL (2004) was able to simulate a quasi-steady state solution in which the heat loss over the interior is balanced by the resulting eddy fluxes.

Most model studies concerning the role of eddies for the convection in the Labrador Sea are based on simplified process models. However, only realistic high-resolution general circulation models are capable to combine all the complex mechanisms, which might be important for the convection process. On the other hand, the problem is that state of the art eddy resolving models tend to show large deficits in simulating observed characteristics of deep water formation in the Labrador Sea (TREGUIER ET AL., 2004). (A review of general circulation models is given in section 3.1).

The aim of this study is to develop a refined model of the general circulation in the North Atlantic without large biases in water mass characteristics and deep water formation. Building on this prerequisite of a realistic representation, we aim at an investigation of the various key processes involved in the deep water formation and its interannual variability in the Labrador Sea. Particular questions to be adressed in this study are:

- What are the reasons for the large deficits of todays general circulation models to simulate deep water formation in the Labrador Sea? Is eddy-mixing a crucial factor to overcome these problems?
- Which sources of eddies can be identified? What is their role in the preconditioning and restratification of the Labrador Sea?
- Which mechanisms determine the interannual variability of Labrador Sea Water formation? Which of these mechanisms are absent or underestimated in non-eddy resolving models?

The structure of the thesis is as follows:

In the following chapter the numerical model is described including an overview of the different experiments discussed in this study. Chapter 3 gives a review of the capability of general circulation models to simulate deep water formation in the Labrador Sea. After a short summary of common problems two key problems are isolated. The first involves the freshwater budget in the Labrador Sea, especially the freshwater import from the Nordic Seas. The second is the role of numerical diapycnal mixing during the restratification process. The outcomes of these studies result in a setup for a basin-scale, eddy resolving model configuration. Chapter 4 describes the characteristics of this improved model setup with focus on Labrador Sea convection. In chapter 5 we discuss the results of sensitivity studies involving the response to idealized forcing scenarios, which allow to separate some mechanisms of interannual deep water formation variability. A hindcast of the period 1989-1997 is described at the end of chapter 5. The last chapter summarizes the results of this thesis.

Chapter 2

The numerical model

2.1 Introduction

The models used in this study are part of the FLAME- hierarchy (*Family of Linked Atlantic Ocean Model Experiments*). The framework of FLAME has been set up to allow systematic investigation of different oceanic processes based on the same numerical code. FLAME includes models of resolution ranging from non-eddy resolving to eddy resolving ($4/3^\circ$, $1/3^\circ$, $1/12^\circ$). Based on the basic FLAME configuration encompassing the Atlantic Ocean from 70°S to 70°N , several subdomains of specific geographical regions were configured depending on the specific objectives of the study (Figure 2.1). In our case the North Atlantic and Subpolar North Atlantic versions in "eddy permitting" ($1/3^\circ$) and "eddy resolving resolution" ($1/12^\circ$) are of particular interest.

The first part of this chapter describes the common model features and characteristics. In the second section a survey of the main experiments used in this study is given. A list of the experiments follows at the end of this chapter.

2.2 General features

The model is based on a refined configuration of the Modular Ocean Model (MOM) (PACANOWSKI, 1995). These GFDL type ocean models are often used for studying the North Atlantic circulation (e.g. BRYAN (1969); COX (1985); BÖNING ET AL. (1995)). We use a parallelized code version of MOM (REDLER ET AL., 1998) rewritten by C. Eden (SPFLAME).

Physical basis are the primitive equations (MÜLLER AND WILLEBRAND, 1989), which are discretized on an Arakawa-B grid (ARAKAWA AND LAMB, 1977). All FLAME-models use an isotropic grid, which means that the meridional equals the zonal extent of each grid box independent of latitude ϕ ($dy \times dx \cdot \cos\phi$). There are 45 non-equidistant levels in the vertical, with spacing of 10 m in the uppermost level and a smooth increase to 250 m at 2500 m depth. Below 2500 m the vertical

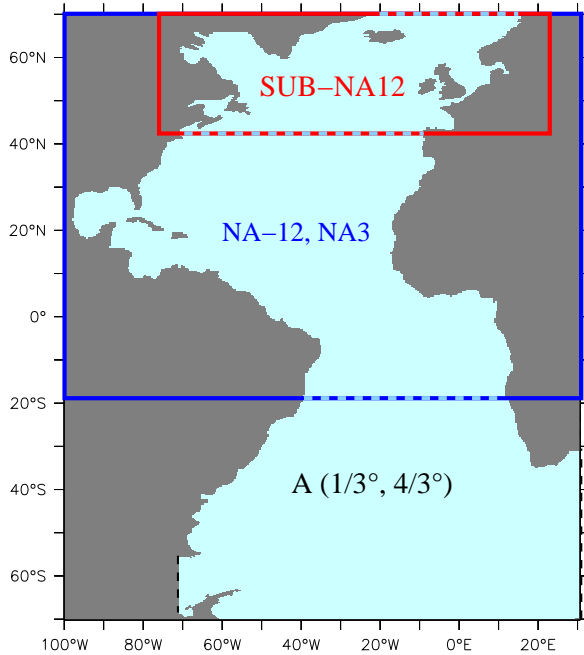


Figure 2.1: Domains of FLAME-configurations: Atlantic (A), North Atlantic (NA), and subpolar North Atlantic (SUB-NA). Dashed lines indicate open boundaries.

grid box thickness is a constant 250 m up to a maximum depth of 5500 m. The model topography was calculated from the ETOPO5 (1988) dataset.

Except for the southern boundary in the Subpolar North Atlantic model, all open boundary formulations follow the approach of STEVENS (1991). For the North Atlantic configurations the prescribed streamfunction at the southern boundary at 18°S is the same as used in DYNAMO GROUP (1997). A new development for this study is an open boundary formulation for the northern boundary (70°N) in the Greenland Sea. For the prescribed streamfunction of the vertical-integrated transport, we adopt modified versions of a streamfunction obtained from an Arctic model developed at the Alfred-Wegener-Institut in Bremerhaven (courtesy of R. Gerdes and J. Brauch). The open boundary formulation will be contrasted with the previous FLAME setups using restoring to climatological temperature and salinity data in a sponge layer in this region. The influence of an open northern boundary is described in section 3.4 in detail. All prescribed temperature and salinity values at the boundaries are taken from a combination of the datasets of LEVITUS AND BOYER (1994) and BOYER AND LEVITUS (1997) [hereafter Levitus]. No restoring is applied in the closed Davis Strait (66°N).

Surface forcing

For the surface forcing the same climatological monthly mean fields as in DYNAMO are used. They originate from a 6-hourly analysis at the ECMWF of the years 1986-88 (BARNIER ET AL., 1995). For studying interannual variability some variations of these forcings were made (a description is given in the next section for the corresponding experiments).

The heat flux includes a relaxation to climatological sea surface temperature (SST) in a formulation following HANEY (1971):

$$Q = Q_0 + Q_2(SST_{model} - SST_{clim})$$

$$\text{with } Q_2 = \left. \frac{\partial Q}{\partial SST} \right|_{SST_{clim}}$$

Here, Q_0 denotes the prescribed heat flux. A flux correction is added in form of a relaxation to climatological SST with a temporal and spatial dependent timescale Q_2 , derived from a linearized form of the bulk formula for the surface heat flux (BARNIER ET AL., 1995).

The freshwater flux into the ocean is realized by a restoring to Levitus sea surface salinities (SSS_{clim}) with a constant timescale of 15 days for the uppermost 10 m deep grid boxes. As in most ocean models, we use this simple freshwater flux formulation due to the large uncertainties in the available precipitation and river runoff datasets.

The models use a simple parameterization of the effect of sea ice. In this "zero-order ice model" surface cooling, surface freshwater fluxes, and surface fluxes of turbulent kinetic energy are set to zero in regions where the sea surface temperature is at or below the freezing point. Surface heating is not altered to allow for heat flux induced sea ice "melting" and wind stress is not altered to account for the drag of sea ice in the ocean.

Except for Q_2 , SST_{clim} , and SSS_{clim} the surface data were linearly interpolated between the monthly means during the model run, filtered according to KILLWORTH (1996) to preserve the monthly means.

Mixing

For lateral mixing of tracers we use diffusion along isopycnal surfaces (approx. neutral surfaces) following REDI (1982) and COX (1987) as a natural choice to parameterize the effect of mesoscale eddies in the eddy permitting model. As an attempt to represent the effect of unresolved (sub-mesoscale) features, this isopycnal mixing scheme is also used in most of the eddy resolving configurations, thereby capitalizing on two advantageous aspects: (1) the horizontal background diffusion, which is needed to control noise on the grid scale, can be slightly decreased compared to "full" horizontal diffusion. This leads to lower diapycnal mixing (for the effects of diapycnal mixing see chapter 3.3); (2) the bottom boundary layer scheme (description later in the text) works more efficiently in combination with isopycnal mixing. The reasons for this connection are not fully understood yet.

The isopycnal diffusion coefficient possesses the same depth dependency $f(z)$ as used in BÖNING ET AL. (1995). For large slopes of neutral surfaces the vertical component of the along-isopycnal diffusive fluxes is getting too large and a tapering of the coefficient is needed for numerical reasons. This leads to an effective isopycnal diffusion coefficient of $ah_{isop}f(z)g(s)$ where z denotes the depth and s the isopycnal slope (see FLAME GROUP (1998) for functions $f(z)$, $g(s)$).

Vertical mixing is parameterized after CUMMINS ET AL. (1990). The vertical diffusion coefficient is set inversely proportional to the static stability N of the water column to account for mixing by internal waves, which is believed to be more efficient at weak stratification. The parameterization of convection is realized in the model using the scheme of RAHMSTORF (1993), which homogenizes water mass properties vertically among unstably stratified boxes. The model also uses the mixed layer parameterization of KRAUS AND TURNER (1967), homogenizing tracers in the wind forced deepening of the surface mixed layer.

A problem in z -level coordinate models is the representation of flows over sills and rough topography. Tracer transport in an overflow situation where dense water crosses a topographic step is accompanied by strong vertical mixing and loss of watermass properties. To overcome this problem, a terrain following bottom boundary layer model (BECKMANN AND DÖSCHER, 1997) with along-isobaths advective and diffusive fluxes was included. The improved representation of the Denmark Strait and Iceland-Scotland Overflow Waters and the consequences for the meridional overturning circulation are described by DENG ET AL. (1999).

2.3 Survey of experiments

2.3.1 Eddy resolving experiments

North Atlantic model

The eddy resolving model has a grid size of $1/12^\circ$ in longitude and $1/12^\circ \cdot \cos\phi$ in latitude, yielding a mesh of about 5 km over the Labrador Sea. The North Atlantic model spans the Atlantic Ocean from 18°S to 70°N . A similar configuration has been used by EDEN AND BÖNING (2002).

In our experiment **NA12** open boundary conditions are implemented at 18°S and at 70°N in the Fram Strait. The western part of the Mediterranean Sea is also embedded in the model domain, a restoring of temperature and salinity to climatological data is applied at 10°E . Starting from a state of rest (Levitus climatology) exp. **NA12** is allowed to spin up for 10 model years forced by the ECMWF climatology described above. To study the interannual variability a hindcast simulation from 1987 until present time follows the spin up phase. This allows for direct comparisons to the large amount of observational data collected during this time period. The variable surface forcing is realized by adding the monthly net heat flux and wind stress anomalies to the ECMWF-based climatology data. The surface flux anomalies were extracted from the NCEP/NCAR reanalysis data (KALNAY ET AL., 1996). A similar variable surface forcing was used in several studies (EDEN AND WILLEBRAND (2001), BÖNING ET AL. (2003), BEISMANN AND REDLER (2003)).

For the horizontal viscosity we use biharmonic mixing in order to minimize the frictional damping on scales larger than the grid scale. All other mixing related issues are described in the general feature section above. The coefficients are given in Table 2.2.

Experiment **NA12** is based on the experience of two previous simulations with the $1/12^\circ$ North Atlantic model. Instead of an open northern boundary in the Greenland Sea, these experiments restore temperature and salinity to climatological data in a sponge layer at a closed boundary. Experiment **NA12-HOR** was used in EDEN AND BÖNING (2002) (their exp. "non-viscous") and was spun-up for 5 years starting from an eddy-permitting version of the model. In contrast to exp. **NA12**, they use horizontal Laplacian diffusion/viscosity and no bottom boundary layer model (BECKMANN AND DÖSCHER, 1997). Experiment **NA12-ISO** starts from the last year of exp. **NA12-HOR** and was spun up for eight years (with support from J.-O. Beismann). In this experiment we switched to isopycnic diffusion and the bottom boundary layer model was included. The results of both simulations are shown in section 3.1.1. Mixing coefficients are given in the Table 2.2 at the end of this chapter.

Subpolar North Atlantic model

Motivated by the computational costs of the basin-scale eddy resolving models, a $1/12^\circ$ Subpolar North Atlantic model was designed. This allows us to do more sensitivity studies. Experiment **SUB_NA12** covers the subpolar gyre from 43°N to 70°N . In contrast to the northern open boundary using a prescribed streamfunction (described above), the streamfunction for the southern open boundary at 43°N is calculated during the integration using a simple Orlanski radiation condition (ORLANSKI, 1976). **SUB_NA12** runs for 11 years starting from a state of rest (Levitus climatology). All mixing parameters are identical to exp. **NA12** and are given in Table 2.2.

For year 8 an "idealized convection tracer" had been embedded. The tracer was initialized with a value of 1.0 within the mixed layer in the Labrador Sea at each time step. The mixed layer depth was defined by the depth where the density difference to the surface layer is greater than 0.01 kg m^{-3} . The tracer is used to study the export pathways of newly formed Labrador Sea Water (section 4.4).

To learn more about the mechanisms of the interannual variability of deep convection some idealized experiments are made, aiming at the response of the system to a sudden switch in either the surface heat flux or the wind stress. Several studies highlighted that the dominant mode of air-sea flux and sea surface temperature variability in the North Atlantic is associated with the North Atlantic Oscillation (NAO). In these experiments we switch immediately from the ECMWF-based forcing to a climatological forcing that corresponds to a persistent high- (or low-) NAO phase. This fixed NAO-like forcing was obtained by using the monthly regression patterns of the heat flux and wind stress time series from the NCEP/NCAR data to the NAO index. These patterns were multiplied by three standard deviations of the NAO index. Note that three standard deviations of the winter time NAO index have been reached several times within the last decades. Three experiments with different forcing changes were performed. Experiment **NAO_HEAT+3** (**NAO_HEAT-3**) was forced with heat flux anomalies

from the regression patterns corresponding to an NAO index of +3 (-3). Experiment **NAO_WIND+3** was forced with wind stress anomalies corresponding to an NAO index of +3. All other forcing data remains the same as in **SUB_NA12**. The same method for building persistent NAO dependent forcing was used in EDEN AND WILLEBRAND (2001). All experiments start in October of year 7 from experiment **SUB_NA-12** due to the fact that the dominant changes occur in winter.

Idealized models

In addition to the realistic setups some simulations with an idealized configuration of the eddy resolving model are performed. In the idealized model experiments we use a linear density equation, no or idealized forcing and a simplified basin geometry and topography. A detailed description is given at the corresponding position in the text.

2.3.2 Eddy permitting experiments

The eddy permitting model is very similar to the z-level model used in DYNAMO. The model domain spans the Atlantic from 18°S to 70°N with a grid size of 1/3° in longitude and $1/3^\circ \cdot \cos\phi$ in latitude. To include the effect of the Mediterranean Sea, temperature and salinity were restored in a sponge layer to climatological data in the Gulf of Cadiz. All eddy permitting models use Laplacian horizontal mixing for viscosity and isopycnic diffusion.

An open question in eddy permitting configurations is the specification of eddy parameterizations. Due to the fact that a 1/3° grid size does not resolve the eddies in the Labrador Sea we include the eddy-induced tracer advection parameterization of GENT AND MCWILLIAMS (1990). The eddy-induced tracer advection (bolus velocity) added to the model velocity, can be thought of as a diffusion of isopycnal thickness. For the thickness diffusivity the same tapering functions as for the isopycnic diffusion coefficient were used (see above). The effect of different thickness diffusion coefficients is discussed in section 3.2.2. Other mixing coefficients are given in Table 2.2 and in the Appendix.

A couple of experiments are made to study the effect of the Nordic Sea exchange. In exp. **NA3_closed** the northern boundary at 70°N in the Fram Strait is closed and temperature and salinities were restored to climatological data in a sponge layer as in DYNAMO. Experiment **NA3_open1** use the streamfunction from the Arctic model (described in the general features section) in an open boundary formulation. In **NA3_open2** we double the strength of the in- and outflow from exp. **NA3_open1**. Further details are described in section 3.2.

2.3.3 List of experiments

Experiment	Viscosity	Diffusion	Forcing	North. Boundary
<i>1/12° North Atlantic</i>				
NA12	biharmonic	isopycnic	NCEP	obc2
NA12-ISO	harmonic	isopycnic	climatological	restoring
NA12-HOR	harmonic	harmonic	climatological	restoring
<i>1/12° Subpolar North Atlantic</i>				
SUB_NA12	biharmonic	isopycnic	climatological	obc2
NAO_HEAT+3	biharmonic	isopycnic	clim. (NAO+3 heat fluxes)	obc2
NAO_HEAT-3	biharmonic	isopycnic	clim. (NAO-3 heat fluxes)	obc2
NAO_WIND+3	biharmonic	isopycnic	clim. (NAO+3 wind stress)	obc2
<i>1/3° North Atlantic</i>				
NA3_closed	harmonic	isopycnic + GM	climatological	restoring
NA3_open1	harmonic	isopycnic + GM	climatological	obc1
NA3_open2	harmonic	isopycnic + GM	climatological	obc2

Table 2.1: List of experiments and main characteristics (see notes below)

Notes:

In all isopycnic diffusion cases a small harmonic background diffusion is added for numerical reasons. GM is the eddy-parameterization following (GENT AND McWILLIAMS, 1990).

The climatological forcing fields originate from a 6-hourly analysis at the ECMWF of the years 1986-88 (BARNIER ET AL., 1995). In the NCEP case the anomalies from the NCEP/NCAR reanalysis data (1987-2003) were added to the clim. forcing.

Different northern boundary formulations at 70°N are applied: a restoring to climatological data in a sponge layer and open boundary conditions (obc); hereby obc1 denotes an annual mean in- and outflow of 6.8 Sv and obc2 of 13.6 Sv.

Lateral Mixing	1/12°	1/3°
<i>Viscosity</i>		
harmonic	$20m^2s^{-1}$	$100m^2s^{-1}$
biharmonic	$2 \times 10^{10}m^4s^{-1}$	-
<i>Diffusion</i>		
harmonic	$40m^2s^{-1}$	-
isopycnic	$50m^2s^{-1}$	$200m^2s^{-1}$
+ harmonic backgr. diff.	$1m^2s^{-1}$	$20m^2s^{-1}$

Table 2.2: Mixing parameters

Chapter 3

Improving the representation of deep convection in the Labrador Sea

3.1 Review: Formation of LSW in general circulation models

Open-ocean deep convection only occurs in a few regions of the world's ocean, characterized by a cyclonic circulation and an intense buoyancy loss to the atmosphere in winter (MARSHALL AND SCHOTT, 1999). The Labrador Sea is one of these regions. However, deep convection in the Labrador Sea is characterized by strong interannual variability. In recent years deep convection reached depths greater than 2000 m (LABSEAGROUP, 1998), but a maximum depth of only 1500m was observed in the late 1990s (PICKART ET AL., 2002). A couple of studies show the connection between Labrador Sea convection and the NAO (DICKSON ET AL. 1996; EDEN AND WILLEBRAND 2001), however the reasons for the variability in the mixed layer depth are not fully understood yet.

One problem for simulating these processes in general circulation models is the high sensitivity of the mixed layer to the chosen horizontal resolution, vertical grid formulation, and mixing parameterization (OSCHLIES 2002; DYNAMO GROUP 1997; CANUTO ET AL. 2004). TREGUIER ET AL. (2004) compare eddy-resolving models in this respect (POP, MICOM, FLAME, and Clipper). They conclude that convection patterns are perhaps the most sensitive feature of ocean models, and present high resolution models are no exception.

This section gives a brief survey of how Labrador Sea convection is represented in general circulation models. Note, that we just report the results here, possible reasons for deficiencies are subject of the following two sections in this chapter.

3.1.1 FLAME

Since the beginning of the *Sonderforschungsbereich 460: Fluctuations of water mass formation and transport processes in the subpolar North Atlantic* in 1996

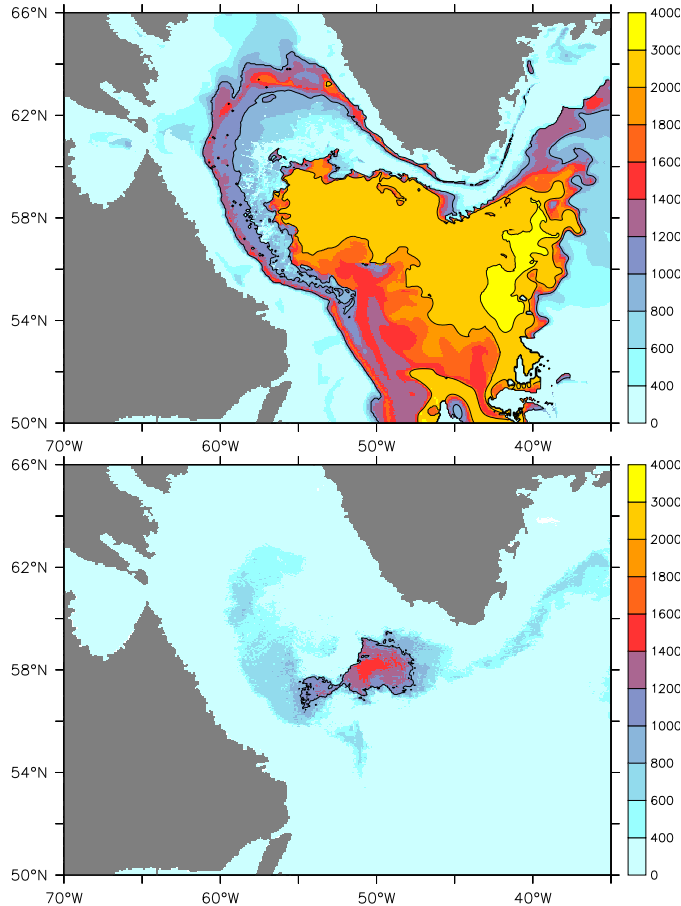


Figure 3.1: March mixed layer depth (m) in **NA12-HOR** (upper) and **NA12-ISO** (lower). The interval of the black contourlines is 1000 m.

a host of experiments with the FLAME-model have been focusing on the North Atlantic Deep Water formation and the associated variability of the large scale circulation. Here, we present results of the eddy-resolving experiments **NA12-HOR**, which is used in EDEN AND BÖNING (2002) (their experiment non-viscous) and **NA12-ISO**. The latter use isopycnic diffusion instead of Laplacian horizontal diffusion and was spun up for 8 years starting from the last year of **NA12-HOR**. A commonly used indicator for convection is the mixed layer depth, where the tracers are vertically homogenized and are in direct contact to atmospheric forcing. We calculate the mixed layer depth by using a potential density criterion, i.e. we are looking for the depth at which σ_0 exceeds its surface value by 0.01 kg m^{-3} .

The mean mixed layer depths in March for the experiments **NA12-HOR** and **NA12-ISO** are shown in Figure 3.1. The only difference between both model setups and hence an obviously important factor for Labrador Sea convection is the lateral mixing formulation (except for the different spin up strategies). **NA12-HOR** uses Laplacian horizontal diffusion while **NA12-ISO** uses isopycnic diffusion and only a small horizontal background diffusion. Nevertheless, there are drastic distinctions in the depth and regional distribution of the mixed layer. In

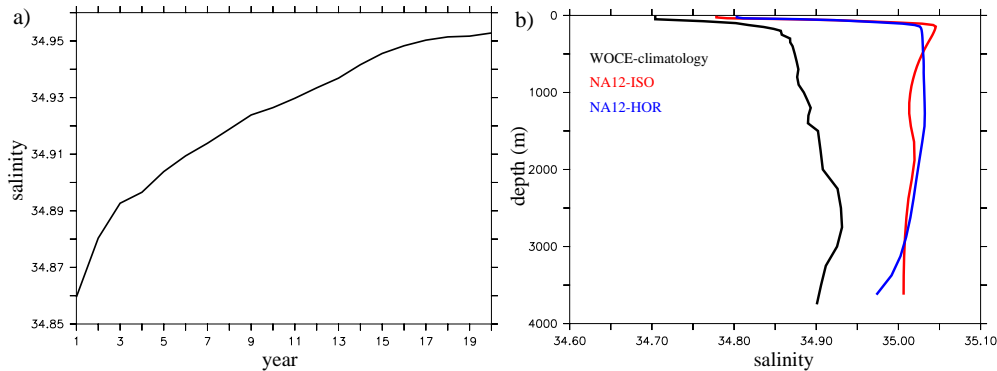


Figure 3.2: a) Increase of the basin-averaged salinity (PSU) during the spin-up of the eddy-permitting experiment **NA3_closed** in the western subpolar gyre ($45\text{-}66^\circ\text{N}, 70\text{-}35^\circ\text{W}$). b) Salinity profile (annual mean in PSU) averaged between $57\text{-}59^\circ\text{N}$ and $51\text{-}49^\circ\text{W}$ of **NA12-HOR**, **NA12-ISO**, and WOCE-climatology (GOURETSKI AND JANCKE, 1998).

experiment **NA12-HOR** the mixed layer depth reaches more than 2000 m over a wide area. The maximum depths of ≈ 3600 m are located outside the Labrador Sea in the vicinity of the Mid-Atlantic Ridge. In contrast, the mixed layer depth in **NA12-ISO** is generally decreased in the whole domain. The area of deep convection is more concentrated in the Labrador Sea reaching maximum depths of ~ 1600 m. No deep convection occurs south of $\sim 54^\circ\text{N}$. **NA12-ISO** is overall in better agreement with observations (Figure 1.3) than **NA12-HOR**. A noticeable discrepancy between **NA12-ISO** and the observational estimates is that the maximum mixed layer depths are more concentrated on the Greenland side of the Labrador Sea.

A further difference between both model setups must be mentioned. The experiment **NA12-ISO** additionally uses the bottom boundary layer (bbl) model of BECKMANN AND DÖSCHER (1997). However, in two experiments with the eddy permitting model, which only differ in using the bbl scheme, there was a slight increase rather than a decrease of the mixed layer depth in the experiment which uses bbl (not shown). Therefore this difference between **NA12-HOR** and **NA12-ISO** cannot explain the large discrepancies in the mixed layer depth between both eddy resolving experiments. Furthermore, the eddy permitting model shows qualitatively the same dependencies on the used lateral mixing as the eddy resolving model (not shown).

Due to the fact that the convection depth depends strongly on the stability of the water column, it is necessary to simulate realistic temperature and salinity distributions. A common problem in regional models (excluding the Arctic) is the strong drift in the water mass properties. It was first noticed in an 1° -North Atlantic model intercomparison by ROBERTS ET AL. (1996) that a salinification occurs in the subpolar gyre. To our knowledge, there is still no solution to overcome this problem. The salinification of the western subpolar gyre during the spin-up phase in our eddy-permitting model **NA3_closed** is documented in Fig. 3.2a

showing the basin-averaged salinity during the spin-up in the western subpolar gyre. The salinity drift is strongest in the first years of the simulation and is still going on after 20 years at lower levels. The drift is more concentrated in the upper water column, which leads to drastic effects for the Labrador Sea Water formation.

Higher resolution does not improve the water mass properties. Fig. 3.2b shows salinity profiles averaged between 57-59°N and 51-49°W in our eddy resolving experiments and for comparison in the WOCE - climatology. Both experiments show intense convection in this region (Fig. 3.1). Underneath the influence of the surface freshwater restoring the model salinities reach values of over 35 PSU. In contrast to observations **NA12-HOR** shows maximum salinities within the LSW. In general the salinity of LSW is at least ≈ 0.1 PSU higher than in the climatology. On the other hand the different mixed layer depths of both experiments (Fig. 3.1) suggest, that the higher salinities (and densities) are not responsible for the extensive deep convection in **NA12-HOR**.

3.1.2 Other OGCMs

Because of the strong sensitivity of the simulated deep convection in the Labrador Sea to model choices as domain sizes and subgridscale parameterizations, a short review of other general circulation models is given in this section.

The DYNAMO-project was a model intercomparison of three eddy permitting models of the North Atlantic (DYNAMO GROUP, 1997). The models differ in the numerical formulation of the vertical discretization, using geopotential levels (LEVEL model), coordinates following surfaces of potential density (ISOPYCNIC), and depth following coordinates (SIGMA). The experimental setups are as similar as possible in all other respects.

Figure 3.3 shows the March mixed layer distributions of all three models. The most striking differences are concentrated in the Labrador Sea. SIGMA has an extremely shallow mixed layer that is nearly less than 250 m deep, without any sign of deep convection. On the other hand LEVEL is deeper than 1000 m over much of the Labrador Sea, reaching almost to the bottom in the center of the gyre, which is in a way analogue to **NA12-HOR**. ISOPYCNIC is in between both other models, with mixed layer depth between 250 m and 1500 m, but the maximum depth are found within the boundary currents which is clearly in disagreement with observations. The variety of solutions illustrate the difficulties of simulating observed mixed layer depth in the Labrador Sea and the sensibility against the specific model architecture.

A more recent model intercomparison by TREGUIER ET AL. (2004) reveals that the problems is not a result of the "low" grid resolution. They compare four state of the art high-resolution models of the (North-) Atlantic Ocean: 1/10°-POP (SMITH ET AL., 2000), 1/12°-MICOM (PAIVA ET AL., 1999), 1/6°-ATL(OPA) (TREGUIER ET AL., 2001), and results from FLAME, i.e. experiment **NA12-HOR**. All experiments had not been run for the purpose of this intercomparison and a possible weakness of the study are the different forcing fields and integration strategies.

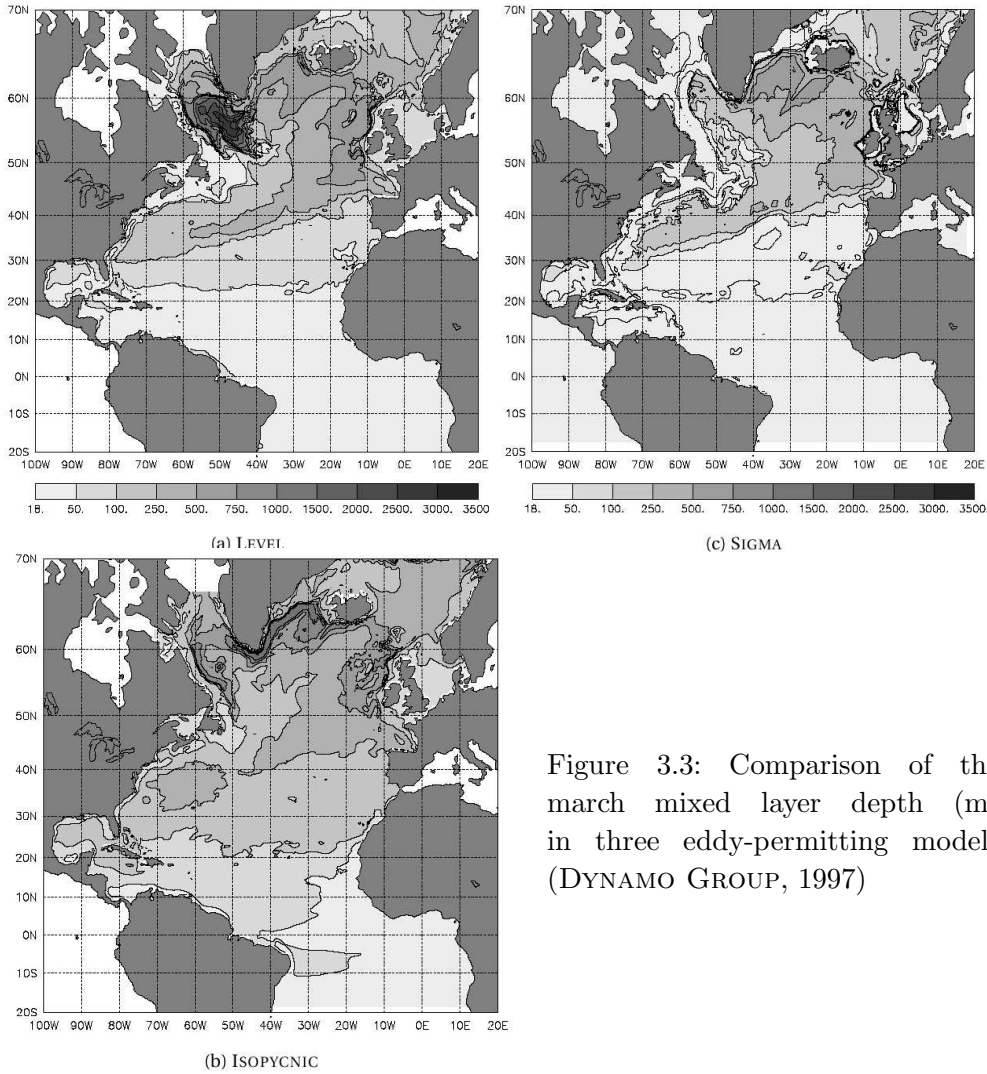


Figure 3.3: Comparison of the march mixed layer depth (m) in three eddy-permitting models (DYNAMO GROUP, 1997)

Figure 3.4a shows the instantaneous mixed layer depth at the end of March interpolated on the section presented in the little schematic above. The authors verified that the instantaneous snapshots are representative for each model experiment. In all models, except POP, convection reaches depths greater than 3000 m in the Labrador and 2500 m in the Irminger Sea. Interannual differences are large (compare both ATL6 mixed layer depths for different years) but the differences between models clearly stand out. POP has a maximum mixed layer depth in the whole Labrador Sea of 1750 m and does not seem to suffer from excessive convection in both basins. In contrast, in ATL6 and MICOM convection reaches the bottom in the Labrador and Irminger Sea, which is clearly in disagreement with observations.

Similar to the FLAME results the water mass properties of all models drift significantly from the initialized climatological values. Figure 3.4b compares the salinity profiles of the different models and a climatology in the central Labrador Sea. The water column in ATL6 and MICOM has become completely homogeneous due to excessive convection. Despite the more realistic convection depth, POP overesti-

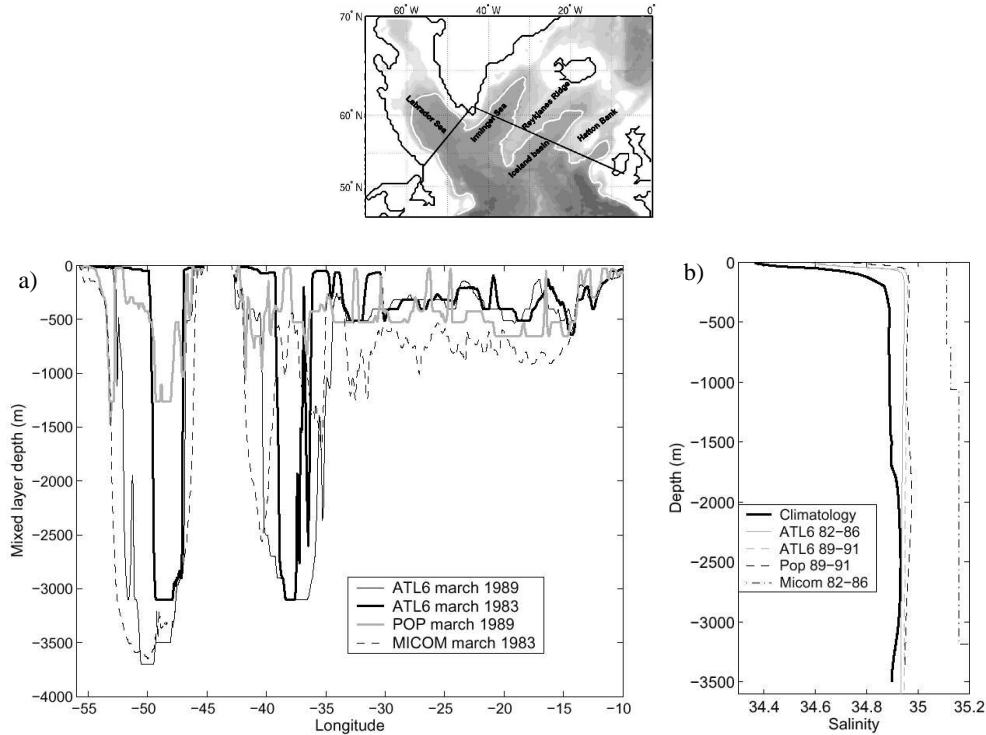


Figure 3.4: From TREGUIER ET AL. (2004): a) The instantaneous mixed layer depth (m) at the end of March along the section above. b) Salinity profiles averaged over $\approx 5^\circ \times 3^\circ$ grid box in the central Labrador Sea.

mates the salinity as the other models do, which suggests that the salinification of the subpolar gyre is not directly linked with local surface forcing and convection. ROBERTS ET AL. (1996), who compared models of 1° resolution, suggested that the reason for the salinization was the restoring of surface salinities to climatological values. In their models the path of the North Atlantic Current (NAC) is too far south compared to the climatology, which leads to large spurious "freshwater" fluxes. Because of the better representation of the NAC path in the high resolution models, TREGUIER ET AL. (2004) find that this process plays a minor role in their models. By examining the spin-up, they show that the salinity anomalies appear in the first year in the East Greenland and downstream boundary current. After a few years all models show a tongue of water with salinities higher than 35 PSU in 700m in the boundary currents around the Labrador Sea. Therefore the authors suggest that the "salt problem" is caused by excessive horizontal transport of salt into the western subpolar gyre.

3.1.3 Summary of common problems

Simulating deep convection in the Labrador Sea is one of the most sensitive features of general circulation models. It was shown that different model architectures and also realizations performed with the same model but with different subgridscale

parameterizations, lead to drastic differences in the simulated mixed layer depths. Observations show large interannual variability in the formation of Labrador Sea Water, but the discrepancies between the different model solutions have at least the same magnitude. Some model intercomparison studies suggest that z-level coordinates may be the best choice for simulating Labrador Sea Water formation in the observed region (in the interior of the Labrador Sea). However, in most models the mixed layer patch is too deep and the convection area is too large in comparison to observations.

All presented model solutions show an unrealistic drift in the water mass properties towards higher salinities in the subpolar gyre. The drift has dramatic consequences for the density range of the Labrador Sea Water simulated in models which, in many cases, begins to overlap with the density of the overflows from the Nordic Seas. This blurred distinction between these water masses leads to a distortion in the spatial patterns of the LSW spreading and associated distribution of dissolved trace gases such as CFCs (BÖNING ET AL., 2003). It has to be mentioned, however, that none of the models are coupled to a realistic ice model nor use observed evaporation, precipitation, and river runoff data for the formulation of freshwater fluxes, whereby the latter fact seems to play a minor role (TREGUIER ET AL., 2004). The salinification of the Labrador Sea Water leads to an increased density in this water mass, but the results of the POP-model and FLAME experiment **NA12-ISO** show that this fact does not necessarily lead to a deeper mixed layer.

3.2 Freshwater budget in the Labrador Sea

The salinification of the Labrador Sea in the model solutions suggests that either a freshwater source is underestimated or a lateral transport of water with high salinity is overestimated. The effect of evaporation minus precipitation, river runoff, and ice-melting in the model is realized by restoring the sea surface salinities towards climatological values. This realization is not able to reproduce variability of these freshwater sources, but it should prevent a drift in the freshwater budget from the climatological state. The freshwater inflow through the Davis Strait, which is important for the salinity fluctuations above the Labrador Shelf (HOUGHTON AND VISBECK, 20002), is not included in the model setups. Instead, after starting a model from climatological state, the salinity anomalies first appear in the East/West Greenland Current (TREGUIER ET AL., 2004). Consequently the salinification of the Labrador Sea seems to originate from an unrealistic low freshwater input from the Irminger Sea.

3.2.1 Sensitivity to northern boundary formulation

A problem of regional model studies is the representation of the lateral boundaries. In the following, we study the role of the northern boundary formulation first by using an eddy-permitting model of the North Atlantic Ocean. All previously shown results are obtained from models using a closed boundary near 70°N. At the closed boundaries temperature and salinity are restored to climatological data in a buffer zone. Figure 3.5a reveals the salinity distribution at 100m in the western subpolar gyre for experiment **NA3_closed**, which uses such a closed boundary formulation. In contrast to the WOCE-climatology (Fig. 3.5b) the model shows a tongue of water with salinities greater than 35 PSU in the East/West Greenland and Labrador Current. The boundary currents around the Labrador Sea are dominated by the "salty" Irminger Current and the portion of the "fresh" East Greenland Current seems to be underestimated. The high salinities within the Irminger Current originate from the North Atlantic Current. This result implies that the freshwater exchange with the Nordic Seas is too weak in the model solution.

To allow for a more effective freshwater exchange across the northern boundary (at 70°N), an open boundary formulation following the approach of STEVENS (1991) was implemented. This formulation allows tracers to leave the model domain at outflow conditions. The water mass properties of inflowing water are obtained from the Levitus climatology. A prescribed barotropic streamfunction is taken from a non-eddy resolving Arctic model developed at the Alfred-Wegener-Institut in Bremerhaven (R. Gerdes and J. Brauch, pers. comm.). After interpolation on our grid under the constraint, that the inflow has to equal the outflow, this streamfunction was used in **NA3_open1**. In a second case, **NA3_open2**, we simply double this prescribed streamfunction, because there is observational and modeling evidence that the in-/outflow may be too weak in the original streamfunction:

- The barotropic streamfunction shows in **NA3_open1** a maximum inflow of 6.8 Sv (annual mean) and 13.6 Sv in **NA3_open2** (Fig. 3.6), but only a little

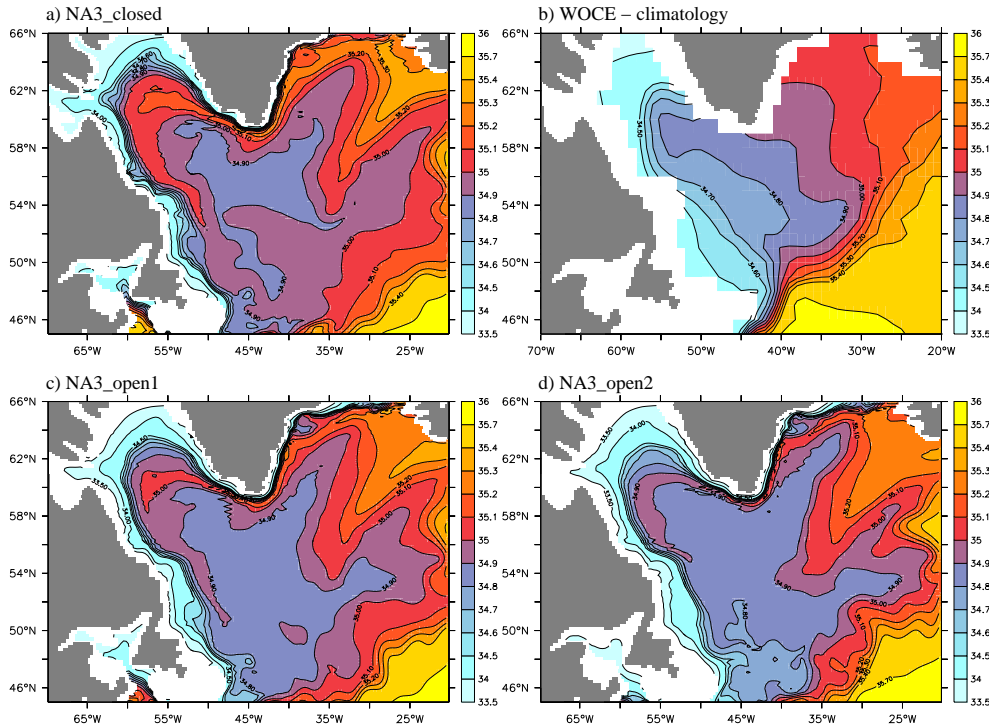


Figure 3.5: Salinity (PSU) at 100m for a) **NA3_closed**, b) WOCE-climatology, c) **NA3_open1** and d) **NA3_open2**

fraction of the inflow enters the subpolar gyre, the greater part recirculates in the Norwegian Basin and leaves the model domain on the eastern side of the open boundary. Only ~ 4 Sv (6 Sv in the doubled inflow experiment) crosses the Denmark Strait, whereby 6 Sv seems to be a more plausible value (HANSEN AND OESTERHUS, 2000).

- There are no transport measurements at 70°N available at the moment, but observations at 75°N show a maximum southward transport of more than 20 Sv (FAHRBACH ET AL., 2001).
- In an eddy permitting version of the Arctic model (AWI, Bremerhaven) the annual mean southward transport at 70°N is ~ 19 Sv, which is significantly higher than in the non-eddy resolving case (6.8 Sv). (Note that we have chosen not to use the eddy permitting model data instead of the one from the coarse resolution model, because the strong boundary current inflow is somewhat more offshore and does not match the prescribed temperature and salinity values of the climatology.)

Figures 3.5c and d show the salinity distributions at 100 m for **NA3_open1** and **NA3_open2**. The tongue of water with high salinities in the boundary currents around the Labrador Sea is significantly lower in **NA3_open1** and **NA3_open2** compared to **NA3_closed**. In **NA3_open2** no water with salinities higher than 35 PSU enters the Labrador Current, but in contrast to the climatology (Fig.

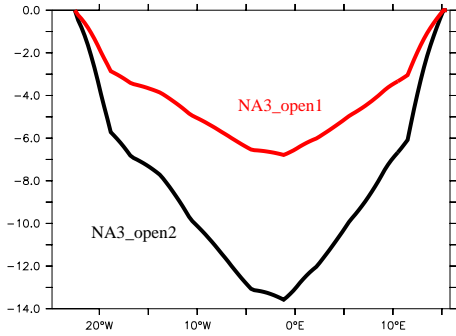


Figure 3.6: Annual mean of the prescribed streamfunctions (Sv) at the open boundary (70°N)

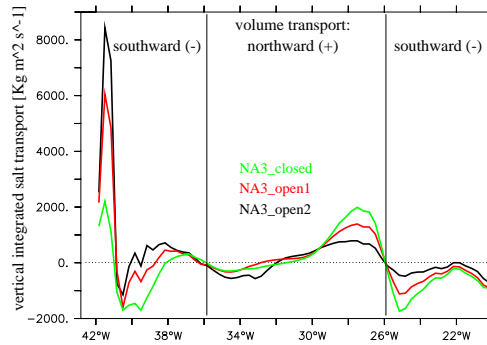


Figure 3.7: Vertically integrated salt transport ($kg\ m^2\ s^{-1}$) at 62°N

3.5b) there remains a small tongue with salinities higher than 34.9 PSU. However, this salinity increase in the West Greenland Current is in good agreement with direct measurements along the WOCE AR7 section (e.g. PICKART ET AL. (2002)) and has most likely disappeared in the smoothed climatology (GOURETSKI AND JANCKE, 1998).

A more quantitative view of the different freshwater fluxes from the Irminger Sea in each experiment is given in Fig. 3.7. We calculate the vertically integrated salt transport $S_{tr} = \int (\mathbf{v}S')dz$ at 62°N through the Irminger Sea, where $S' = S - 35$ and S denotes salinity. The black vertical lines separate the section in a northward flowing part in the middle from the southward flowing conjunction of the Irminger Current and East Greenland Current in the west. Note that a positive salt transport in the southward flowing western part of this section denotes a positive freshwater flux into the Labrador Sea. The southward flowing part in the eastern section is related to the Irminger Current on the eastern side of the Reykjanes Ridge. The open boundary experiments show lower salt transport around the Reykjanes Ridge (30°W - 22°W), because of an increased salt transport in the Nordic Seas and out of the model domain. The strong salt transport around the Reykjanes Ridge in **NA3_closed** recirculates and leaves the Irminger Sea on the western side of this section. The weak East Greenland Current (at 42°W) in this experiment is not able to compensate the positive salt flux into the Labrador Sea. The freshwater transport in the East Greenland Current has increased in **NA3_open1** and is greatest in **NA3_open2**. The lower salinities in the Labrador Sea in the experiments with open boundaries are therefore the combined result of a stronger East Greenland Current freshwater transport and a lower Irminger Current salt transport.

3.2.2 The lateral exchange between boundary currents and interior

Figure 3.8 [left] shows the difference in salinity between the cases **NA3_open2** and **NA3_closed** at 500 m. As mentioned above the salinity in the boundary currents

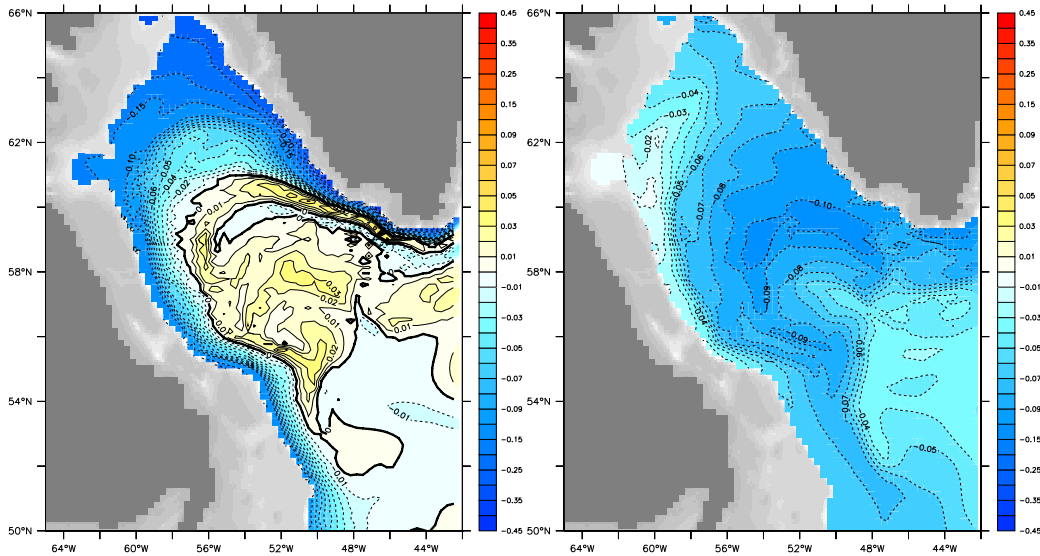


Figure 3.8: Effect of eddy-mixing: salinity difference at 500 m depth in the experiment **NA3_open2** - **NA3_closed**. The coefficient for thickness diffusion is $200 \text{ m}^2 \text{ s}^{-1}$ (left) and $2000 \text{ m}^2 \text{ s}^{-1}$ (right)

is significantly decreased in the experiments with open boundaries (up to 0.2 PSU at 500 m). But the effect is absent in the interior of the Labrador Sea. In contrast, a slight increase in the salinity of up to 0.03 PSU is found in the regions where intense convection occur. This result points towards a too weak exchange between boundary currents and the interior Labrador Sea.

An open question in eddy permitting configurations is the specification of eddy parameterizations. In a model with a horizontal grid resolution of $1/3^\circ \times 0.4^\circ$ BÖNING AND BUDICH (1992) demonstrated, that the model resolves the scale of the energetic eddies in the subtropical gyre, but obviously fails in higher latitudes. Therefore, we have to parameterize the effect of eddies on tracers in our eddy permitting model. The widely used parameterization after GENT AND MCWILLIAMS (1990) adds to the model velocity an eddy-induced tracer advection (bolus velocity), which can be expressed as a diffusion of isopycnal thickness. The bolus velocity is linearly dependent on the thickness diffusion coefficient, which therefore determines the strength of the parameterized eddy-mixing. A common value for the thickness diffusion in non-eddy resolving models is $2000 \text{ m}^2 \text{ s}^{-1}$. In our eddy permitting model a more moderate value of $200 \text{ m}^2 \text{ s}^{-1}$ is usually adopted (BÖNING ET AL. (2003), BEISMANN AND REDLER (2003)).

In order to asses the effect of the eddy parameterization, we rerun our experiments using a thickness diffusion coefficient of $2000 \text{ m}^2 \text{ s}^{-1}$. The difference in salinity at 500 m between **NA3_open2** - **NA3_closed** with higher thickness diffusion is shown in Fig. 3.8 [right]. The stronger eddy-mixing enhances the communication between boundary currents and the interior of the Labrador Sea. The freshwater signal due to the open boundary now reaches the region of intense convection in the interior. The salinity in the whole Labrador Sea is decreased up to a value of

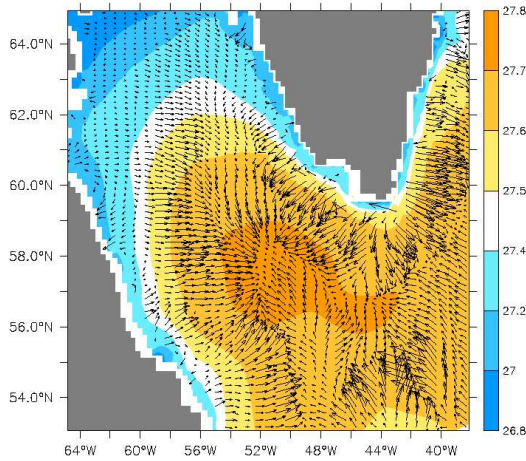


Figure 3.9: Potential density ($kg\ m^{-3}$) and bolus velocities at 100m in **NA3_open2** with high thickness diffusion ($m^2\ s^{-1}$)

0.1 PSU in **NA3_open2**.

The bolus velocities in 100 m (Fig. 3.9) are upgradient of the mean density σ_0 . The strongest velocities are found between the boundary currents, especially the East- and West Greenland Current, and the interior, which leads to an intensified freshwater exchange.

The representation of the North Atlantic Deep Watermasses in each experiment compared to the WOCE-climatology is shown in Fig. 3.10. In the low eddy-mixing case both model experiments fail to represent the observed water mass characteristics. The Labrador Sea Water in both experiments has densities higher than $27.8\ kg\ m^{-3}$. **NA3_open2** has slightly warmer temperatures in the upper water column and significantly lower salinities in the "overflow water masses" compared to **NA3_open1**. The high eddy-mixing experiments reveal that a combination of an open boundary and an adequate representation of the eddies is needed to simulate water mass properties in agreement with observations.

Similar results as in **NA3_open2** with high eddy-mixing are found in a further experiment in which the thickness diffusion coefficient is increased only in the Labrador and Irminger Sea (not shown). The aim of this experiment was to investigate, whether the better representation of the water masses can be understood as a result of locally increased eddy mixing. A problem of using a high thickness diffusion coefficient in the whole model domain are drastic changes in the large scale circulation (e.g. a very broad Gulf Stream), clearly undesirable in models with eddy-permitting resolution. HAINE ET AL. (2003) come to the same conclusion from a different background. They use an eddy permitting model to study the uptake of anthropogenic tracers (CFCs). In an experiment with high thickness diffusion the CFC uptake was in good agreement with observations in the subpolar gyre, but was characterized by large deficits in the subtropics. In contrast, the CFC uptake in a similar experiment with low thickness diffusion was in good agreement with observations in the subtropical gyre but showed deficits in the subpolar gyre. The results emphasize the need for a laterally varying eddy parameterization especially in eddy-permitting models. VISBECK ET AL. (1997) proposed a method to calculate a variable eddy transfer coefficient. Their coefficient is proportional

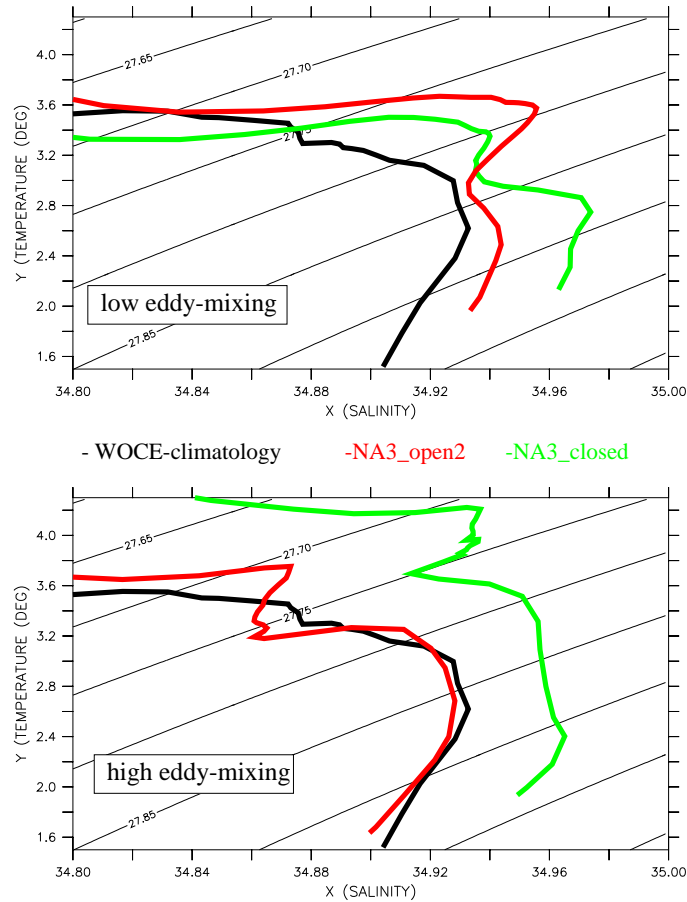


Figure 3.10: Annual mean of temperature ($^{\circ}C$) vs. salinity (PSU) distributions in the central Labrador Sea ($58^{\circ}N$, $53^{\circ}W$) in the eddy-permitting experiments with low eddy-mixing (upper panel) and high eddy-mixing (lower panel).

to the Eady growth rate of the unstable baroclinic waves and to the square of a length scale of the baroclinic region. This parameterization might improve a couple of aspects concerning the general circulation, but fail in regions where eddy variability is generated by barotropic instabilities, local surface or topographic forcing. The dominant eddy source in the Labrador Sea is the eddy separation in the West Greenland Current at Cape Desolation due to barotropic instability and strong topographic interaction (EDEN AND BÖNING, 2002). These eddy sources are untouched by the parameterization after VISBECK ET AL. (1997).

The results of this section give a first impression of the important role of eddies in the Labrador Sea. To overcome the problems with the eddy parameterization and to study the role of eddies in more detail, eddy resolving models are used in the following.

3.3 The role of diapycnal mixing: an idealized process study

Since the work of BRYAN (1987), it has been known that ocean model dynamics are quite sensitive to the level of diapycnal mixing. In z-level (sigma-coordinate) models the effective diapycnal mixing depends both on the mixing parameterization and the chosen advection scheme (GRIFFIES ET AL., 2000), usually leading to magnitudes much higher than observational estimates.

The aim of this section is to show that there is a simple relation between simulated mixed layer depths and the amount of diapycnal mixing. This might explain some of the discrepancies between observed and simulated convection depths.

3.3.1 A simple channel model

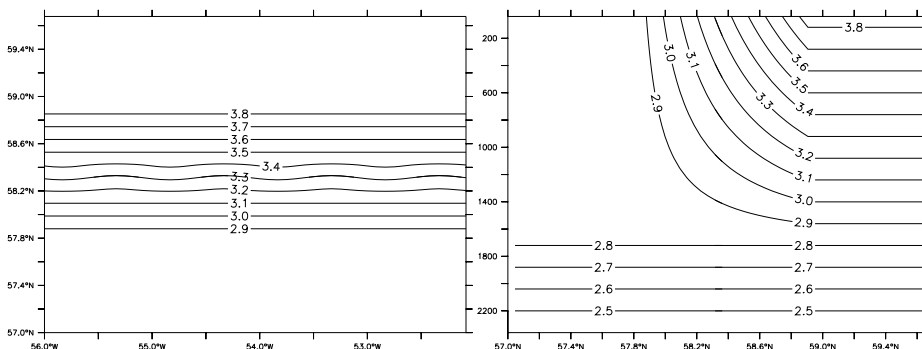


Figure 3.11: Initial condition: sea surface temperature (left panel), meridional temperature section (right panel) both in $^{\circ}C$.

To simulate the restratification process a simple channel is used. The channel was initialized with an analytical temperature field corresponding to an idealized section through the Labrador Sea after deep convection (Figure 3.11). There are no variations in zonal direction except for a little sine-like disturbance to avoid total zonal symmetry. At the western and eastern boundaries cyclic boundary conditions are implemented. The model has a horizontal grid spacing of $1/12^{\circ}$ by $1/12^{\circ} \cos \phi$ with ϕ being the latitude and 30 equidistant levels (80 m each) in the vertical. To keep things simple we use no surface forcing and a linear density equation $[\rho = -\alpha T]$ with $\alpha = 0.2 \times 10^{-3} \frac{kg}{km^3}$. A series of experiments was done differing only in the formulation of the lateral mixing (Table 3.1). A higher horizontal diffusivity coefficient increases the implicit diapycnal mixing. Each experiment was integrated over one year. The parameters of experiment BIH2 are similar to the $1/10^{\circ}$ -model study of SMITH ET AL. (2000). Experiment HOR corresponds to the $1/12^{\circ}$ -model used in EDEN AND BÖNING (2002) (their exp. NON-VISCOUS) and ISO correspond to the experiment NA12-ISO. (Obviously isopycnal diffusion has no effect if using a linear density equation; it is nevertheless used here to mimic our realistic setup and to test numerical interferences. However, a further experiment without isopycnal diffusion (not shown) yields exactly the same results.)

Experiment	Viscosity	Diffusion	Isopycnic diffusion
BIH1	Biharm.: $2.7 \times 10^{10} m^4/s$	Biharm.: $2.0 \times 10^{10} m^4/s$	-
BIH2	Biharm.: $2.7 \times 10^{10} m^4/s$	Biharm.: $0.9 \times 10^{10} m^4/s$	-
HOR	Harmonic: $20m^2/s$	Harmonic: $40m^2/s$	-
ISO	Harmonic: $20m^2/s$	Harmonic: $10m^2/s$	$50m^2/s$

Table 3.1: List of channel-experiments and horizontal mixing parameters

3.3.2 Restratification in the channel model

Winter time convection generates a well mixed patch of nearly uniform density. In our setup this patch encompasses the southern half of the channel reaching a depth of 1700m. If the radius of the patch is greater than the Rossby radius of deformation, it is prone to baroclinic instability (MARSHALL AND SCHOTT, 1999). From a numerical experiment in which a cylinder of dense homogenous fluid was placed in a resting stratified fluid, JONES AND MARSHALL (1997) demonstrate that a rim current arises, which is cyclonic on the top and anticyclonic below. The corresponding "rim" current in our case is shown in Figure 3.12a. Subsequently this current becomes unstable and baroclinic eddies grow (Figure 3.12b,c). The mixed patch is breaking up and the dense fluid disperses over the whole domain by geostrophic eddies (Figure 3.12d). In our idealized experiments only this lateral eddy-transport is responsible for the restratification.

The restratification process can be also described as a transformation of available potential energy (APE). APE is the difference between a fluid's potential energy (PE) and the potential energy of a corresponding reference state, which can be reached by adiabatically rearranging the fluid to a state of zero horizontal density gradients. The buoyancy loss to the atmosphere during convection leads to sloping isopycnals and thus the ocean gains APE. In a purely adiabatic ocean the entire APE is transformed into eddy potential energy (EPE) and into eddy kinetic energy (EKE), where it is finally dissipated.

Figure 3.13 shows the evolution of PE¹ in our experiment BIH1 referenced to zero after one year of integration. After a few days the PE rapidly decreases to a value near zero. After the vigorous restratification it is only the vertical diffusion which slightly increases the potential energy furthermore. The timescale for the restratification of $\tau_{restrat} \approx 3$ months appears as a plausible value for the Labrador Sea and is close to the theoretical value of $\tau_{restrat} \approx 75days$ (also shown) following JONES AND MARSHALL (1997). From numerical experiments they find that for a mixed layer patch with radius r , depth h , and a buoyancy jump at its edge of magnitude Δb the timescale for the restratification process is $\tau_{restrat} \approx 56(r/\sqrt{h\Delta b})$. The initial values for our channel-setup of $r = 220km$, $h = 1700m$, and $\Delta b = 2.125 \times 10^{-3}ms^{-2}$ correspond to a timescale of also $\tau_{restrat} \approx 75days$.

The evolution of PE for the different channel experiments is shown in Figure 3.14a. All experiments start under the same initial conditions. Here we normalize

¹We show PE since APE cannot uniquely defined

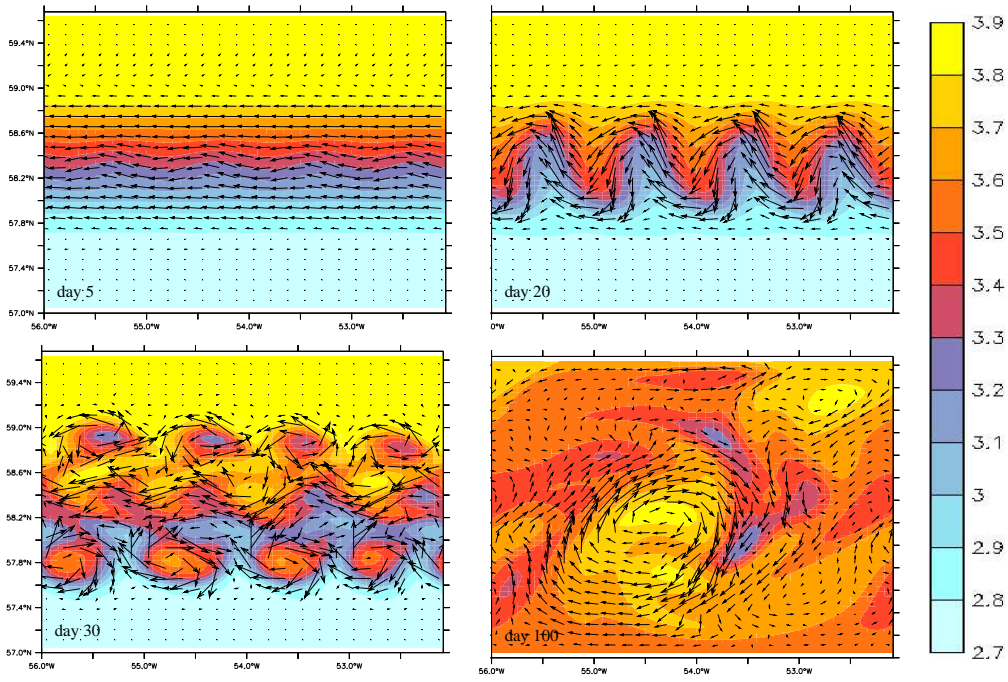


Figure 3.12: Sea surface temperature ($^{\circ}C$) and -velocities for experiment BIH1 for day 5, 20 ,30, 100 (every second vector plotted)

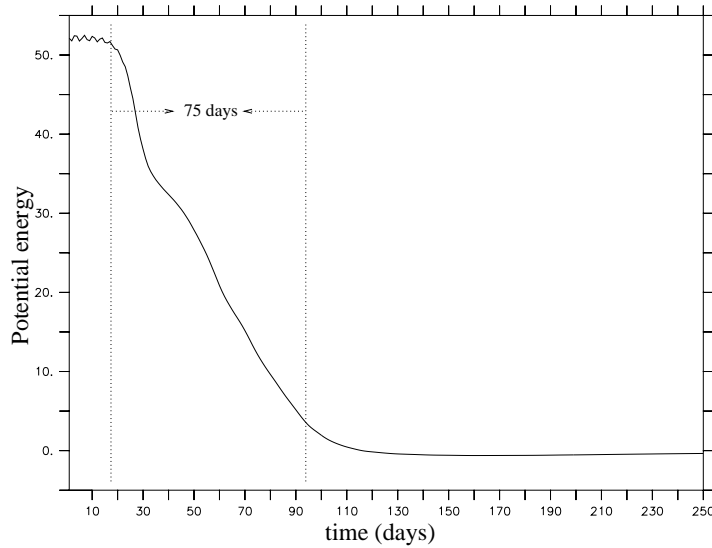


Figure 3.13: Loss of potential energy ($kg\ m^{-1}\ s^{-2}$) during the restratification process in experiment BIH1. The PE is referenced to zero after one year of integration. 75 day is the expected restratification timescale for our model setup following JONES AND MARSHALL (1997)

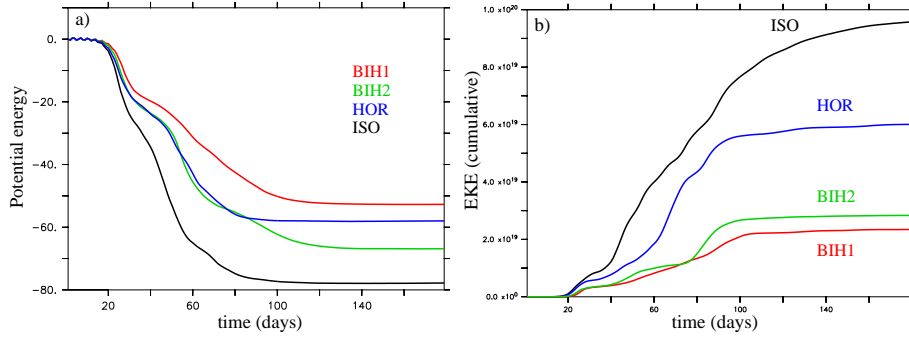


Figure 3.14: a) Time series of potential energy ($kg\ m^{-1}\ s^{-2}$) for exp. BIH1, BIH2, HOR, and ISO; PE being normalized to zero at the beginning. b) Eddy kinetic energy (cm^2/s) cumulatively integrated over the time period

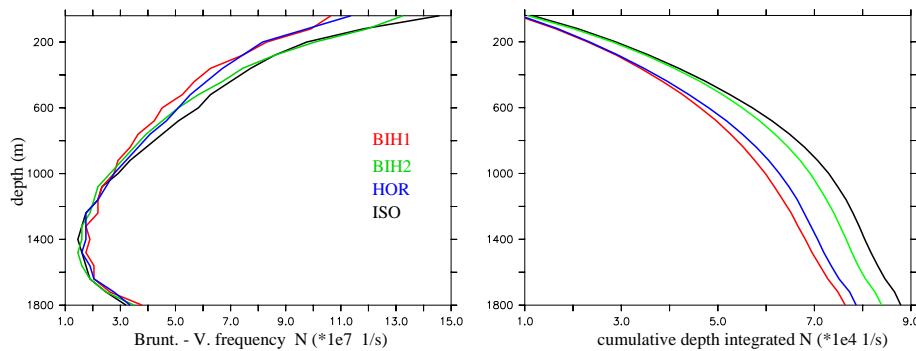


Figure 3.15: Stratification (Brunt-Väisälä frequency N (1/s)) after 1 year of integration (left), cumulative depth integrated N (right)

the PE at the beginning of each integration. The restratification process in all cases is finished at similar timescales, although the experiments with biharmonic mixing need a few days longer. The remarkable result is the difference in PE loss. BIH1 loses only $\sim 64\%$ of the PE compared to ISO. Distinguishing between the harmonic and biharmonic mixing experiments clearly shows that the loss of PE is controlled by the amount of diapycnal mixing, i.e. lower diapycnal mixing leads to an increased PE loss. As a consequence hereof, the eddy kinetic energy (EKE) is increased in case of lower diapycnal mixing, i.e. more of the available potential energy is converted to EKE. Figure 3.14b displays the cumulative increase of the basinwide EKE in the four experiments. (The EKE has been defined here as $v'^2/2$.) Because of the effective frictional damping on the grid scale, experiments with biharmonic mixing obviously produce less EKE compared to the harmonic experiments.

The different PE loss has strong consequences for the stratification of the water column and thus to the preconditioning for the subsequent winter. The stratification after one year of integration for all experiments is shown in Figure 3.15 [left]

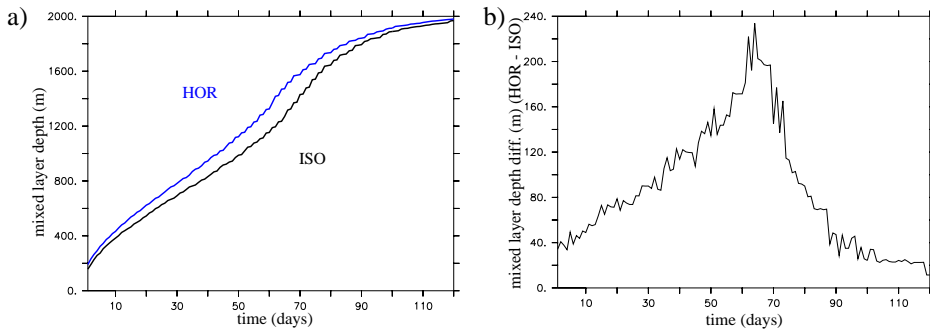


Figure 3.16: a) Time series of the mixed layer depth (m) for exp. ISO and HOR (beginning after 1 year) at constant cooling of 200 W/m^2 in a 1-dim mixed layer model. b) Difference in the mixed layer depth (HOR-ISO).

using the horizontal average of the Brunt-Väisälä frequency¹. With higher diapycnal mixing level the water column becomes less stratified after restratification. Because of the low differences in N at each depth, Figure 3.15 [right] displays the cumulative integral of N starting at the surface.

A simple 1-dimensional mixed layer model is used to study the effect on the convection depth in the following winter. This mixed layer model only exchanges water mass properties vertically among unstably stratified grid boxes (convective adjustment). We take the basinwide averaged density profiles of ISO and HOR after one year and apply a cooling at the top with a constant surface heat flux of 200 W/m^2 (Fig. 3.16a). There is a noticeable difference between both experiments of $O(100\text{m})$ (Fig. 3.16b). After ~ 70 days the mixed layer in ISO reaches the more stratified lower water column underneath the idealized "Labrador Sea Water", which is normally the end of the surface cooling in a more realistically forced model. This explains the lower differences in mixed layer depth between both experiments in the last 50 days.

The difference of $O(100\text{m})$ in the mixed layer depth is reached after only one convective cycle and the effect may accumulate in the following years.

3.3.3 Applications for the realistic model

We have demonstrated that there is a connection between numerical diapycnal mixing and simulated mixed layer depth. These results may help us to explain the large differences in the previous model studies. The mixed layer depths of the realistic model setups which correspond to the channel experiments ISO and HOR are shown in Figure 3.1. The maximum convection depth of over 3500 m in experiment **NA12-HOR** is decreased to a value of about 1600m in **NA12-ISO**. Note, that **NA12-ISO** additionally uses the bottom boundary layer (bb) model after BECKMANN AND DÖSCHER (1997) which may add to the different behaviors. However, in two additional experiments with the eddy permitting model

¹Brunt-V. frequency $N = \sqrt{-\frac{g}{\rho_0} \frac{\partial \rho}{\partial z}}$

(not shown), which only differ in using the bbl model, there was a slight increase rather than a decrease of the mixed layer depth in the experiment which uses bbl.

Further evidence for a connection between diapycnal mixing and simulated convection depth is given in the study of TREGUIER ET AL. (2004). They found in a high resolution model intercomparison that the $1/10^\circ$ -POP model (SMITH ET AL., 2000) show shallower (and even more realistic) convection depth compared to other models (e.g. FLAME experiment **NA12-HOR**). A possible explanation is provided by the behavior of BIH2, which uses the same mixing parameters as the POP model: this experiment experiences the second most PE loss during the restratification process (Figure 3.14a). This leads to a more stratified ocean (Fig. 3.15) compared to our experiment HOR (**NA12-HOR**).

There have been clear indications that the breakup of the mixed patch by "rim current eddies" cannot be the main restratification mechanism (e.g. KATSMAN ET AL. (2004); see also chapter 5 of this thesis), but the role of numerical diapycnal mixing on the mixed layer depth should be independent of the different eddy sources.

Chapter 4

Characteristics of the improved eddy-resolving model

4.1 Introduction

An improved eddy resolving model is designed based on the results from the previous chapter:

- the northern open boundary condition successfully used in the $1/3^\circ$ -experiment **NA3_open2** is implemented to improve the advective part of the freshwater budget, and thereby to prevent a salinification of the subpolar North Atlantic
- the numerical diapycnal mixing is minimized by using isopycnic diffusion together with only a small horizontal background diffusion

In this chapter we discuss salient aspects of the improved model solution from our experiment **SUB_NA12** after the spin-up phase. For a quantitative model assessment it should be noted that the climatological forcing is based on the years 1986-88, which corresponds to a medium NAO-phase. The most recently collected data (since 1996) encompass a period of transition to a low NAO-phase with rather weak convection depths in the Labrador Sea.

4.2 General circulation in the Subpolar North Atlantic

4.2.1 Upper ocean circulation

As an overview of the upper circulation, Figure 4.1 shows the velocities at 75 m depth underneath the Ekman layer in experiment **SUB_NA12** in comparison to the surface velocities derived from 1992-98 drifter data (FLATAU ET AL., 2003). Ekman velocities are subtracted from the drifter data. Velocities greater than 30 cm/s are shown in red in both cases. In general, the model circulation is in good

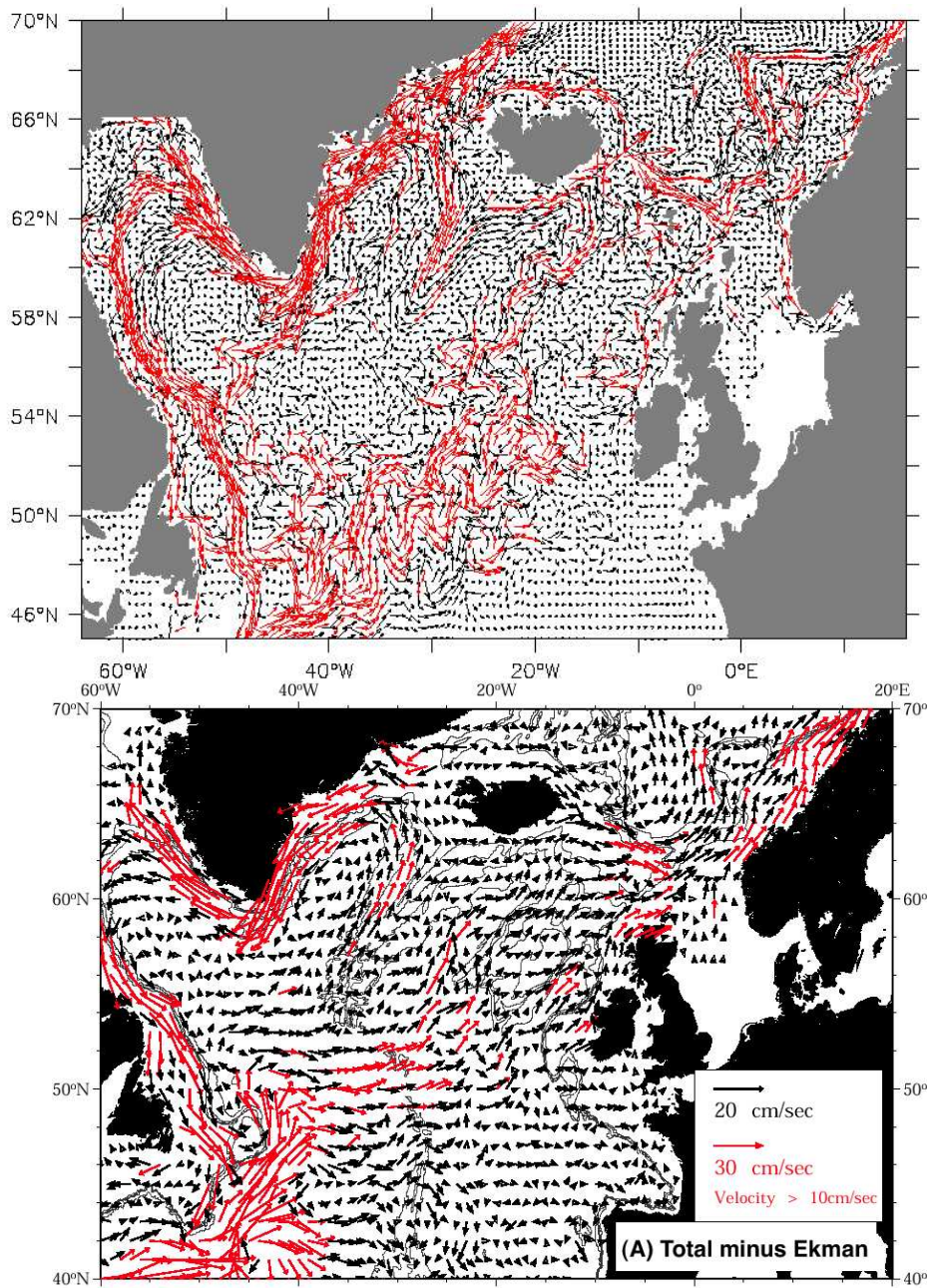


Figure 4.1: Upper panel: velocities at 75m underneath the Ekman layer (3y mean, every 6th vector is plotted). Lower panel: surface velocities from drifter data minus Ekman velocities derived from 1992-98 NCEP/NCAR-data (FLATAU ET AL., 2003)

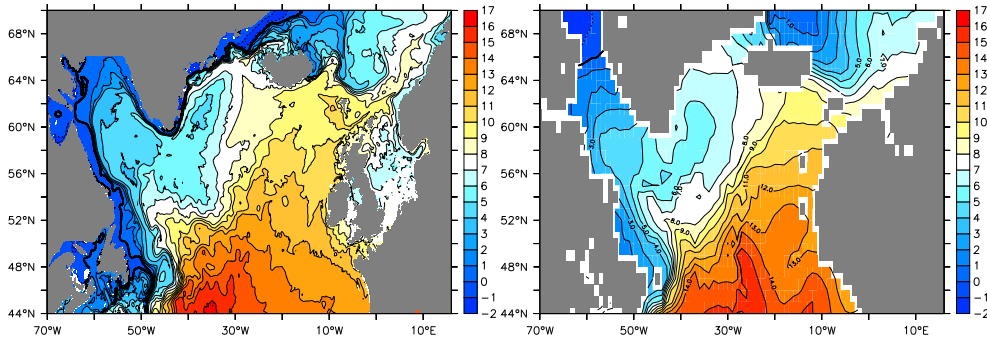


Figure 4.2: Annual mean temperatures ($^{\circ}\text{C}$) at $z=50\text{m}$ from experiment **SUB_NA12** (left panel) and WOCE-climatology (GOURETSKI AND JANCKE, 1998) (right panel)

agreement with the observations and is able to simulate the main flow characteristics: The North Atlantic Current entering the model domain on the western side of the southern boundary flows to the northeast and splits up into two main branches at 54°N . One branch reaches the Norwegian Sea at the western side of the Iceland-Faeroe Ridge and the second branch crosses the Faeroe-Shetland Channel. Velocities in the model tend to be larger than in the observations, but note that the drifter data were interpolated on an 1° -grid and smoothed using a 5-day running mean filter which may lead to a decrease in the velocity maxima. The model solution also contains the anticyclonic loop (called Northwest Corner) of the North Atlantic Current touching the southern Labrador Sea at $\sim 54^{\circ}\text{N}$. The Northwest Corner is characterized by relatively high temperatures (see Fig. 4.2 for a more distinct view) and high eddy-activity (see Fig. 5.2).

The subpolar gyre is completed by the Irminger (IC), East Greenland (EGC), West Greenland (WGC), and Labrador Current (LC) which are also in good agreement with the observations. In contrast to the drifter data the model shows two branches in the connection between WGC and LC, whereby the southern branch is associated with the eddies separated at Cape Desolation (see chapter 5 for details). Both branches are also described in observational studies (e.g. CUNY ET AL. (2002)). A further noticeable discrepancy can be found on the eastern side of the Reykjanes Ridge. The drifter data show a weak northward flow in this region, whereas the model solution provides southward velocities feeding the IC with warm and salty North Atlantic Current water. FLATAU ET AL. (2003) demonstrated that the northward flow is associated with the low NAO-phase in the late 90's and that under high NAO conditions (early 90's) the flow is southward in this region. Using drifter data from 1990-2000 and a somewhat different interpolation method JAKOBSEN ET AL. (2003) also obtained southward flow to east of the Reykjanes Ridge.

As discussed later in the text, a possible recirculation of the LC into the Labrador Sea has strong impacts on the convection region. Such an anticyclonic circulation in the interior of the Labrador Sea was first mentioned by LAVENDER ET AL. (2000). A similar recirculation pattern is found in the model. This recirculation reaches the

interior Labrador Sea at $\sim 57^\circ\text{N}$, 52°W before it turns east into the Irminger Sea, whereas it reaches the Labrador Sea at $\sim 59^\circ\text{N}$, 55°W in the study by LAVENDER ET AL. (2000). A weak recirculation branch turning into the Irminger Sea can be also identified in the surface drifter data (Fig. 4.1).

These minor differences in the upper circulation between model and observations seem to have no serious effect on the near surface temperature distribution (Fig. 4.2), which is in good agreement with the observations.

4.2.2 Deep circulation

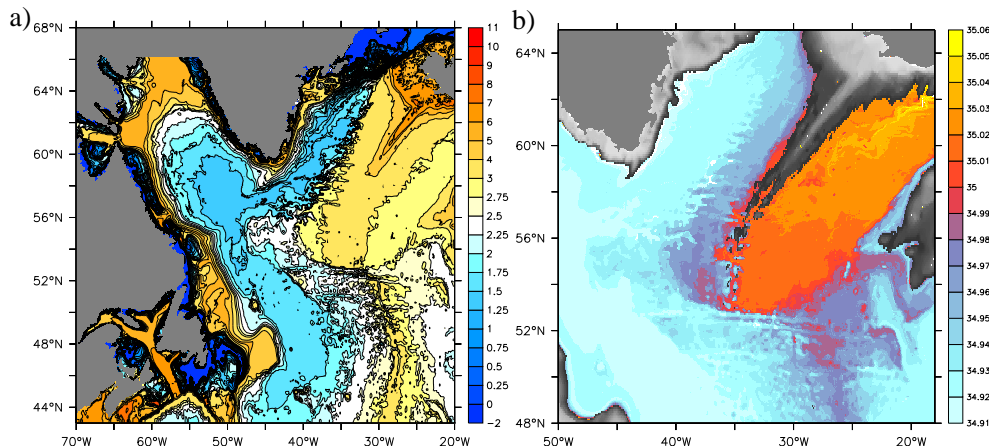


Figure 4.3: a) Cold inflow of Denmark Strait Overflow Water in the Subpolar North Atlantic represented by the annual mean bottom temperature ($^{\circ}\text{C}$). b) Leakage of Iceland-Scotland Overflow Water into the western basin as represented by the annual mean bottom salinity (PSU) at depths deeper than 1600m

The deep circulation in the Subpolar North Atlantic is closely connected to the formation and transport of North Atlantic Deep Water (NADW). The upper branch of NADW is formed by the Labrador Sea Water (LSW). A detailed description of LSW formation and export is given in the next chapter. The lower branch is associated with the overflow water masses entering the subpolar gyre across the sills between Greenland and Scotland. To overcome the problems of z-level models in representing flows across such sills, we use the bottom boundary layer model of BECKMANN AND DÖSCHER (1997) (see Chapter 2.2 for details). The large-scale impacts of the resultant representation of the overflows are given by DENG ET AL. (1999) and are not part of this study. In the subpolar gyre we distinguish between the dense Denmark Strait Overflow Water (DSOW) and the somewhat lighter Iceland-Scotland Overflow Water (ISOW). Due to large entrainment the product waters of ISOW in the western part of the subpolar gyre are often called "Gibbs Fracture Zone Water" (GFZW).

The DSOW provides the lower limb of the Deep Western Boundary Current (DWBC) with the coldest bottom temperatures in the subpolar gyre. Figure 4.3a shows the spreading of DSOW in the Subpolar North Atlantic in **SUB_NA12** on

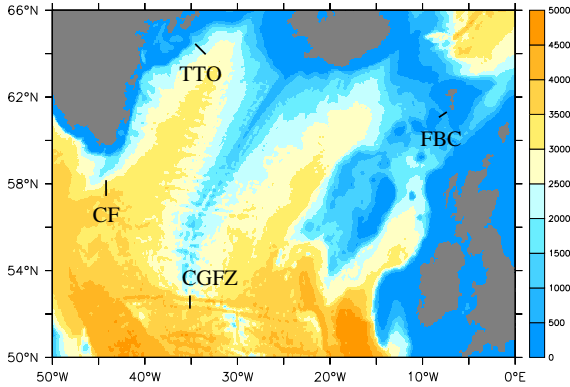


Figure 4.4: The location of moored arrays superimposed on the bathymetry (m) of the eastern North Atlantic. CF: Cape Farewell; CGFZ: Charlie-Gibbs Fracture Zone ; FBC: Faroe Bank Channel

the basis of the annual mean bottom temperatures. The tongue of cold temperatures follows the DWBC on the eastern side of Greenland. South of Greenland the spreading seems to be not concentrated in the relative narrow DWBC following the continental slope around the Labrador Sea, which may represent a model artefact of the bottom boundary layer scheme. Nevertheless, the bottom temperatures in the central Labrador Sea of 1.4°C are in close agreement with observations (e.g. PICKART ET AL. (2002)).

Location	Reference/Experiment	Salinity (PSU)	Temperature ($^{\circ}\text{C}$)
TTO	DICKSON AND BROWN (1994)	34.83 - 34.90	0 - 3.0
	SUB_NA12	34.92	1.2 - 2
	NA12_ISO	35.01 -35.02	2.2 - 2.5
CF	CLARKE (1984)	34.9 - 34.93	1.4 - 3.0
	SUB_NA12	34.91 - 34.93	1.4 - 2.2
	NA12_ISO	35.01 -35.03	2.3 - 2.6
FBC	SAUNDERS (1990)	34.9 - 35.1	-0.71 - 3.0
	SUB_NA12	34.9	-1.4 - 0
	NA12_ISO	34.9 -34.93	-1.8 - 0
CGFZ	SAUNDERS (1994)	34.94 - 34.975	2.4 - 3.35
	SUB_NA12	34.95 - 35	1.8 - 3.2
	NA12_ISO	34.99 -35.01	2.8 - 3.2

Table 4.1: Characteristic of the overflows at selected sites shown in Fig. 4.4

The ISOW is characterized by a salinity maximum compared to the surrounding water masses (DSOW,LSW). The ISOW enters the western part of the subpolar gyre through gaps in the Reykjanes Ridge (especially the Charlie-Gibbs Fracture Zone). The leakage through these gaps is presented in Fig. 4.3b by the annual mean bottom salinity. The high bottom salinity signal fades away in the western part where the ISOW lies above the lower DSOW. Nevertheless, two pathways of ISOW can be identified there. One narrow branch follows the Irminger Current on the western side of the Reykjanes Ridge, while a second broader wedge seems to spread westward directly into the Labrador Sea.

Direct comparisons of temperature and salinity values of experiment **SUB_NA12** and **NA12_ISO** with the observed characteristics of the overflows at selected

sites are given in Table 4.1. The locations of the sites are shown in Fig. 4.4. The simulated overflow properties (annual mean) are mostly in the range of the observed variability. Both model experiments use the bottom boundary layer model following BECKMANN AND DÖSCHER (1997), but **NA12_ISO** uses in contrast to **SUB_NA12** no open northern boundary. The main effect emerging here are higher salinity and temperature values of the DSOW in **NA12_ISO** at TTO and CF. However, since the effect of temperature and salinity are nearly compensating, differences in density between the model cases are rather weak.

4.3 Deep convection in the Labrador Sea

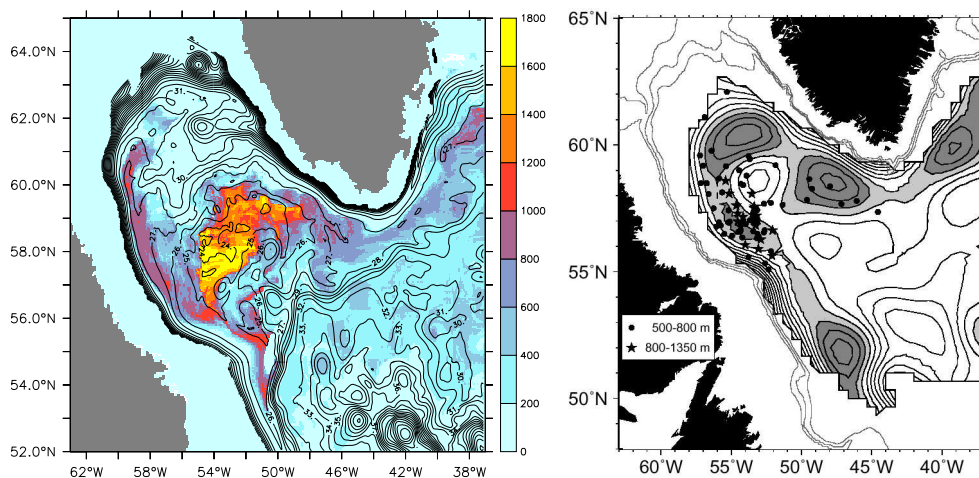


Figure 4.5: March mean of the mixed layer depth (m) and winter mean (J/F/M) of the dynamic height (cm) at 700m. Left: model solution , right: obtained from 1996-98 float data (LAVENDER ET AL., 2002) (for mixed layer depth only 1997). The low dynamic height regions are shaded in grey

4.3.1 Mixed layer depths

Deep convection in the Labrador Sea occurs in late winter, reaching maximum depths usually in late March. In chapter 3 we discussed the problems of numerical models in quantitatively reproducing convection regions and depth. The refined model configuration obtained by taking into account the critical factors identified in the previous chapter, exhibits a climatological mixed layer distribution closer to the observational estimates (Fig. 4.5).

The maximum mixed layer depths are found on the LC side in the central Labrador Sea. More regions of deep convection are located on the WGC side in the central Labrador Sea and in a small branch just offshore the northeastern LC. The simulated mixed layer reaches a maximum depth of ~ 1800 m which seems to be a plausible value according to the climatological forcing obtained from the years 1986-88. The maximum values in the observations obtained by float data reach

only 1350m in 1997. In both cases deep convection mainly occurs in regions of low dynamic height or cyclonic circulation. The convection area in the model is apparently constrained by the WGC, LC, "Cape Desolation eddies" and the anticyclonic recirculation. The recirculation in the observations extent far into the central Labrador Sea building a further local dynamic height maximum at $\sim 60^\circ\text{N}$. In the model there is also a local dynamic height maximum in this area, associated with the strong anticyclonic eddy formation at Cape Desolation. In contrast to the LAVENDER ET AL. (2002) interpretation of the float data it is, however, disconnected from the recirculation.

KÄSE ET AL. (2001) have demonstrated that the recirculation can be explained as a locally wind-driven circulation in the presence of topography interacting with the baroclinic flow field due to the Greenland-Scotland overflow. Necessary elements therefore appear to be the proper representation of the bottom topography and the path of the dense NADW flow. In contrast to our model study, KÄSE ET AL. (2001) used partially filled bottom cells, which improves interaction of topography with the circulation. As mentioned earlier, the DSOW in our model is not concentrated in the DWBC around the Labrador Sea. A possible connection between the DSOW signal and the recirculation might prevent a recirculation gyre reaching further to the north in our simulation. However, the patch of deepest convection appears to be localized between the recirculation and the boundary current. The simulated convective patch is, in contrast to the observations, continuously deep in the interior of the Labrador Sea. An interaction between the deep convection patch and the recirculation might be another possibility, which prevents a more northeast reaching recirculation in the model.

The critical role of eddies in setting the convection region is shown in Fig. 4.6 by a snapshot of the mixed layer depth and the velocities at 100 m. MARSHALL AND SCHOTT (1999) pointed out that a large scale cyclonic circulation is a necessary precondition for open-ocean deep convection. The cyclonic circulation preserves the weak stratification in the interior by inclining the isopycnals towards the surface (doming). Anticyclonic circulation on the other hand prevents deep convection even in individual mesoscale features, e.g. the coherent anticyclonic eddy at 59°N , 57°W . The anticyclonic eddies are more frequent and easier to detect than the cyclonic eddies. A weak cyclonic eddy structure can be identified at e.g. 57°N , 51°W . The anticyclonic eddies formed at Cape Desolation are well stratified due to a freshwater cap, which originates from the fresh onshore part of the West Greenland Current over the shelf. These eddies cause a nearly complete shutdown of convection (further details are given in section 5.2 in the following chapter). Other regions, like the meandering recirculation, seem also to be prone for generating coherent eddy structures. As a consequence, the form of the whole convective patch is not a simple homogeneous cylinder, as often assumed in idealized process studies, but rather a complex structure dispersed by geostrophic eddies.

The Labrador Current is characterized by a baroclinic part along the shelf with an offshore edge near the ~ 2000 m isobath, and a more barotropic part named "deep" Labrador Current, roughly above the 2500 m isobath (CUNY ET AL., 2002). The

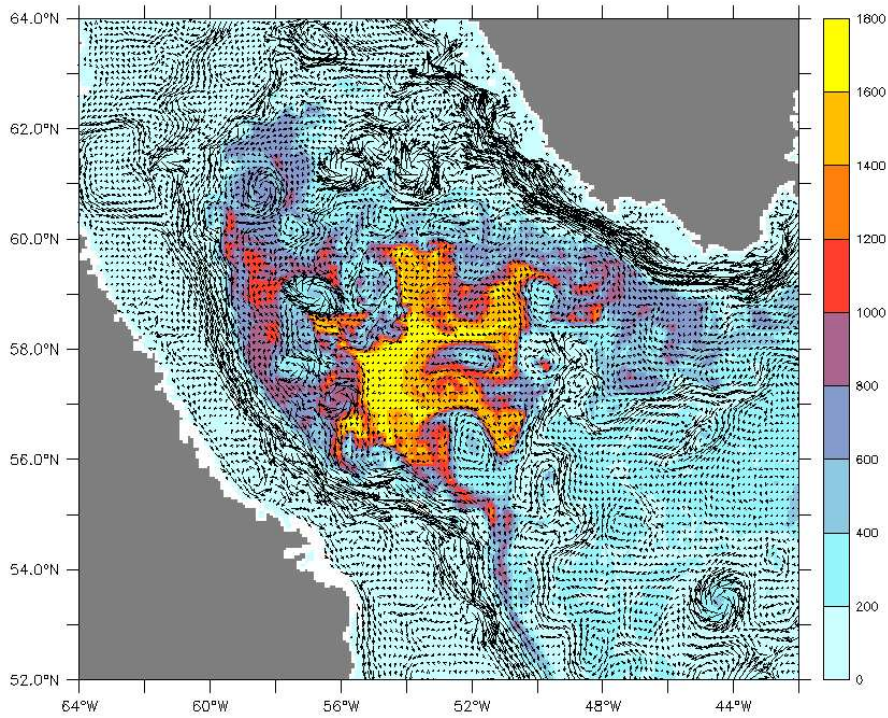


Figure 4.6: Snapshot of the mixed layer depths (m) and velocities in 100m (15. March) in experiment **SUB_NA12**

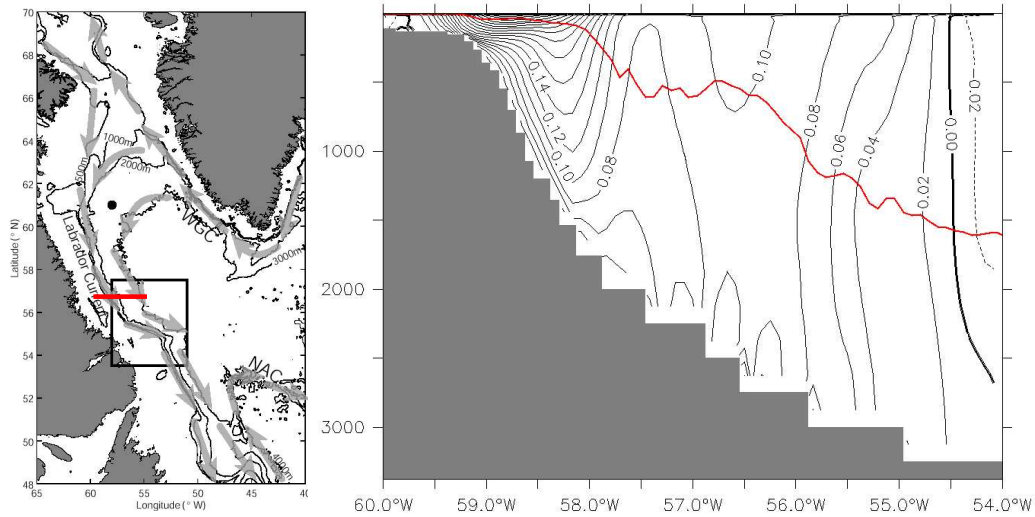


Figure 4.7: Schematic circulation in the Labrador Sea (CUNY ET AL., 2004) [left panel]. Annual mean of the meridional velocity at 57°N (red line in the schematic) from experiment **SUB_NA12**. Note that positive values indicate a flow to the south. Contour interval is 0.02 m s^{-1} . The red curve denotes the March mean mixed layer depth [right panel]

3000 m isobath is often considered as the offshore edge of the Labrador Current. Figure 4.7 shows a schematic view of the boundary currents in the Labrador Sea (CUNY ET AL., 2004). The deep Labrador Current appears closely connected to the pathway of the Cape Desolation eddies. There is observational evidence that convection may also occur in the deep Labrador Current (PICKART ET AL. (2002), CUNY ET AL. (2004)). A section through the Labrador Current at 57°N from experiment **SUB_NA12** is given in Fig. 4.7. The model is obviously capable of simulating both parts of the Labrador Current along the observed isobaths. The red curve denotes the mean of mixed layer depths in March. The mixed layer reaches depths of ~ 500 to 1000 m within the deep Labrador Current. PICKART ET AL. (2002) found mixed layer depths of 825 m within the deep Labrador Current in March 1997. In **SUB_NA12** the mixed layer deepening in and nearby the deep Labrador Current starts somewhat earlier (beginning of February) than in the interior Labrador Sea (mid-February) (not shown), which is in agreement with observational estimates (CUNY ET AL., 2004). Recently P. Brandt et al.¹ calculated water mass transformation rates from **SUB_NA12** using the simulated heat- and freshwater fluxes. They found that a considerable part of the newly formed Labrador Sea Water is formed in the deep Labrador Current. However, PICKART ET AL. (2002) found that the product of convection above the Labrador slope would be hardly differentiable from the interior product once advected away from the Labrador Sea.

4.3.2 Water mass properties

In the eddy permitting experiments the open northern boundary prevents a salinification of the subpolar gyre. In those experiments (as shown in section 3.2) the LSW is only affected by the resulting increased freshwater import by the boundary currents, if the exchange with the interior is effectively parameterized. In an eddy resolving model version as used here, this effect should be adequately represented by the explicitly simulated eddy field.

Figure 4.8 shows the effect of the open boundary on the water mass properties in the central Labrador Sea. The LSW is characterized by the local salinity minimum compared to the surrounding water masses. A typical density range for LSW in observational studies is $\sigma_0 = 27.74 - 27.80$, whereas the salinity minimum of LSW is nearly disappeared in the smoothed climatology. The open northern boundary in **SUB_NA12** leads, in agreement with the climatology, to much fresher and colder LSW compared to experiment **NA12_ISO** with closed northern boundary. We define the LSW range in **SUB_NA12** as $\sigma_0 = 27.76 - 27.81$, still somewhat denser than in the observation but significantly improved compared to the previous model studies. These improvements in the water mass properties also extend to the DSOw and ISOW as well. Surprisingly, the salinity and temperature changes in the overflows due to the open boundary formulation seems to be density compensated.

¹Brandt, P., A. Funk, F. Schott, L. Czeschel and C. Eden (2004): Role of the eddy field for the export of newly formed Labrador Sea Water within the Labrador Current - Poster presentation at CLIVAR-workshop on North Atlantic thermohaline circulation variability

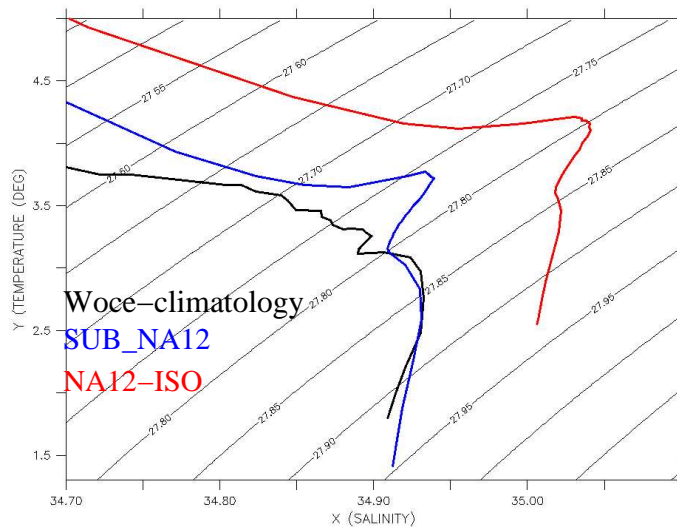
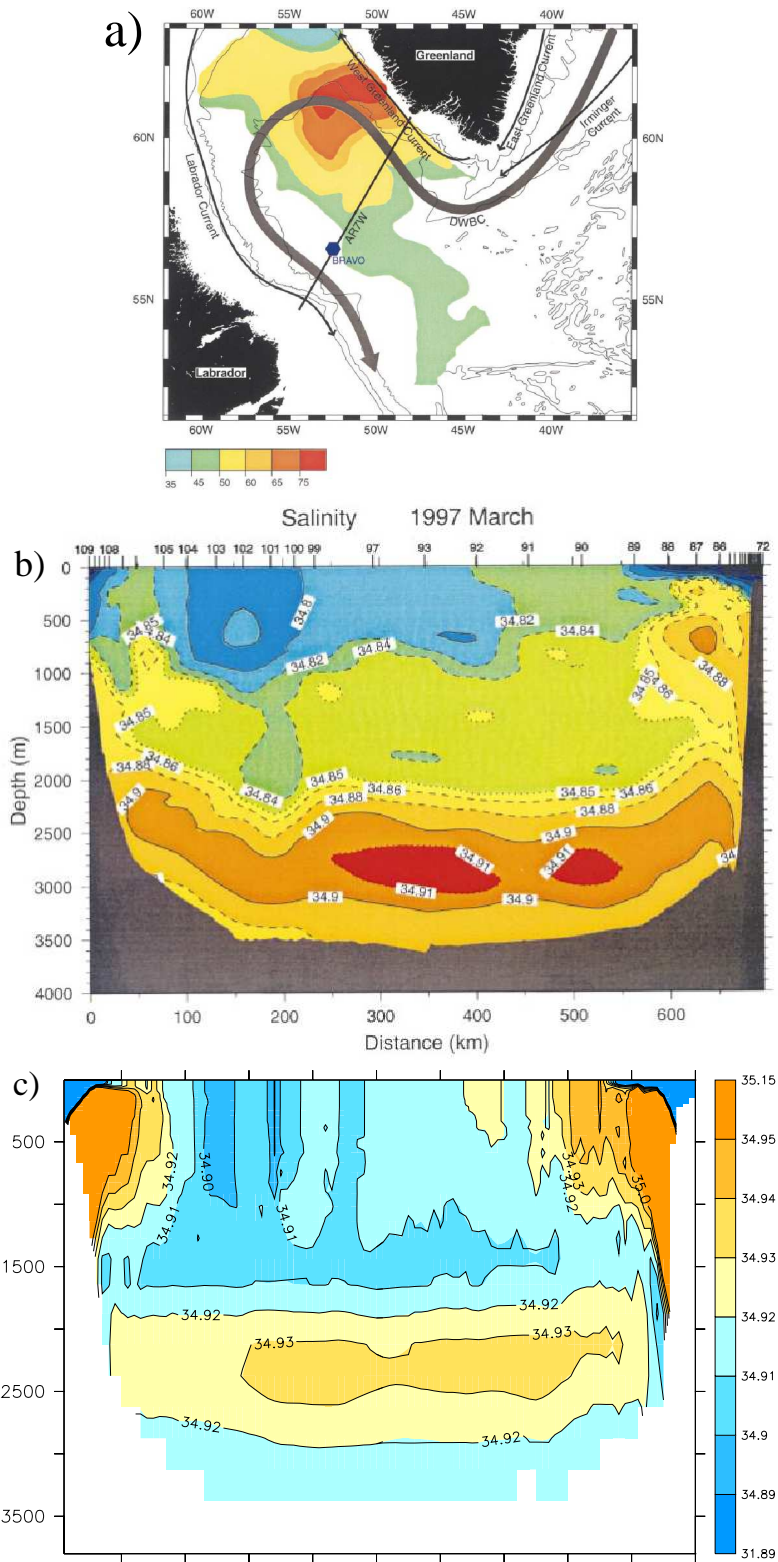


Figure 4.8: Annual mean of the potential temperature ($^{\circ}C$) vs. salinity (PSU) distribution at $56.5^{\circ}N$ and $53^{\circ}W$ from the WOCE-climatology (black) (GOURETSKI AND JANCKE, 1998), experiment **SUB_NA12** with open northern boundary (blue), and **NA12-ISO** with closed northern boundary (red).

A salinity section during active convection along the WOCE AR7W hydrographic line for experiment **SUB_NA12** is compared to observations (PICKART ET AL., 2002) in Fig. 4.9. The simulated salinities are, in general, somewhat higher than in the observations, which might be explained by the climatological forcing used at the surface and the lateral boundaries of the model. In contrast to the quasi-steady state model solution, observations show a freshening of the deep water masses in the North Atlantic over the past 4 decades (DICKSON ET AL., 2002). Therefore this comparison is a more qualitative analysis. The simulated and observed section show a very similar salinity distribution. The boundary currents are characterized by very low near surface salinities and high salinities below. Despite the open northern boundary formulation (see also Fig. 3.5), the salinities of up to 35.15 PSU in the warm and salty slope part of the boundary currents, especially in the Labrador Current, are overestimated in the model. A further salinity maximum is related to the ISOW below ~ 2000 m and above the lower saline DSOW at the bottom. The deep convection is concentrated in the southern half of the section. The newly formed Labrador Sea Water reaches depths of more than 1000m in the observations and ~ 1700 m in the model. Note that the AR7W section is a bit south of the region of deepest convection (1400 m) in 1997 (PICKART ET AL., 2002). The water mass in the observations with salinities between 34.82 - 34.85 PSU is associated with LSW formed in the deep convection years in the early to mid-90's.

While there are still some differences in the details of the salinity distribution between experiment **SUB_NA12** and the observations, the model solution appears to be remarkably improved compared to experiment **NA12-ISO** (Fig. 4.9d). In **NA12-ISO** salinities of newly formed LSW are higher than 34.99 PSU and the

4.3. DEEP CONVECTION IN THE LABRADOR SEA



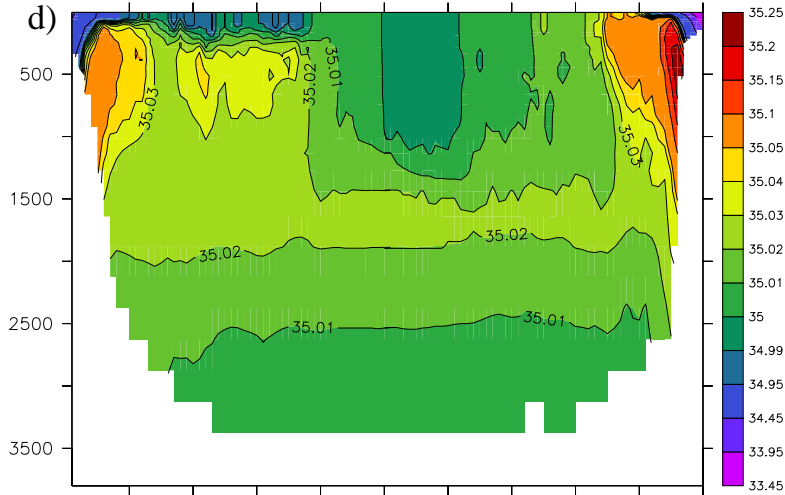


Figure 4.9: a) Location of AR7W hydrographic section. The color represents the standard deviation of sea surface height anomaly (mm) as measured from satellite altimetry (PICKART ET AL., 2002). b) Salinity (PSU) along AR7W during active convection in March 1997 (PICKART ET AL., 2002). c) Salinity along AR7W in **SUB_NA12** (March mean). d) Salinity along AR7W in **NA12-ISO** (March mean). Note that different and unequally spaced color bars have to be used in each figure to visualize the variety of salinity ranges.

location of deep convection is concentrated on the Greenland side. The highest salinities in **NA12-ISO** in the central Labrador Sea (at ~ 1800 m depth) seems to be rather a consequence of mixing with the boundary currents than an salinity maximum which can be associated with ISOW.

4.4 Export of Labrador Sea Water

The deep convection in the Labrador Sea creates the relatively homogeneous Labrador Sea Water, with unique characteristics of low salinity, low vertical density gradient and high anthropogenic tracer concentrations. These signals can be traced as the LSW spreads laterally into other regions. LSW follows three primary pathways away from the formation region (SY ET AL. (1997), Fig. 4.10a): north-eastward into the Irminger Sea, eastward near 50°N , and southward as part of the Deep Western Boundary Current (DWBC).

The low vertical density gradient of LSW leads to a minimum in the large-scale potential vorticity PV given by

$$PV = \frac{f}{\rho_{ref}} \frac{\partial \rho}{\partial z},$$

where f denotes the Coriolis parameter. The spreading of the low PV signal in **SUB_NA12** on the $\sigma_0 = 27.79$ surface is shown in Fig. 4.10b. The model is capable

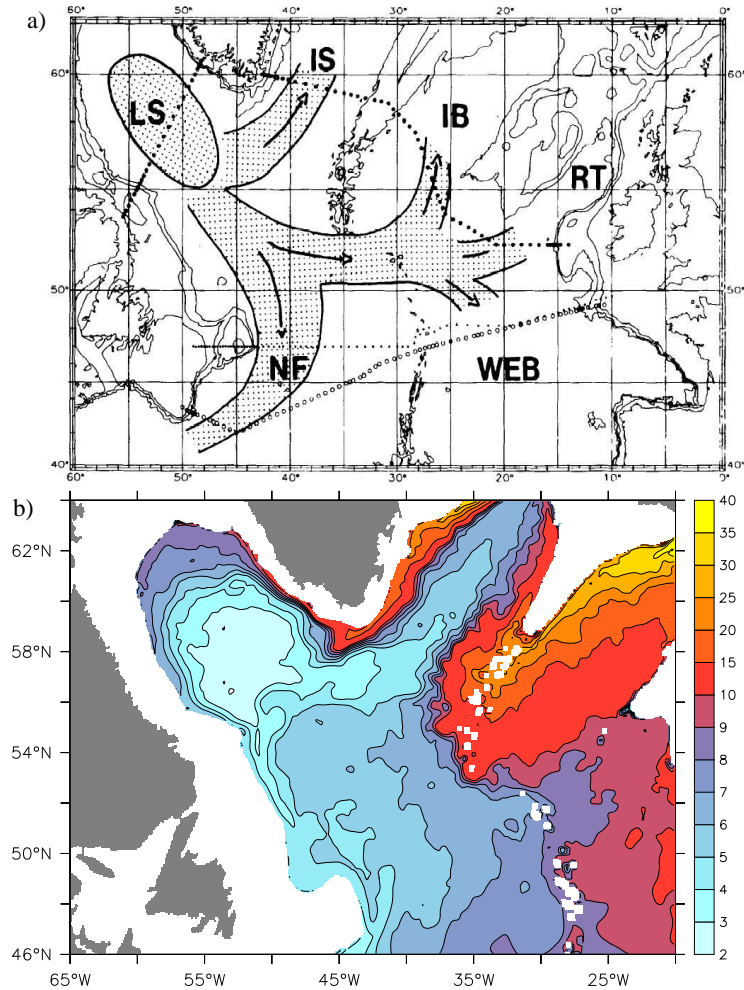


Figure 4.10: a) LSW export pathways (SY ET AL., 1997). b) Annual mean of the large-scale potential vorticity ($\times 10^{10} m^{-1} s^{-1}$) on $\sigma_0 = 27.79$ for experiment **SUB_NA12**.

of reproducing the three observed main pathways. The lowest PV concentrations are found in the formation region in the interior Labrador Sea. The most significant pathway of LSW is the DWBC with PV-values lower than $5 \times 10^{10} m^{-1} s^{-1}$. A further major pathway is the export of LSW into the Irminger Sea, which can be associated with the anticyclonic recirculation (Fig. 4.5). The export of LSW in the eastern part of the subpolar gyre is characterized by somewhat higher PV concentrations due to mixing with surrounding water masses.

Further information, especially on the export timescales, is provided by an idealized "convection tracer" as described in section 2.3.1. The simulated LSW encompasses the density classes from $\sigma_0 = 27.76$ to $27.81 kg m^{-3}$ (Fig. 4.8). We split the LSW into an upper part ($\sigma_0 = 27.76 - 27.78$) and a lower part ($\sigma_0 = 27.9 - 27.81$). The spreading of newly ventilated LSW is shown in Fig. 4.11 by the vertical average of the idealized convection tracer in the upper and lower LSW part. The tracer is initialized by a value of 1 at each time step within the mixed layer in a regional

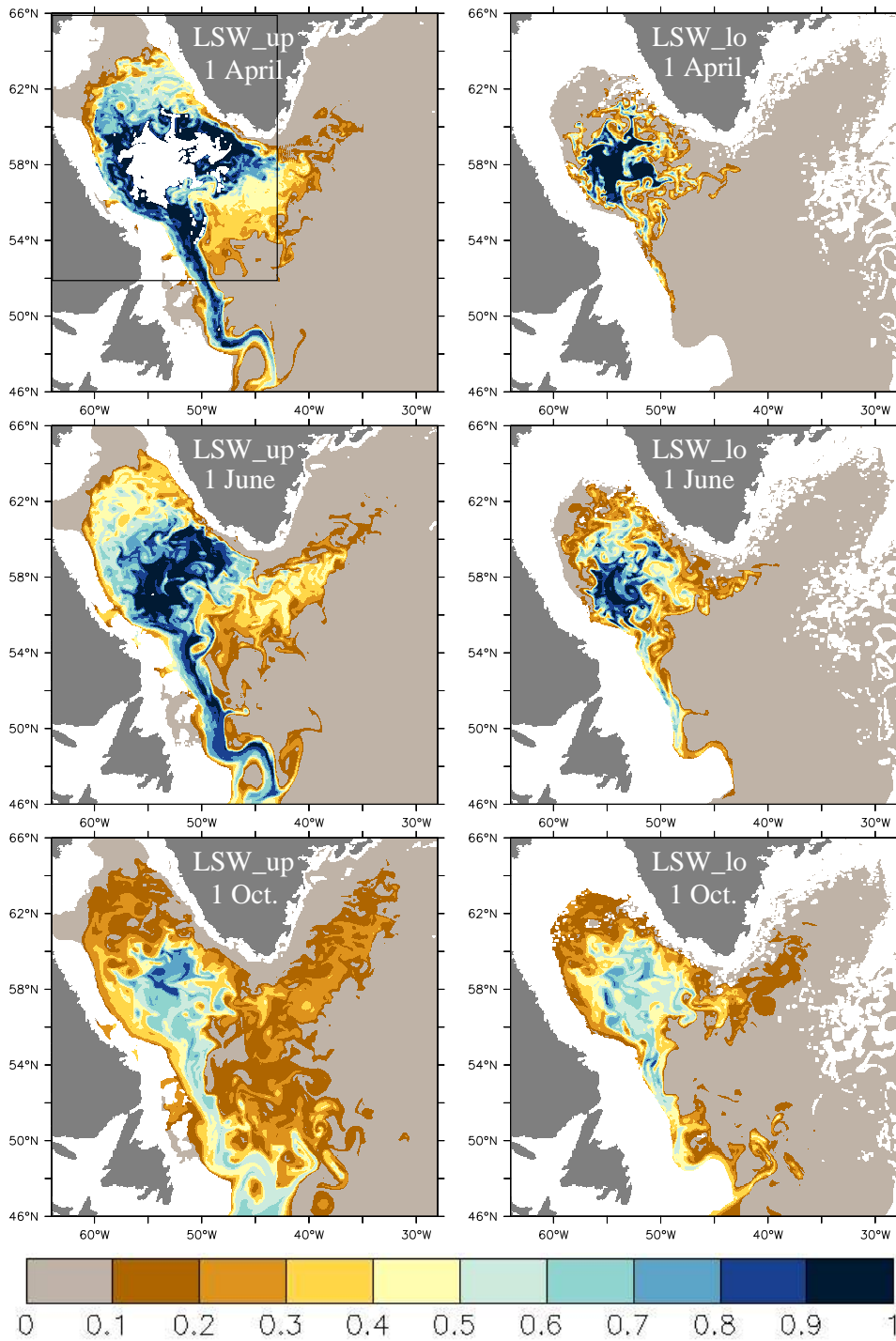


Figure 4.11: Spreading of an idealized convection tracer at selected times. The tracer is initialized with a value of 1 within the mixed layer in the black contoured box. The left column shows the vertical average between the isopycnal surfaces $\sigma_0 = 27.76 - 27.78$, which represents the upper part of the simulated LSW (LSW_up). The right column represents the lower part between $\sigma_0 = 27.79 - 27.81$ (LSW_lo).

”Labrador Sea-box” (also shown).

In late winter (1. April) the upper LSW shows a rapid export along the DWBC with tracer concentrations close to the initialized values of 1, which indicates that a large fraction of this water mass originates from convection in the deep Labrador Current. Note, that the deepening of the mixed layer in the deep Labrador Current starts in early February. The northeastward spreading from the LSW formation region with mean tracer concentrations ranging from 0.2 - 0.8 can be associated with strong eddy-stirring due to the ”Cape Desolation eddies” (compare Fig. 4.6 and 4.9a). The lower LSW part in late winter is concentrated in the interior Labrador Sea and the largest part is still in contact with the atmosphere. Some irregular offshoots with lower tracer concentrations indicate the presence of strong eddy-mixing. In spring (1. June) the upper LSW shows a strong tracer signal in the DWBC; a second branch reaches the Irminger Sea with tracer concentrations around 0.4, which can be associated with the recirculation. The ongoing restratification can be seen in the area of the Cape Desolation eddies, where the tracer concentrations decrease relative to April. In fall (1. October) the upper LSW has reached wide parts of the Irminger Sea, which is in agreement with the 6 month transition timescale of this export pathway suggested by SY ET AL. (1997). The tracer shows no evidence for an export pathway from the formation region directly to the eastern subpolar gyre. The spreading into the east is instead characterized by a loop through the western boundary current. The spreading of the lower LSW takes the same pathways but is obviously slower.

We define the annual LSW formation rate as the volume of newly formed LSW in winter. The volume of LSW (between $\sigma_0 = 27.76$ to 27.81 kg m^{-3}) in the region shown in Fig. 4.11 reaches its minimum in January and its maximum in April. The annual formation rate, calculated by the difference between the monthly mean volume of April minus January, ranges from 5.9 Sv to 6.6 Sv in the last three years of experiment **SUB_NA12**. Typical formation rates from observational estimates range from 2-3 Sv in years of weak forcing to 12 Sv in years of intense atmospheric forcing (SMETHIE AND FINE (2001); RHEIN ET AL. (2002)). The formation rate can also be estimated by using the idealized convection tracer. The tracer is initialized with zero at 1 January, and from then onward set to a value of 1 within the mixed layer. Consequently the formation rate can be simply derived from the maximum integrated tracer content within the LSW layer, which is reached in April. Using this method we obtain an annual formation rate of 16.7 Sv. But in contrast to the volume, the tracer initial condition at 1 January is zero and only $\sim 66\%$ of the tracer content leaves the Labrador Sea until the subsequent January. Using the difference between April and the subsequent January we obtain 5.6 Sv, which is very similar to the volumetric estimate of 5.9 Sv in this year. The volumetric estimate describes the net water mass transformation into the density range of LSW, whereas the significant higher (16.7 Sv) ”tracer inventory estimate” describes the rate of ventilation, i.e. how much water received new atmospheric impressed tracer properties, like e.g. CFCs.

In this chapter it has been shown that the ”new” model is capable to simulate the characteristics of the subpolar gyre in good agreement with observations, except

of two noticeable differences: 1) the model overestimates the salinities in the warm and salty parts of the West Greenland Current and Labrador Current; 2) the anticyclonic recirculation in the Labrador Sea extends northwestward only to about $\sim 57^\circ\text{N}$, 52°W before it turns east into the Irminger Sea, whereas in observations it reaches $\sim 59^\circ\text{N}$, 55°W (LAVENDER ET AL., 2000). However, the localization of deep convection and the water mass properties of newly formed Labrador Sea Water are remarkably improved compared to previous model solutions, so that the model can now be used with more confidence to assess underlying mechanisms of deep convection and its variability.

Chapter 5

Mechanisms of deep water formation

5.1 Introduction

Like most regions of the subpolar North Atlantic, the Labrador Sea is characterized by a net annual heat loss to the atmosphere which, in steady state, must be balanced by a net convergence of heat due to the ocean circulation. The heat needed to balance the annual surface heat loss, is supplied to the region by the boundary currents that flow cyclonically around the convecting interior (GASCARD AND CLARKE (1983), PICKART ET AL. (2002)). Several studies highlight that the exchange between the boundary currents and the interior is regulated by lateral eddy fluxes with contributions from boundary current instabilities (KATSMAN ET AL. (2004), SPALL (2004)) and the instability of the convective patch (JONES AND MARSHALL (1997), LEGG ET AL. (1998)).

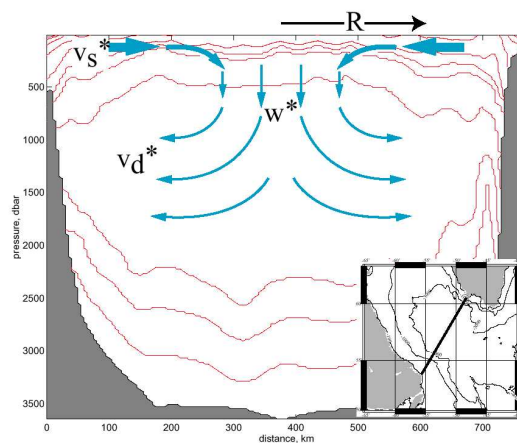


Figure 5.1: A potential density section across the Labrador Sea superimposed on a schematic of the anticipated eddy-induced circulation (KHATIWALA AND VISBECK, 2000)

Figure 5.1 shows schematically how these lateral eddy fluxes are thought to organize restratification after convection (KHATIWALA AND VISBECK, 2000). The eddies transport buoyant low salinity water at the surface from the boundary currents towards the interior and newly ventilated Labrador Sea Water at depth towards the boundaries. Together they comprise an "eddy-induced overturning circulation".

The above mentioned model studies are based on simple process models, which might disregard various aspects concerning deep water formation in the Labrador Sea. In this chapter the impacts of eddies (and associated eddy-mixing) in a realistic general circulation model are studied.

5.2 Mesoscale variability

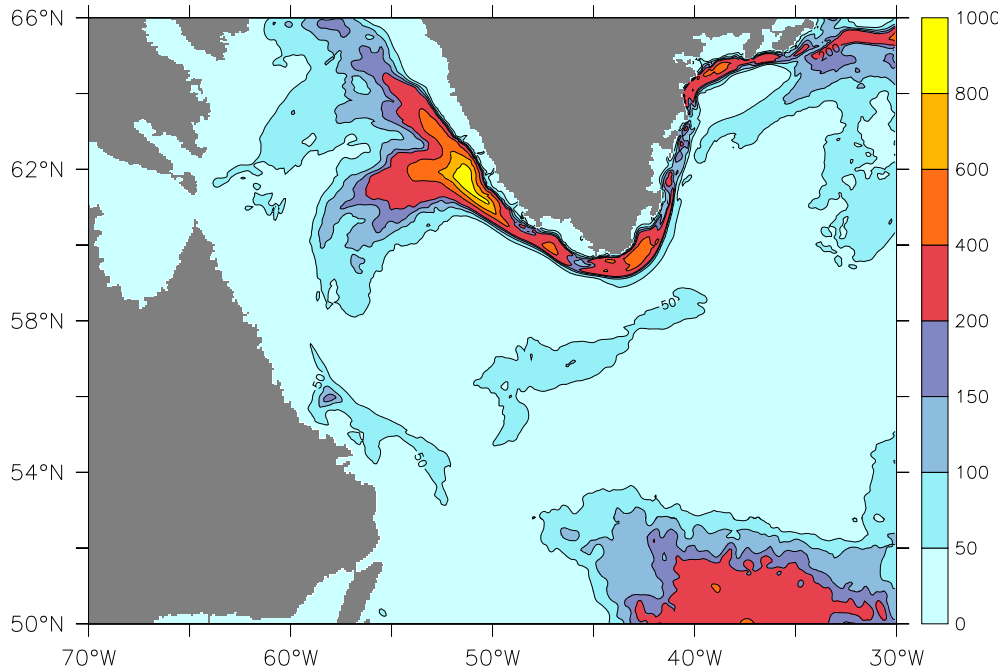


Figure 5.2: Eddy kinetic energy (cm^2/s^2) from **SUB_NA12** averaged over the top 100m and 3 years. Note the unequally spaced contour interval.

The distribution of eddy-activity in the western part of the subpolar North Atlantic is shown in Fig. 5.2 using the eddy kinetic energy (EKE) averaged over three years and the upper 100m. The EKE is defined as:

$$EKE = \frac{1}{2} \overline{(u'^2 + v'^2)},$$

whereby the overbar denotes the time average (one month) and primes denote the deviations from the mean.

Overall the distribution of EKE is in good agreement with observations from the T/P and ERS satellite data (Fig. 1.5), from BRANDT ET AL. (2004). (Note that the

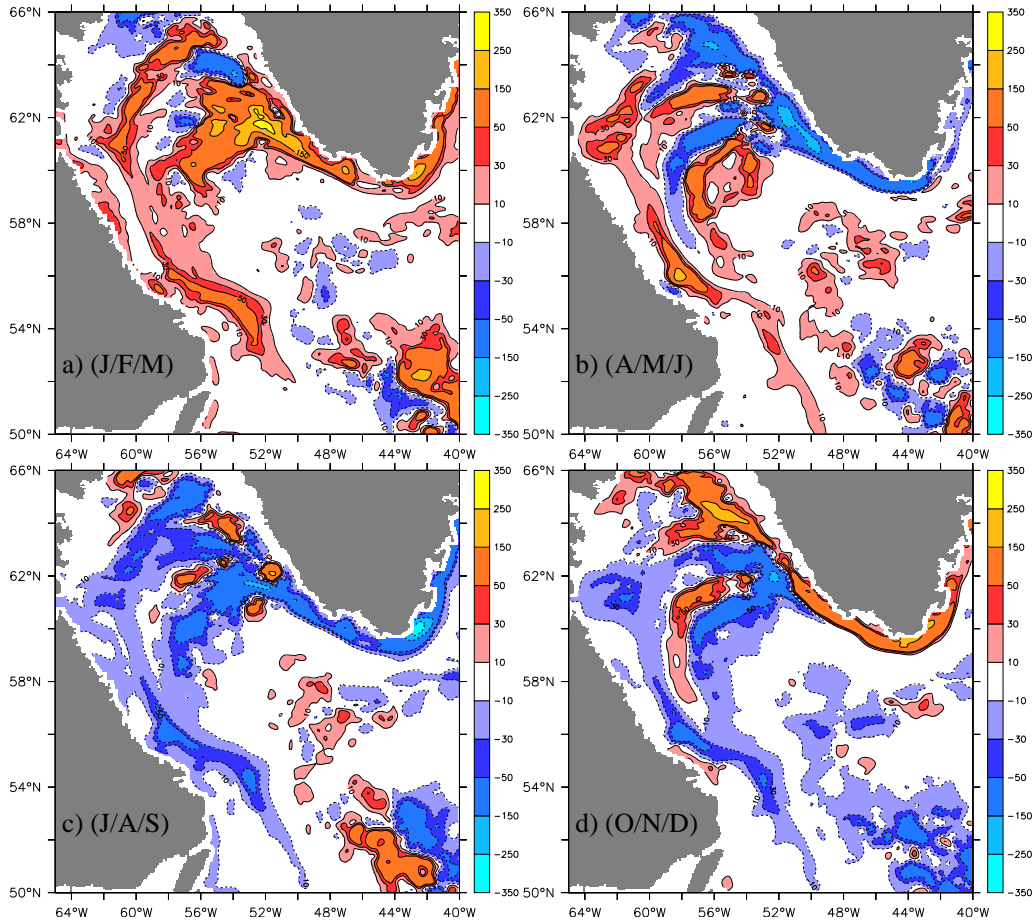


Figure 5.3: Seasonal anomalies of the eddy kinetic energy (cm^2/s^2) from exp. **SUB_NA12** averaged over the top 100m and 3 years. Note the unequally spaced contour interval.

satellite data represent the EKE distribution at the surface). The most prominent feature in the mean EKE field is the loop of the North Atlantic Current called "Northwest Corner" entering the western subpolar gyre from the south at $\sim 55^\circ N$. The simulated EKE in the Northwest Corner, i.e. 200 to 400 cm^2/s^2 is somewhat lower than in the observations (600 to 1000 cm^2/s^2), which is most likely related to the southern open boundary at $43^\circ N$, since the forcing at the open boundary (obtained from monthly mean data) reduces the "natural" variability of the North Atlantic Current. The maximum simulated EKE, with values of more than 600 cm^2/s^2 , extends from the West Greenland Current at $\sim 61^\circ N$ into the interior Labrador Sea, obviously associated with the separation of "Cape Desolation eddies" (see also Fig. 4.6). These EKE maximum also show up in the satellite data with values ranging from 600 to 800 cm^2/s^2 . The whole East- and West Greenland Current are also characterized by high EKE in the model, which is confirmed by EKE estimates based on surface drifter data (FRATANTONI, 2001), showing values of 300 to more than 500 cm^2/s^2 compared to ~ 200 to 600 cm^2/s^2 in the model. Another area of moderately enhanced EKE can be found in the Labrador Current,

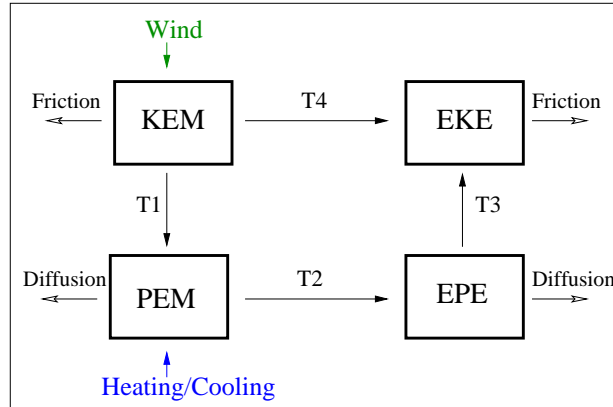


Figure 5.4: Mean energy cycle for a closed oceanic basin, driven by steady winds and buoyancy forcing. The schematic is redrawn from BÖNING AND BUDICH (1992). The energy components are mean kinetic energy (KEM), eddy kinetic energy (EKE), mean available potential energy (PEM), and eddy available potential energy (EPE). T(1-4) represents the energy transfer terms.

with values up to $200 \text{ cm}^2\text{s}^{-2}$, and in the anticyclonic recirculation area between $55\text{-}59^\circ\text{N}$ (up to $100 \text{ cm}^2\text{s}^{-2}$). Overall, the EKE distribution is very similar to the high resolution model-studies presented by EDEN AND BÖNING (2002) and SMITH ET AL. (2000).

The seasonal cycle of EKE from experiment **SUB_NA12** is shown in Fig. 5.3 as seasonal anomalies from the annual mean. The EKE in the boundary currents around the Labrador Sea is characterized by a pronounced seasonal cycle. The highest eddy activity occur in the winter season (J/F/M) with an increase of $\sim 25\%$ in the Cape Desolation area and of more than 100% in the Labrador Current (LC) compared to the annual mean. In spring (A/M/J) the EKE remains high in the LC and around the region of deep convection. In contrast, negative EKE anomalies are found during spring in the West Greenland Current (WGC) and along the main pathway of the branch separated from WGC following the 3000 m isobath (see schematic in Fig. 3.7). The summer (J/A/S) is generally characterized by the lowest eddy activity. In autumn (O/N/D) the situation seems to be opposite to the spring conditions. Positive EKE anomalies are found in the WGC upstream of Cape Desolation and in the separated branch along the 3000 m isobath. The LC and wide parts of the interior Labrador Sea show negative EKE anomalies. In contrast to the boundary currents around the Labrador Sea, the EKE signal in the North Atlantic Current (Northwest Corner) shows no pronounced seasonal cycle.

The evolution of EKE in time, per unit mass, is given by:

$$\begin{aligned} \frac{\partial}{\partial t} EKE &= T3 + T4 + \text{advect. terms} + \text{diffusion and dissipation}, \\ \text{with } T3 &= -g\overline{\rho'w'} \\ T4 &= \frac{1}{\rho_0} \left(\overline{u'u'} \frac{\partial \bar{u}}{\partial x} + \overline{u'v'} \left(\frac{\partial \bar{u}}{\partial x} + \frac{\partial \bar{v}}{\partial y} \right) + \overline{v'v'} \frac{\partial \bar{v}}{\partial y} \right), \end{aligned}$$

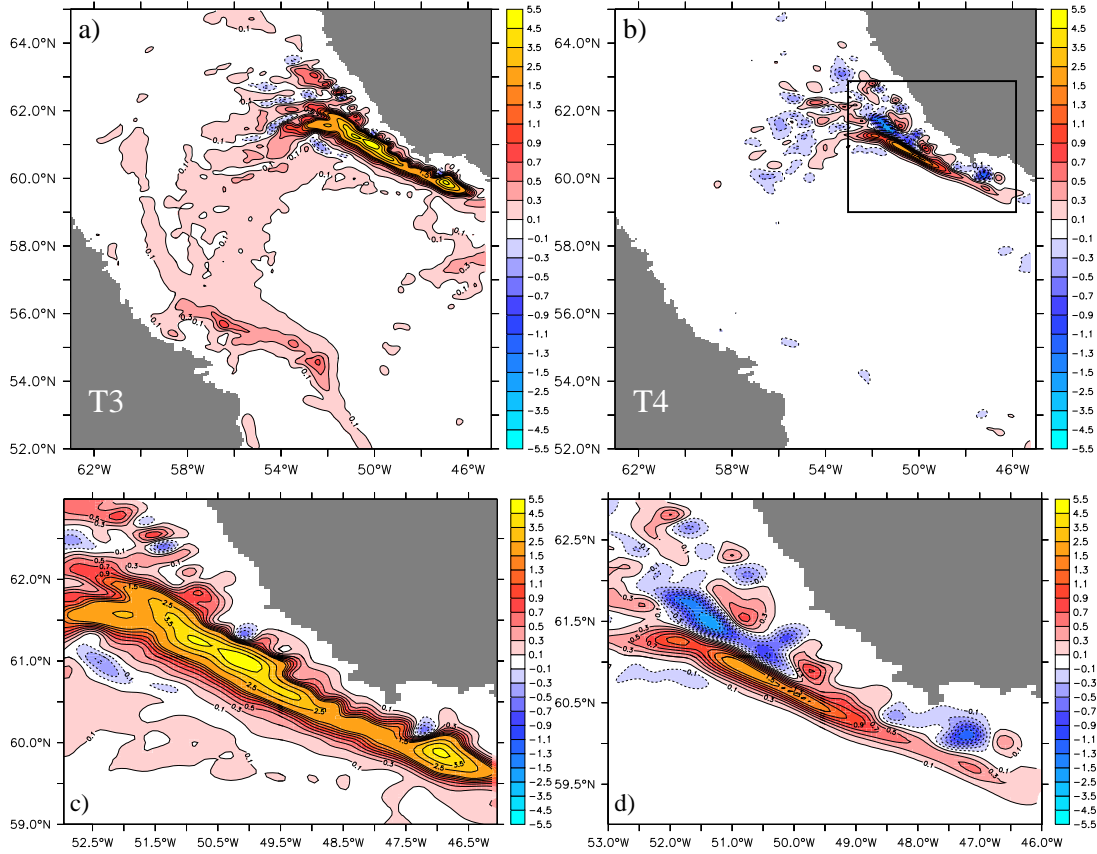


Figure 5.5: a) Vertically integrated transfer from eddy potential energy to eddy kinetic energy (**T3**). b) Vertically integrated transfer from mean kinetic energy to eddy kinetic energy (**T4**). A zoom into the Cape Desolation area (black contoured box) is given in c) for **T3** and d) for **T4**. Both transfer terms are averaged over the winter month (J/F/M) of 3 following years, $\times 10^5 m^3 s^{-3}$. The data have been horizontally smoothed (Hanning window over 7 grid boxes) prior the plotting.

where u , v , and w denote the velocity components, g the gravitational acceleration, and ρ_0 a reference (in situ) density. The energy transfer term **T4** represents the conversion of mean kinetic energy into eddy kinetic energy, which is associated (if positive) with barotropic instability. **T3** represents the conversion of eddy potential energy in eddy kinetic energy. A schematic view of the whole mean energy cycle (originally introduced by LORENZ (1955)) is shown in Fig. 5.4. If integrated over a closed domain, an energy component can change by the work of external forces (wind, buoyancy) or by diffusion/dissipation or by energy transfers due to interaction with other energy components (**T1-4**). The conversion of mean available potential energy into eddy available energy (**T2**) describes baroclinic instability. In this study we concentrate on the terms **T3** and **T4**, which directly affect the EKE. **T3** can be associated with baroclinic instability plus the effect of diffusion acting on the eddy potential energy. Note, that the energy budget cycle presented in Fig. 5.4 is only valid if integrating the terms over a closed oceanic basin, and

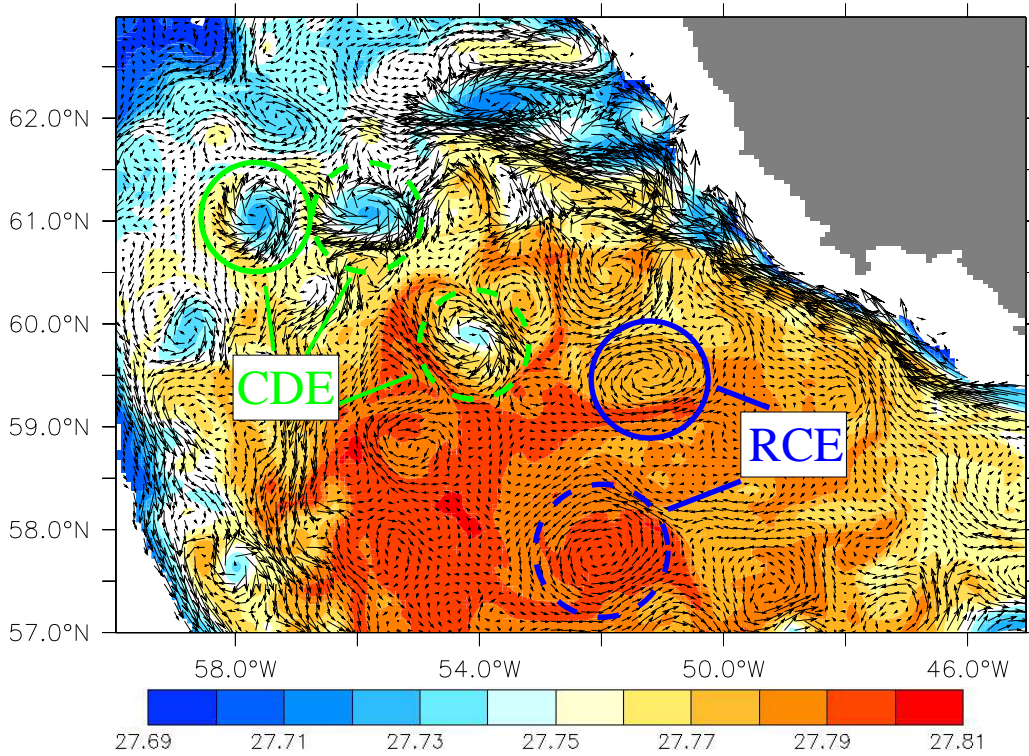


Figure 5.6: Snapshot of potential density ($kg\ m^{-3}$) and velocities at 600 m depth (4. April). A Cape Desolation eddy (CDE) shown in Fig. 5.7 is marked by a green circle. A rim current eddy (RCE) shown in Fig. 5.7 is marked by a blue circle. Further examples are marked by a dashed circle in the corresponding color.

that in our following regional study the transport of energy due to mean and eddy advection and due to divergence of mean and eddy pressure work are involved as well.

The vertically integrated transfer terms T3 and T4 for the winter months (J/F/M) are shown in Fig. 5.5. The conversion of eddy potential energy into EKE (T3) takes place in wide parts of the boundary currents, with a pronounced maximum in the area around Cape Desolation. A second local maximum is found in the LC at $\sim 54\text{--}56^\circ\text{N}$, which is related to the region of enhanced EKE in winter (Fig. 5.3a) and also east of the convection region at $\sim 58^\circ\text{N}$. Thus, these positive conversion rates are concentrated around the region of deep convection. This indicates a direct connection between the edge of convection and baroclinic instability.

The conversion of mean kinetic energy into EKE (T4) is concentrated in a narrow region at Cape Desolation. The negative values at $\sim 61.5^\circ\text{N}$, 51.5°W seem to compensate parts of the T3 term in this area. The strong eddy formation at Cape Desolation is obviously not a direct result of deep water formation but rather triggered by the local bathymetry, which explains the increase of barotropic (EDEN AND BÖNING, 2002) and baroclinic (BRACCO AND PEDLOSKY, 2004) instabilities. Figure 5.6 shows a snapshot of the potential density distribution and velocities at 600 m depth in early spring (4. April). At that time the deep convection phase

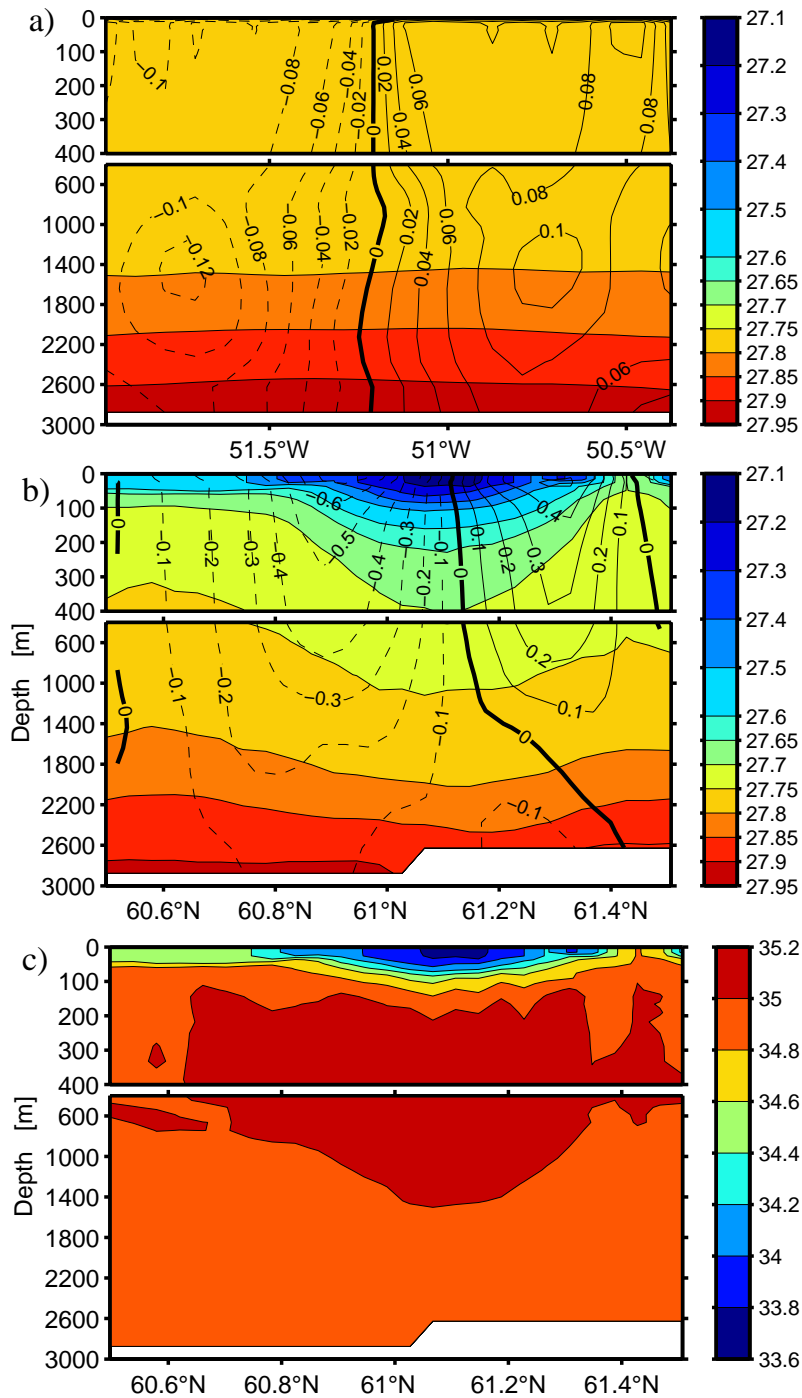


Figure 5.7: Potential density structure ($kg m^{-3}$) of a typical coherent a) "rim current eddy". and b) "Cape Desolation eddy". The contours show the velocity structure ($m s^{-1}$). c) Salinity structure (PSU) of the same Cape Desolation eddy. Note the split-up of the depth axis to highlight the top 400m. The locations of both eddies are marked in Fig. 5.6.

runs out and the restratification process is in progress. The dense mixed patch of newly formed Labrador Sea Water is dispersed by geostrophic eddies. At least two different "classes" of coherent eddies can be identified. The first and dominating class are the "Cape Desolation eddies" (CDE). The Cape Desolation eddies are in general anticyclones originating in the West Greenland Current where the 3000 m isobath branches off the continental slope. They can easily be identified by the low density compared to the surrounding waters. Their main pathway follows the "deep" Labrador Current along the 3000 m isobath, but sometimes they also reach the interior (e.g. at 60°N, 54°W). The second class are predominantly cyclonic "rim current eddies" (RCE). Only a limited amount of rim current eddies can be identified and they can be found only in the interior Labrador Sea. A few eddies, for example at 59°N, 55.5°W and 60.5°N, 52°W, are of ambiguous type, possibly the result of interaction between Cape Desolation- and rim current eddies. However, the spreading of the dense mixed patch suggests that all types of eddies are involved in the restratification process.

Figure 5.7 shows the differences in the vertical structure between both classes of eddies. The rim current eddy (Fig. 5.7a) contains water in the upper ~ 1600 m with densities corresponding to newly formed Labrador Sea Water. The low stratification is related to a near barotropic velocity structure with maximum velocities of $\sim 0.1 \text{ m s}^{-1}$. The density structure suggests that rim current eddies are formed during the deep water formation process. They can be found predominantly in the period March to June. The Cape Desolation eddy (Fig. 5.7b) on the other hand is well stratified. The velocities are surface intensified with maximum values of $\sim 0.6 \text{ m s}^{-1}$ leading to a more baroclinic structure. The salinity structure (Fig. 5.7c) of the same eddy shows a pronounced freshwater cap in the upper ~ 75 m. Obviously the water mass structure of these eddies originates from both parts of the WGC: the fresh and cold Arctic Water on the shelf and the warm and salty Irminger Water on the continental slope at depth between ~ 100 m and 1400 m (see also Fig. 4.9c). As a consequence of the stratification, the Cape Desolation eddies suppress deep convection (Fig. 4.6). PICKART ET AL. (2002) suggest that these eddies are responsible for the more stratified water column at the Greenland side along the WOCE AR7W section (Fig. 4.9b), which results in lower mixed layer depths in this region during convection.

In a five-year observational record from mooring data in the central Labrador Sea, LILLY ET AL. (2003) find both types of eddies (rim current eddies, Cape Desolation eddies) with very similar velocity structures compared to the model simulation. Their observations suggest that both types occur in the central Labrador Sea in roughly equal shares. In contrast to the simulation, the observed rim current eddies are without exception anticyclonic and have radii of only 5-10 km. In a further observational study STEFFEN AND D'ASARO (2004) found 4 cyclonic rim current eddies with radii ranging from 1 to 5 km. The horizontal resolution of "only" ~ 5 km in our model might explain the low number of coherent rim current eddies.

In an idealized process model, KATSMAN ET AL. (2004) demonstrate the importance of Cape Desolation eddies for a restratification in observed timescales. They

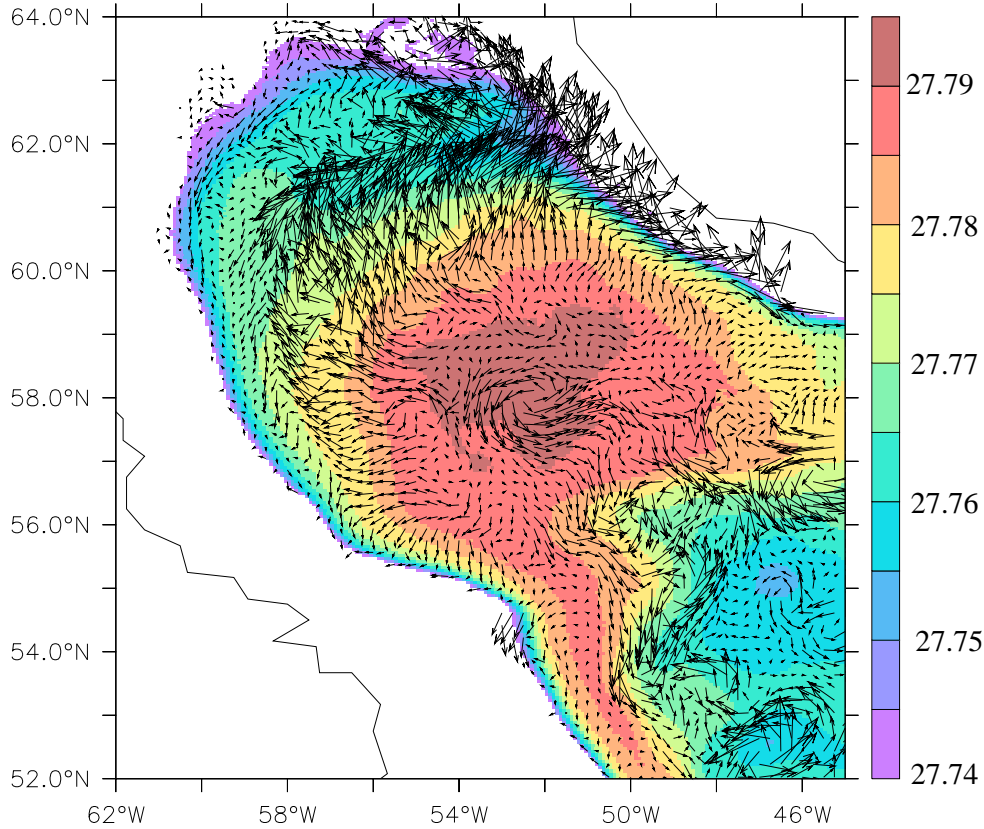


Figure 5.8: Annual mean potential density ($kg\ m^{-3}$) and horizontal eddy density flux at 1000 m depth

suggest that the heat transported by these eddies is sufficient to balance the net annual heat loss to the atmosphere.

Figure 5.8 shows the annual mean potential density and the horizontal eddy density flux $\overline{\rho' \mathbf{u}}$ at 1000 m depth. The eddy flux is generally downgradient leading to a transport of dense Labrador Sea Water towards the boundary current, which is consistent with the view of an "eddy-induced overturning circulation" (Fig. 5.1). The strength of the eddy density flux is not uniformly distributed around the region of deep convection, as often shown by simple process models. Maximum eddy fluxes occur in the region associated with the generation and pathway of Cape Desolation eddies. Obviously, in agreement with the study of KATSMAN ET AL. (2004), they contribute to a large part to the eddy-induced restratification. A second area of increased eddy density fluxes are found along the recirculation (section 4.3.1), where, however, a large part of the eddy fluxes show up as rotational fluxes, i.e. perpendicular to the density gradient, and therefore do not contribute to the restratification process.

In contrast to the eddy density flux at 1000 m depth, the near surface fluxes (not shown) are approximately one order of magnitude stronger but very noisy. Moreover they show dominantly rotational fluxes (along contours of σ_0). It is therefore difficult to identify a clear tendency near the surface that the eddies transport

buoyant low salinity water from the boundary currents towards the interior, which would be expected by the "classical view" of an eddy-induced overturning (Fig. 5.1) and the water mass characteristics of the dominating Cape Desolation eddies (Fig. 5.7b and c). As mentioned in the introduction of this chapter, the cyclonic boundary currents supply the heat which is needed to balance the annual surface heat loss and it is supposed that the exchange between the boundary currents and the interior is regulated by lateral eddy fluxes. The strongest lateral eddy fluxes in our simulation occur within and nearby the fluctuating "deep" Labrador Current, which makes it impossible to separate clearly between boundary currents and interior. For these reasons it is difficult to quantify the role of eddies in the heat budget of the Labrador Sea. However, more independent evidence for the important role of eddies in the restratification process is given in the following.

Time series of moorings in the Labrador Sea have revealed some important details of the evolution of the restratification process (LILLY ET AL., 1999). After winters of deep convection the newly formed Labrador Sea Water is found to be capped by a stratified layer of about 1000 m thickness in summer. The upper part of the water column becomes rapidly warmer and saltier. This generally occurs in late March, while the ocean is still cooled by the atmosphere, indicating that at least part of the restratification process is governed by oceanic processes. The fact that the restratification is rapid and deep reaching, points to a mechanism involving lateral eddy fluxes.

To assess the effect of "resolved" eddies on the restratification timescale, potential density sections through the region of deep convection at the beginning of the restratification process (April) and 6 months later (September) are shown in Fig. 5.9. The upper row shows the results from the eddy resolving experiment **SUB_NA12**. The remaining subfigures show the results from the eddy permitting experiment **NA3_open2**, which uses the eddy-induced tracer advection parameterization of (GENT AND MCWILLIAMS, 1990). The middle row represents the results from the low eddy-mixing case and the lower row shows the high eddy-mixing case introduced in chapter 3.2. Note the different density classes of newly formed Labrador Sea Water.

In April, the isopycnals are generally inclined towards the surface within the convective patch. Experiment **SUB_NA12** shows already some evidence for the beginning restratification process by a slightly flattening of the isopycnals. The fluctuation in the depths of some isopycnals (e.g. $\sigma_0 = 27.79$) points to eddy activity, which is in some respects in agreement with observations (LILLY ET AL., 1999). In September the isopycnals are flattened in all cases in the top ~ 400 m. Underneath the surface layer the isopycnals are predominantly flattened in the eddy resolving experiment (**SUB_NA12**), especially in the region of increased eddy fluxes (Fig. 5.8) on the western side. The eddy permitting model on the other hand shows underneath the top 400 m large amounts of unstratified Labrador Sea Water with vertical extensions very similar to the April conditions. This lack of intense restratification seems to be unaffected by the choice of the thickness diffusivity coefficient, which determines the strength of the parameterized eddy-mixing.

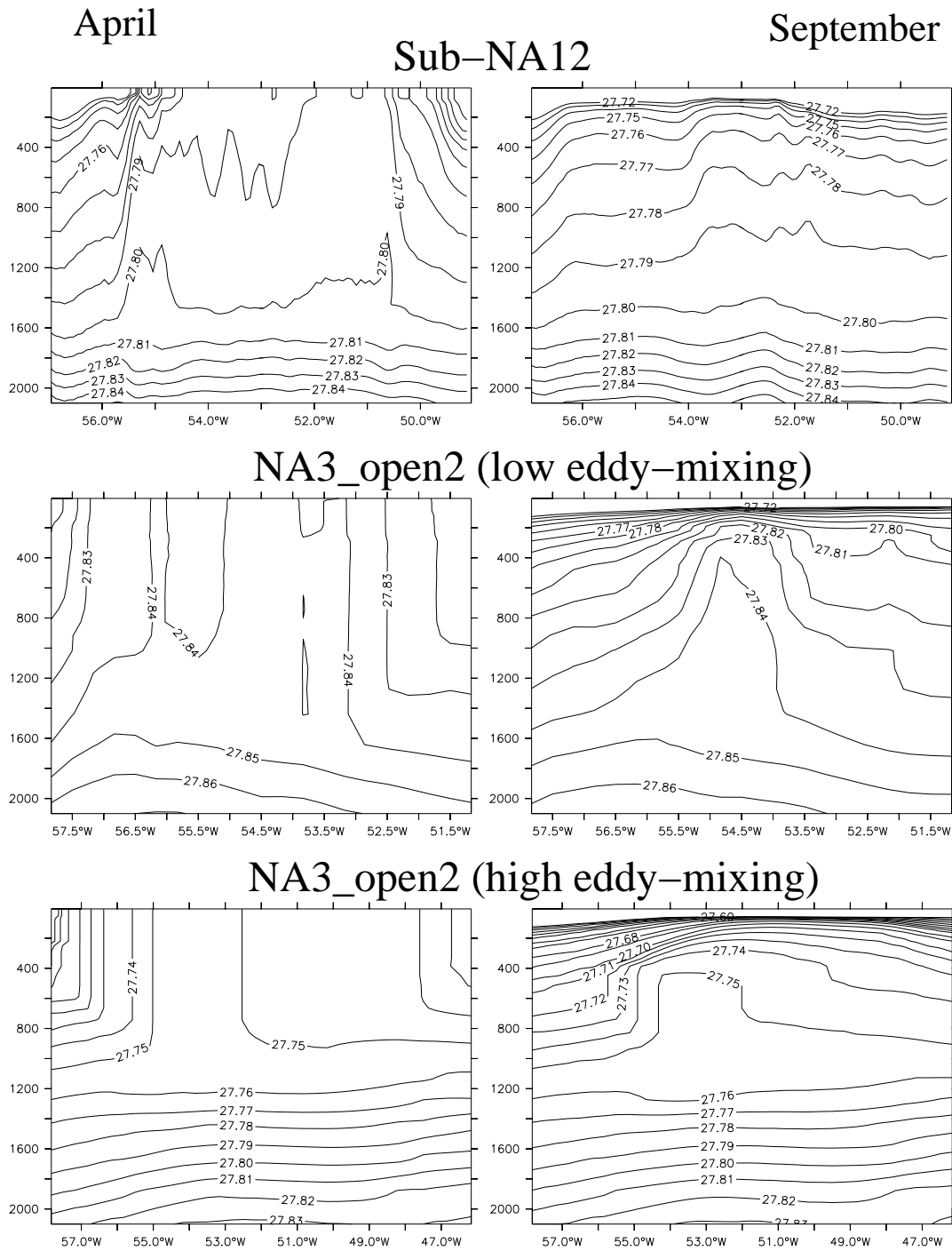


Figure 5.9: Monthly mean potential density (σ_0 in $(kg\ m^{-3})$) sections through the region of deep convection for the eddy resolving case **SUB_NA12**, the eddy permitting case **NA3_open2** with moderately parameterized eddy-mixing, and in the lower column the eddy permitting experiment **NA3_open2** with high parameterized eddy-mixing.

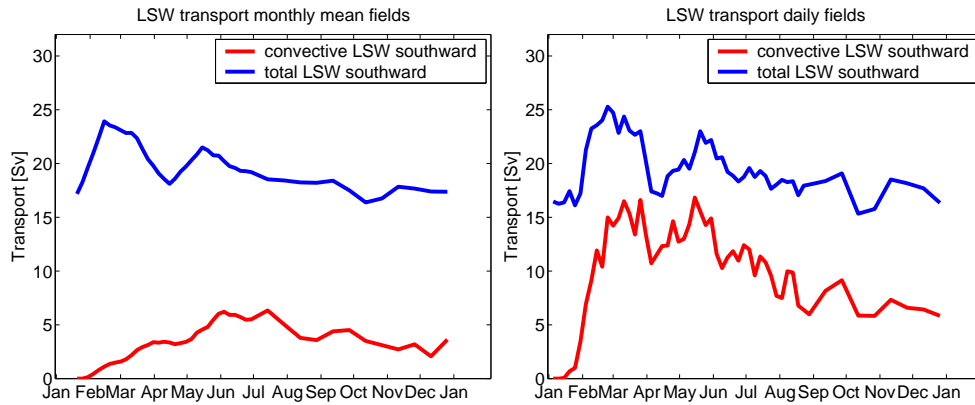


Figure 5.10: Transport (Sv) of Labrador Sea Water at $\sim 53^\circ\text{N}$ in the Labrador Current obtained from a Lagrangian drifter simulation (explanation in the text).

A possible explanation of this insensitivity of restratification to the value of thickness diffusion is the following: for large slopes of isopycnals the vertical component of the thickness diffusivity is getting too large and a tapering of the coefficient is needed (see chapter 2). This tapering reduces the parameterized eddy-mixing to zero in cases of vertical isopycnals, which results in an ineffective or at least delayed restratification of the Labrador Sea.

More evidence for an eddy-induced restratification is given by a float simulation based on velocity fields of **SUB_NA12** (P. Brandt et al. ¹). A Lagrangian drifter technique was employed to answer the question, when a particle that leaves the Labrador Sea via the Labrador Current was the last time in contact with the atmosphere, i.e. within the mixed layer. The starting point was a section through the Labrador Current at $\sim 53^\circ\text{N}$, and the drifters were calculated backward from this section to find the location and time of subduction. The calculation of a specific drifter stops if it enters the mixed layer. Moreover, each drifter represents a fraction of the transport in this section (BLANKE AND RAYNAUD, 1997). The calculation was performed for daily and monthly mean fields to elucidate the role of eddies in the export of newly formed Labrador Sea Water. Figure 5.10 shows the results for the Labrador Sea Water density range, where the blue curves denote the total LSW transport and the red curve denote the transport of newly ventilated LSW, i.e. water masses that originate from the mixed layer during the same year. The results obtained by the daily mean fields (including the eddies) indicate that a large part of the water exported within the Labrador Current was in contact with the atmosphere during the same year. This water is exported almost instantaneously with maximum values of ~ 16 Sv during March to May. Results obtained by using monthly mean fields (without eddies) indicate on the other hand that there is a strongly reduced export of newly formed LSW with maximum values in June to August of ~ 6 Sv pointing to the important role of eddies for the restratification.

¹Brandt, P., A. Funk, F. Schott, L. Czeschel and C. Eden (2004): Role of the eddy field for the export of newly formed Labrador Sea Water within the Labrador Current - Poster presentation at the CLIVAR-workshop on North Atlantic thermohaline circulation variability.

In this section it has been demonstrated that the restratification process is much more complex than often assumed in simple process models (for example the diapycnal mixing study in section 3.3). The dominant EKE signal in the Labrador Sea at Cape Desolation is obviously not a direct consequence of deep convection. Nevertheless, two different eddy "classes" can be identified: well stratified Cape Desolation eddies, which are responsible for the dominant EKE signal, and rather unstratified rim current eddies, which are obviously formed during the deep water formation process. Both types contribute to the restratification process and are important for a restratification in observed timescales.

5.3 Response to idealized forcing

General circulation models provide the possibility of exploring the response of the system to a sudden switch in either the heat flux or the wind stress. In such idealized experiments we switch immediately from the ECMWF-based forcing used in experiment **SUB_NA12** to a climatological forcing that correspond to a persistent high NAO(+3) or low NAO(-3) phase. In the case of **NAO_HEAT+3** (**NAO_HEAT-3**) only the heat flux is altered, which represents an increased (decreased) heat loss to the atmosphere in the Labrador Sea. In the case of **NAO_WIND+3** only the wind stress is increased (see chapter 2.3.1 for details). The aim of these idealized experiments is to separate mechanisms of interannual deep convection variability.

The impacts of the idealized forcing changes on the convection depths in the first March under NAO-like forcing are shown in Fig. 5.11. A relation between the heat loss to the atmosphere and the depths to which convection occurs is evident. The simulated annual heat loss averaged over the Labrador Sea (the black contoured box illustrated in Fig. 4.11) is 54.3 W m^{-2} in **NAO_HEAT-3**, 74.5 W m^{-2} in the reference case, 94.9 W m^{-2} in **NAO_HEAT+3**, and 69.85 W m^{-2} in **NAO_WIND+3**. The March mean mixed layer depths depend strongly, as expected, on the level of this heat loss. The maximum depths in **NAO_HEAT-3** is below ~ 1200 m, increasing up to values of ~ 2000 m in **NAO_HEAT+3**. The area in which deep convection occurs is very similar in both "heat flux changed" experiments, which indicates that the preconditioning is to a large extent independent from heat flux variability on this short timescales.

In **NAO_WIND+3** the maximum mixed layer depths of ~ 1600 m to 1800 m are similar to those in the reference experiment, but the area in which convection occurs is significantly decreased. This decrease is concentrated in the region of the significant EKE maximum (Fig. 5.2), which is associated with the separation of well stratified Cape Desolation eddies. The resulting Labrador Sea Water formation rates are 5.9 Sv in the reference case, 1.3 Sv in **NAO_HEAT-3**, 7.6 Sv in **NAO_HEAT+3**, and 4.6 Sv in **NAO_WIND+3** (calculated after the volumetric estimate presented in section 4.4). The "wind effect" appears therefore as a relevant factor decreasing deep water formation in the Labrador Sea. We show in the following that an increased wind stress leads to higher generation of well stratified Cape Desolation eddies, which are capable to suppress deep convection.

The response of the EKE distribution due to an increased wind stress and an increased heat loss are shown in Fig. 5.12. The basin-wide averaged EKE in the top 400 m increases to $48.5 \text{ cm}^2/\text{s}^2$ in **NAO_HEAT+3** compared to **SUB_NA12** ($43.1 \text{ cm}^2/\text{s}^2$). The thin green line denotes the 3000 m isobath, which is a rough separation between the "deep" Labrador Current and the interior. The deep Labrador Current corresponds approximately to the main path of the Cape Desolation eddies. In experiment **NAO_HEAT+3** an EKE increase shows up in the region of the Cape Desolation eddies as well as in the interior of the Labrador Sea, indicating that a combination of Cape Desolation- and rim current eddies are involved.

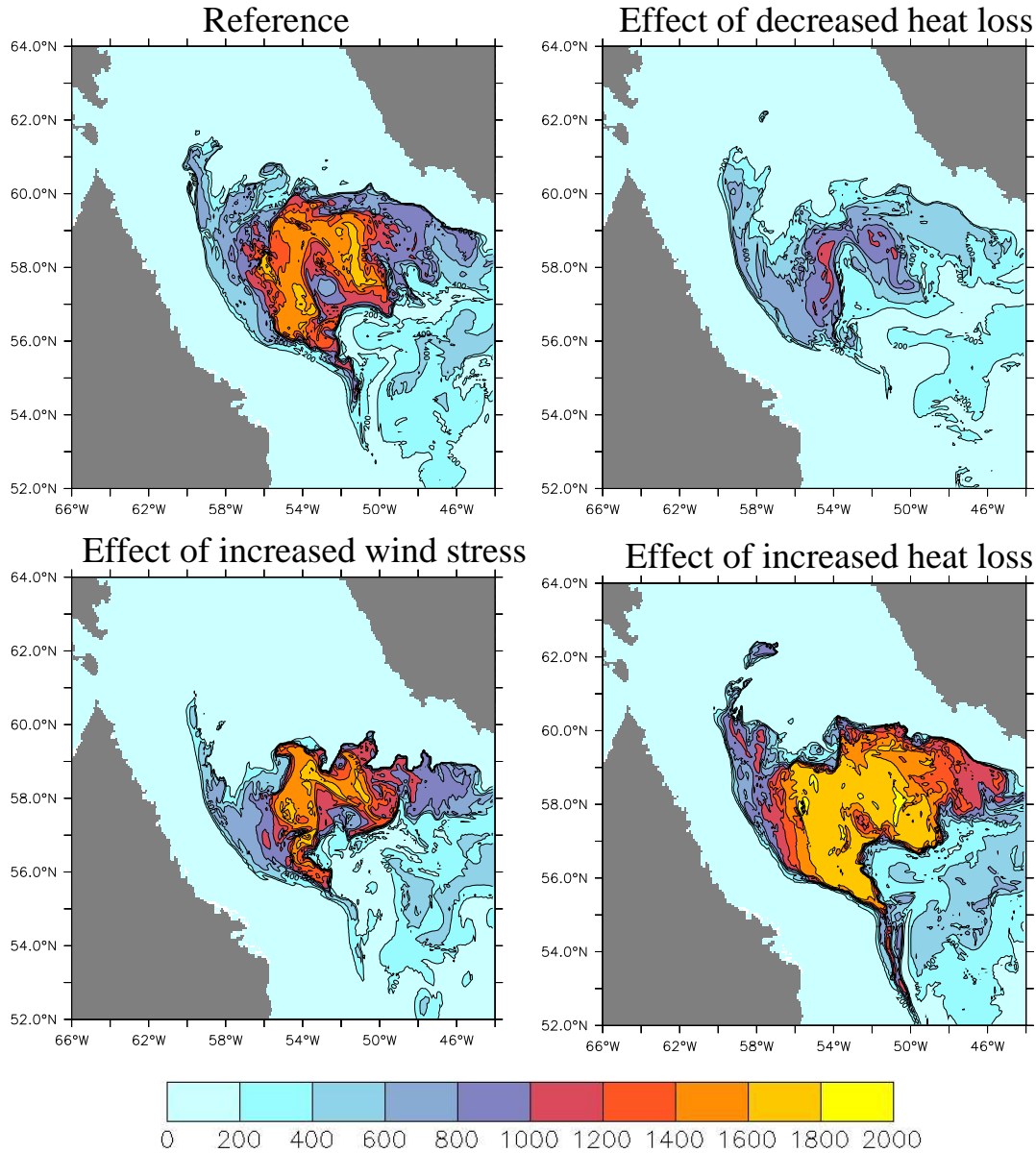


Figure 5.11: March mean mixed layer depths (m) in the first year after a sudden switch to NAO-like forcing. The effect of a decreased heat loss to the atmosphere is shown by **NAO_HEAT-3**, the effect of an increased heat loss by **NAO_HEAT+3**, and the effect of an increased wind stress by **NAO_WIND+3**.

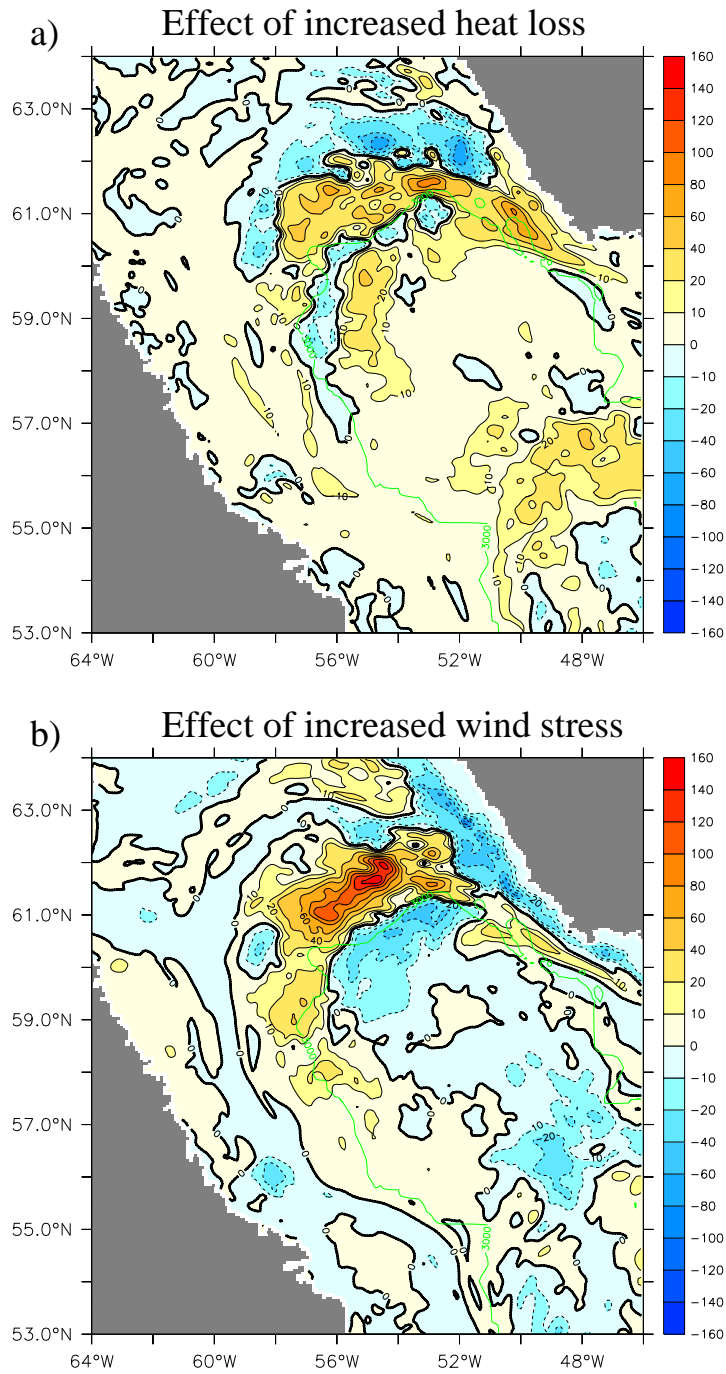


Figure 5.12: a) EKE response due to an increased heat loss (difference between **NAO_HEAT+3** - **SUB_NA12**). b) EKE response due to an increased wind stress (difference between **NAO_WIND+3** - **SUB_NA12**). The EKE (cm^2/s^2) is averaged over 3 years and over the top 400m in all experiments before plotting the difference. The thin green line denotes the 3000 m isobath.

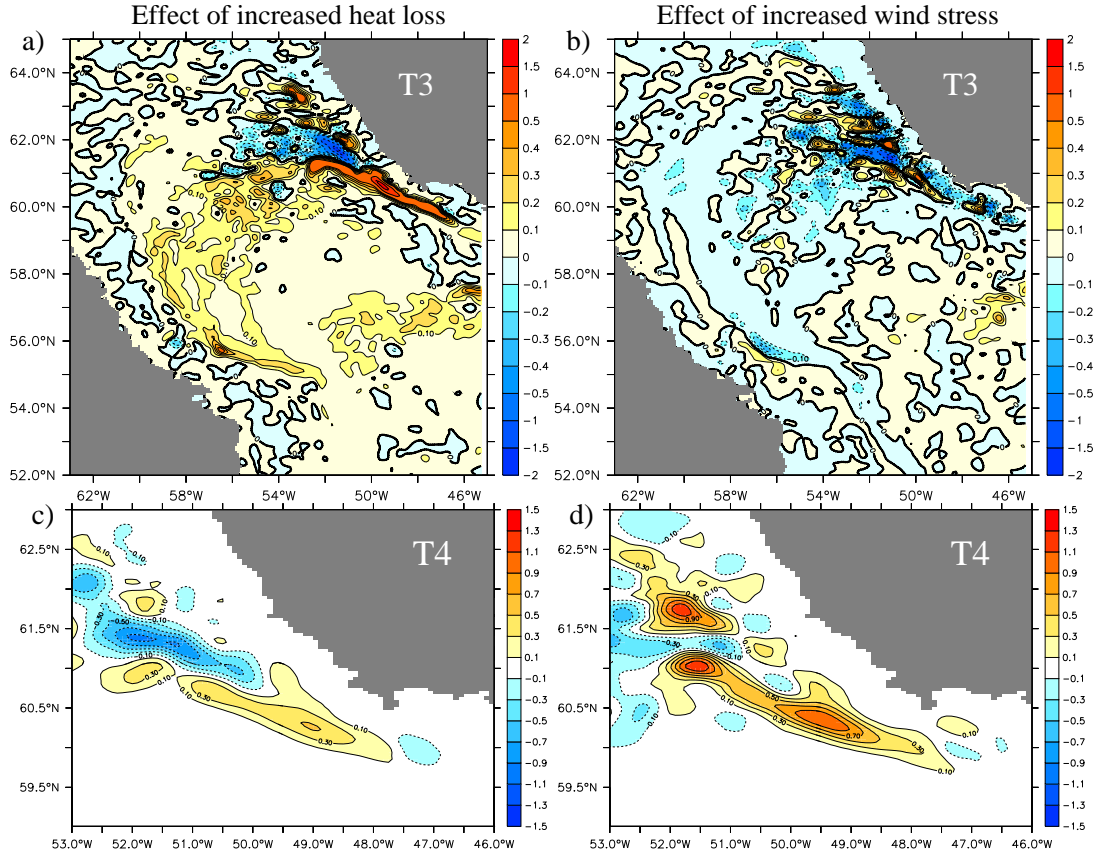


Figure 5.13: Vertical integrated transfer terms T3 and T4. The left column shows the effect of increased heat loss (**NAO_HEAT+3 - SUB_NA12**) for a) T3 and c) T4. The right column shows the effect of increased wind stress (**NAO_WIND+3 - SUB_NA12**) for b) T3 and d) T4. The T4 terms are shown in the Cape Desolation region marked in Fig. 5.5b. The transfer terms are plotted in the same way as in Fig. 5.5.

The EKE increase is concentrated in regions where the largest eddy density fluxes are found (Fig. 5.8).

In experiment **NAO_WIND+3** (Fig. 5.12b) the EKE is strongly enhanced in the formation region and along the pathway of the Cape Desolation eddies. The EKE increase of 40 to 160 cm^2/s^2 in this region is significantly higher than in **NAO_HEAT+3** (20 to 100 cm^2/s^2). An EKE decrease occurs at the baroclinic shelf part of the WGC and in parts of the interior of the Labrador Sea with, however, lower magnitudes compared to the increase at Cape Desolation. The basin-wide averaged EKE in the top 400 m increases to 44.6 cm^2/s^2 in **NAO_HEAT+3** compared to **SUB_NA12** (43.1 cm^2/s^2), whereby the increase in winter ($\sim 10\%$) is significantly higher than the annual mean. Overall, the EKE response in **NAO_WIND+3** indicates a relation between formation of Cape Desolation eddies and the wind stress.

Figure 5.13 shows the effects of the increased wind stress and heat loss on the

transfer terms T3 and T4 over the Labrador Sea. In **NAO_HEAT+3** the conversion of eddy available potential energy into EKE (T3) is increased approximately around the region of deep convection, which implies that at least parts of this eddy source are directly related to the enhanced deep water formation.

The effect of wind stress on T3 (Fig. 5.13b) is very noisy in the Cape Desolation area and weak in the remaining areas. The conversion of mean kinetic energy into EKE (T4), associated with barotropic instability, is less influenced by heat flux (Fig. 5.13c) changes but obviously increased in **NAO_WIND+3** (Fig. 5.13d). This points to an increase in the mean kinetic energy, i.e. a stronger West Greenland Current transport. (Note that all statements are related to interannual variability and possible interactions on longer timescales are not within the scope of this study.)

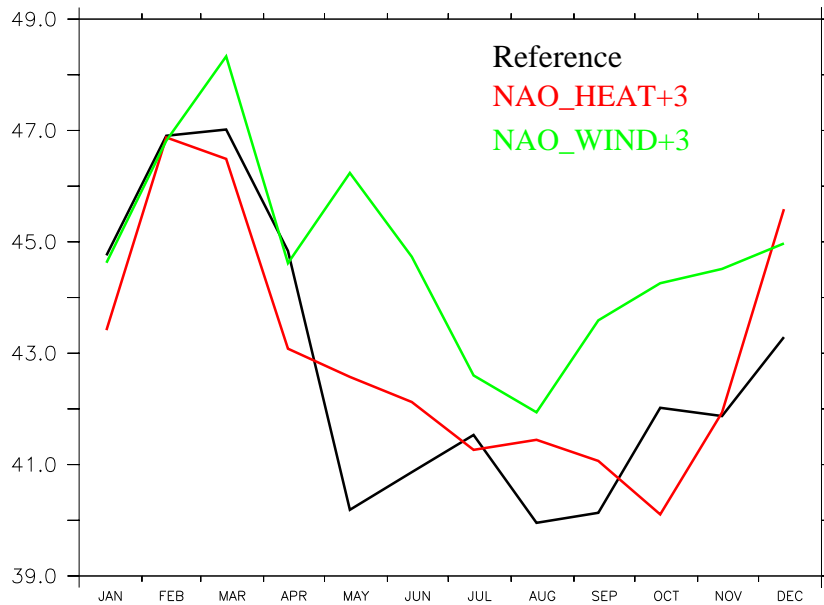


Figure 5.14: Annual cycle (averaged over 3 years) of the barotropic West Greenland Current transport (Sv) at 48°W for **SUB_NA-12** (black line), **NAO_HEAT+3** (red), and **NAO_WIND+3** (green).

An increased wind stress has consequences for the barotropic cyclonic circulation around the Labrador Sea. The annual cycle of the West Greenland Current transport at 48°W is shown in Fig. 5.14 for the three experiments. The WGC transport is characterized by a pronounced seasonal cycle with maximum transports in winter, which might explain large parts of the seasonal cycle in the EKE maximum at Cape Desolation (Fig. 5.3). The relation between the WGC transport and the EKE at Cape Desolation is also shown by EDEN AND BÖNING (2002). The WGC transport is significantly increased in **NAO_WIND+3** due to an increased wind stress, which leads to more conversion of mean kinetic energy to eddy kinetic energy (Fig. 5.13d) and therefore to enhanced EKE (Fig. 5.12b) at Cape Desolation. There are no significant differences between **NAO_HEAT+3** and **SUB_NA-12**, but the EKE is increased (at lower level) in the Cape Desolation area as well,

which indicates that the WGC transport might not be the only factor determining the EKE in that region.

The results of the idealized experiments are summarized in the following.

A positive NAO-phase leads to higher EKE in the Labrador Sea. The EKE increase is the combined effect of deeper convection (rim current eddies) and a higher generation of Cape Desolation eddies primarily as a consequence of a stronger boundary current transport. The enhanced heat loss to the atmosphere is related to stronger Labrador Sea Water formation. But a stronger heat loss to the atmosphere in positive NAO-phases is also associated with an increased wind stress. An increased wind stress on the other hand, leads to significantly lower formation of Labrador Sea Water due to stronger generation of Cape Desolation eddies. This might provide a possible explanation for the observed disagreement in specific years between strong heat loss and missing strong convection activity in the Labrador Sea.

5.4 Hindcasting the "WOCE" period 1989-1997

In order to assess the combined effect of wind stress and heat flux induced variability a hindcast of the period 1989-1997 using realistic forcing is made (see section 2.3.1 for details). This period allows for direct comparison to the large amount of observational data collected during the "World Ocean Circulation Experiment" (WOCE). In contrast to the previously discussed $1/12^\circ$ -model studies, the model domain in this experiment (**NA-12**) includes also the tropical and subtropical North Atlantic. The model was spun-up for ten years using the same climatological forcing as experiment **SUB_NA-12**. After the spin-up phase the characteristics of deep water formation in the Labrador Sea are very similar in both models. As an example, the annual mean temperature versus salinity distributions in the central Labrador Sea at 57°N , 54°W are shown in Fig. 5.15.

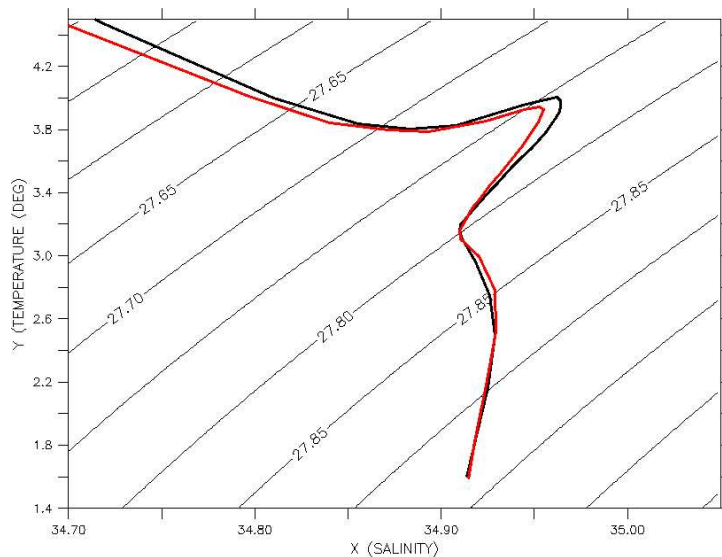


Figure 5.15: Annual mean of the temperature ($^\circ\text{C}$) vs. salinity (PSU) distribution in the central Labrador Sea (57°N , 54°W) after the 10 year spin-up phase for North Atlantic experiment **NA-12** (black) and the subpolar North Atlantic experiment **SUB_NA-12** (red).

After the spin-up phase the density range of Labrador Sea Water is, similar to the subpolar North Atlantic model, between 27.76 and 27.81 kg m^{-3} . In specific years during the period 1989-1997 parts of the Labrador Sea Water are formed beyond this density range. Figure 5.16 shows the annual Labrador Sea Water formation rates during this time period. The calculation follows the "volumetric estimate" method introduced in section 4.4 using a LSW density range from 27.75 to 27.82 kg m^{-3} . Also shown are the mean winter (D/J/F) heat flux anomalies over this period averaged over the Labrador Sea (in a box shown in Fig. 4.11). The LSW formation follows in general the trend of lower heat loss to the atmosphere during the 90s. Maximum LSW ($4.4 - 6 \text{ Sv}$) is formed in the years 1989 to 1991 and the minimum (2.2 Sv) is reached in year 1996. This general trend is in agreement with

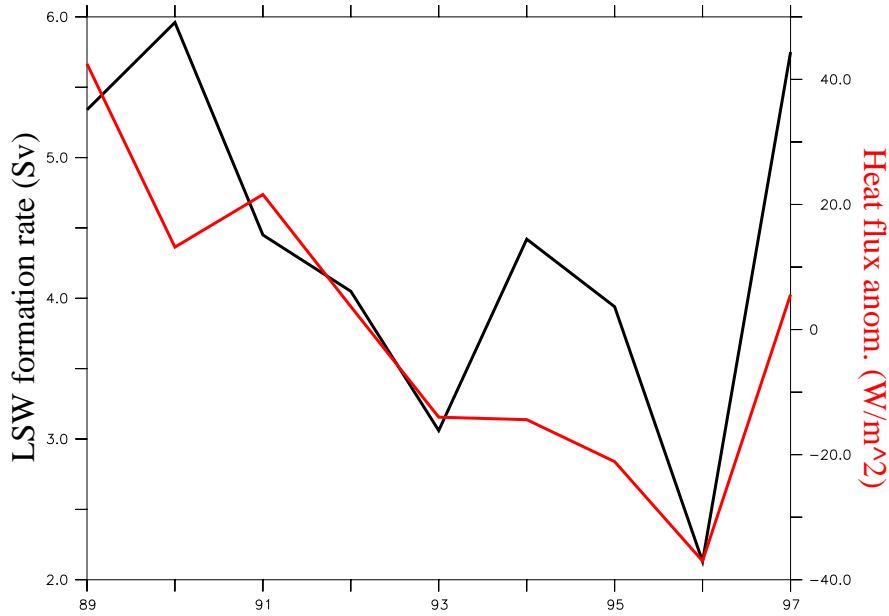


Figure 5.16: Labrador Sea Water formation rates (Sv) in black and simulated winter heat flux (heat loss to the atmosphere) anomalies ($W m^{-2}$) over the Labrador Sea in red.

several modeling and observational studies (e.g. LAZIER ET AL. (2002), BÖNING ET AL. (2003)). Several years indicate that the heat loss to the atmosphere is not the only factor which determines LSW formation (e.g. 1990). None of the years reach the maximum(minimum) values of 7.6(1.3) Sv of the idealized NAO+3(-3) experiments discussed in section 5.2, although the winter NAO-index ranges from 5.08 in 1989 to -3.78 in 1996 (extended version of HURRELL (1995)). This might be explained by the "wind effect" presented in the previous chapter, but no significant relation between EKE in the Labrador Sea, West Greenland Current transport, and NAO-Index can be found in this short time period (not shown). The time period is obviously too short for a statistical assessment.

Figure 5.17 shows the LSW formation rate anomalies of experiment **NA-12** and from an eddy permitting Atlantic FLAME model used in BEISMANN AND REDLER (2003). This eddy permitting model is very similar to our experiment **NA3_closed** with low thickness diffusivity (see section 3.2). Due to the salinification of the LSW the density range of LSW in this model is defined between 27.82 and 27.92 $kg m^{-3}$, which allows only a qualitative comparison. However, the mean formation rate averaged over this period is 5.5 Sv in the eddy permitting case and 5.3 Sv in **NA-12**. Both model solutions show in general the same trend of a decreasing LSW formation from the early 90s to 1996 and an increase in 1997. The amplitude is larger in the eddy permitting case, with LSW formation anomalies ranging from +3 Sv in 1989 to -3.6 Sv. The formation anomalies in **NA-12** on the other hand only range from +1.5 Sv in 1990 to -2.4 Sv in 1996. Thus convection in the eddy permitting model appears to be more sensitive to heat flux changes than **NA-12**. A summary of the collected hydrographic data during the 90s in the central

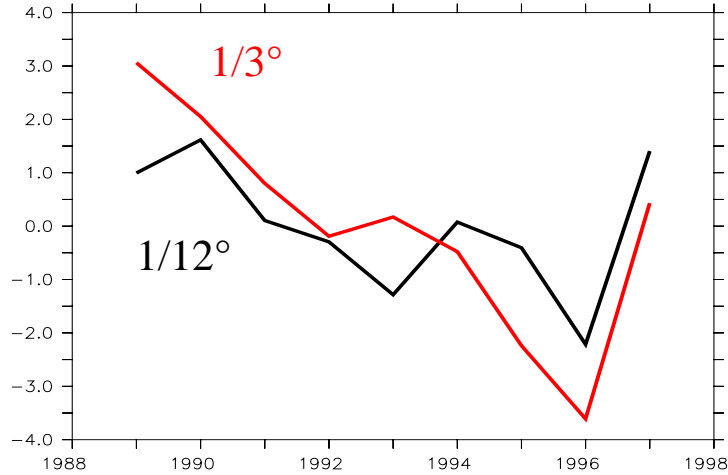


Figure 5.17: Labrador Sea Water formation rate anomalies (Sv) from the eddy resolving experiment **NA-12** and an eddy permitting FLAME Atlantic model (BEISMANN AND REDLER, 2003).

Labrador Sea is given by LAZIER ET AL. (2002). Figure 5.18 shows the summer to summer evolution of $\sigma_{1.5}$ (potential density relative to 1500 db) in the central Labrador Sea from the model compared to observations. The LSW is characterized by the low vertical density gradient between ~ 400 m and 2000m depth in both cases. As shown in section 4.3, the LSW in the model is slightly denser ($\sigma_{1.5}$: 34.7 - 34.66 $kg m^{-3}$) compared to the observations (34.70 - 34.62). Note that the observations in Fig. 5.18b encompass the period 1987 to 2001 while the model time series ends already in 1997. The vertical density gradient in the observations decreases during 1988 to 1994, corresponding to strong LSW formation during this period. The thickness between the 34.7 and 34.66 isopycnal of 400 m in 1988 increases to a value of 2300 m in 1994. After 1994 the thickness decreases again to a value of ~ 800 m in year 2000. Therefore the period after 1994 is named " multiyear restratification phase" (LAZIER ET AL., 2002). A similar tendency shows up as well in the model solution, but the temporal changes in the vertical density gradients are smaller than in the observations. In the model, the thickness between the isopycnals 34.74 and 34.72 of ~ 200 m in year 1989 increases to its maximum value of 800 m in year 1993 and decreases afterwards to ~ 380 m in year 1997.

It has been shown in the previous section that the wind stress has an impact on the generation of well stratified Cape Desolation eddies and thus on the region of deep convection. In specific years another wind induced effect causes Labrador Sea convection variability. Figure 5.19 shows the March mean mixed layer depths (a,c) and the near surface density (σ_0) at 20 m (b,d) for the years 1992 and 1989. Also shown are the wind stress (a,c) and the associated Ekman transport (b,d). The distribution of the mixed layer depths and the near surface density in the year 1992 is very similar to the climatological forced case. The Cape Desolation eddies transport low buoyant surface waters in the interior which suppress deep convection. In specific years however, like 1989, the wind stress is parallel to the

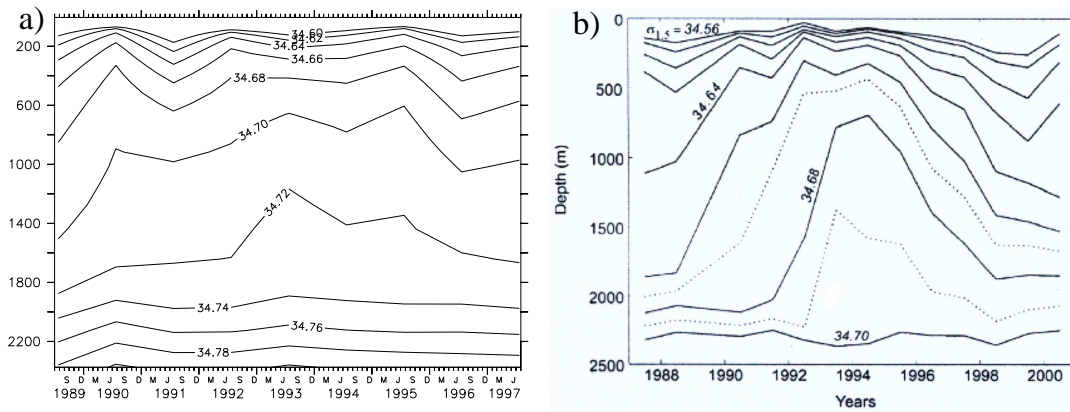


Figure 5.18: Summer to summer evolution of potential density (σ_{1500}) in the central Labrador Sea from a) experiment **NA-12** and b) observations (LAZIER ET AL., 2002). Note the somewhat longer time period in the observations.

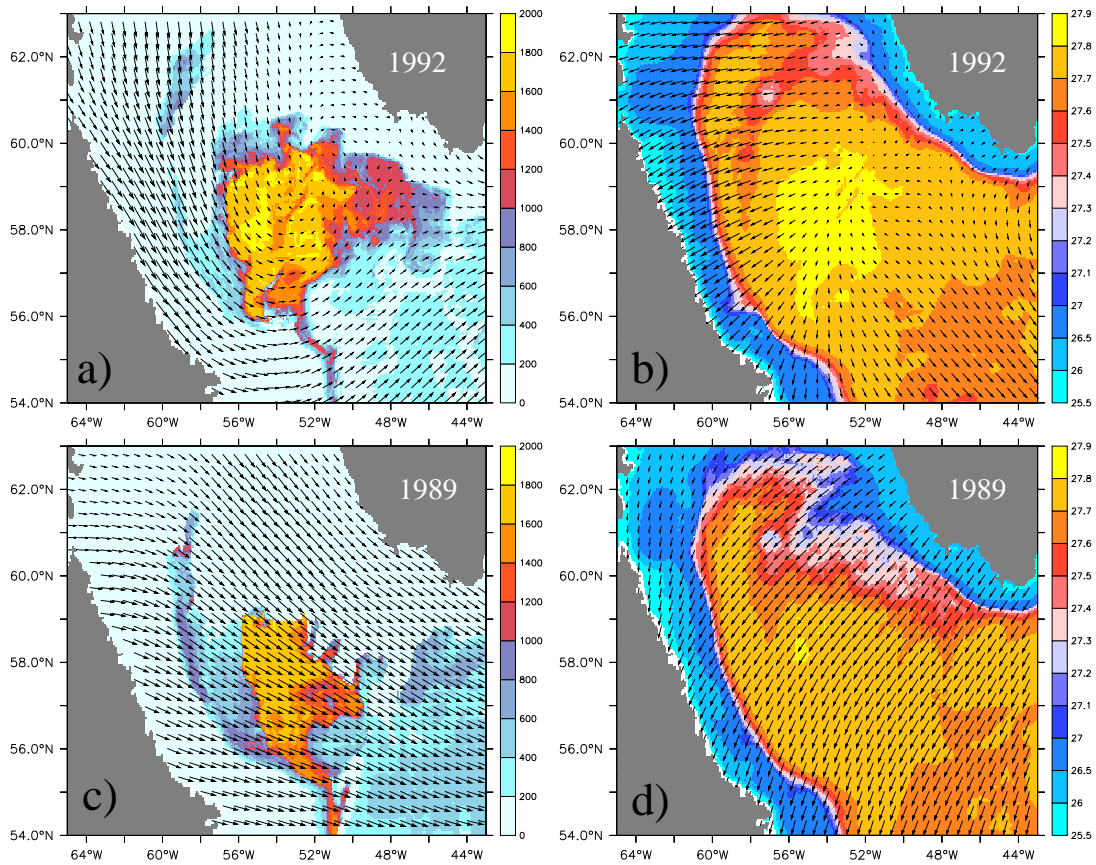


Figure 5.19: Mixed layer depth (m) and wind stress in a) 1992 and c) 1989. Potential density ($kg\ m^{-3}$) at 20 m depth and Ekman transports in b) 1992 and d) 1989 (in each case the March mean is shown).

coast west of Greenland and causes an anomalous Ekman transport of relatively fresh and cold shelf water off the coast towards the interior. This low buoyant water stratifies the water column on the Greenland side of the Labrador Sea. In such cases deep convection occurs only on the Labrador side.

The horizontal gradient in the mixed layer depths seems somewhat too strong on the edge between the low buoyant water and the dense convective patch. Probably this is a result of the monthly mean wind stress forcing in the model, which causes a nearly continuous Ekman freshwater transport during one month in such specific case. Daily varying wind stresses might help to overcome this problem. PICKART ET AL. (2002) suggest that the Cape Desolation eddies are responsible for the more stratified Greenland side along the WOCE AR7W section (see Figure 4.9); probably the Ekman transport is able to contribute to this stratification as well.

The mixed layer depth distributions in the years 1989 and 1992 are also a good example for the difference between water mass transformation into the Labrador Sea Water density class and ventilation of LSW (section 4.4). The region of enhanced mixed layer depths is obviously greater in year 1992 than in year 1989, which results in a higher ventilation of LSW in 1992, i.e. more water is marked with atmospheric impressed tracer properties (e.g. CFCs). But the LSW formation rate (Fig. 5.16) in year 1992 of 4 Sv is significantly lower than in 1989 (5.4 Sv). The reason is that in 1992 large amounts of dense LSW formed in the previous "strong" winters have remained in the interior Labrador Sea (Fig. 5.18).

It should be noted here that the model integration of **NA-12** is at the time of this writing no yet completed and further analysis of the hindcast simulation (year 1989 to 2004) will follow.

Chapter 6

Conclusions

The aim of this study is to develop a model of the general circulation in the North Atlantic Ocean without biases in water mass characteristics and deep convection in the Labrador Sea to investigate various key processes involved in the Labrador Sea Water formation and its interannual variability.

Ocean general circulation models (OGCMs) have tended to show large deficits in simulating observed characteristics of deep water formation in the Labrador Sea. The simulation of winter mixed layer depths is one of the most sensitive features of OGCMs. It was shown that different model architectures and also realizations performed with the same model but with different subgridscale parameterizations, lead to drastic differences in the horizontal extension and depth of the dense convective patch.

In a review of North Atlantic models ranging from eddy permitting to eddy resolving resolution, it has been shown that in most cases the simulated mixed layer depth is too deep and the convection area is too large in comparison with observations. All models show an unrealistic drift in the water mass properties towards higher salinities in the subpolar gyre. The drift has dramatic consequences for the density range of Labrador Sea Water which, in many cases, begins to overlap with the densities of the overflows from the Nordic Seas. This blurred distinction between these water masses leads to a distortion in the spatial patterns of the LSW spreading and associated distribution of dissolved trace gases such as CFCs (BÖNING ET AL., 2003).

Freshwater budget in the Labrador Sea

The salinification in the Labrador Sea in the model solutions suggests, that either a freshwater source is underestimated or a lateral transport of water with high salinity is overestimated. TREGUIER ET AL. (2004) demonstrate that after starting a model from climatological state, the salinity anomalies first appear in the East- and West Greenland Current. Consequently the salinification of the Labrador Sea originates from an unrealistic low freshwater input from the Irminger Sea. The

advective freshwater input from the Irminger Sea is the combined result of the "salty" Irminger Current and the "fresh" East Greenland Current.

Previous model studies typically used a closed boundary near 70° where temperature and salinity are restored to climatological data in a buffer zone. In an eddy permitting ($1/3^\circ$) FLAME model of the North Atlantic it has been demonstrated that the freshwater exchange with the Nordic Seas is underestimated in such a configuration. A too large fraction of the salty water within the North Atlantic Current feeds the Irminger Current instead of leaving the subpolar gyre through the Nordic Sea. The East Greenland Current on the other hand, which transports fresh and cold Arctic Water through the Labrador Sea, is underrepresented.

To allow for a more effective freshwater with the Nordic Seas, an open boundary formulation following the approach of STEVENS (1991) was implemented in the eddy permitting model. The prescribed streamfunction is taken from a non-eddy resolving Arctic model developed at the Alfred-Wegener-Institut at Bremerhaven (R. Gerdes and J. Brauch, pers. comm.) while the water mass properties of inflowing water are still obtained from climatological data. The model with such an open boundary formulation shows a drastic freshening (up to 0.2 PSU) of the boundary currents around the Labrador Sea compared to the "closed boundary" case, but the effect of increased freshwater import is absent in the interior Labrador Sea.

Several studies highlight the role of eddies for the exchange between boundary currents and the interior Labrador Sea. The eddy permitting model resolves the scale of the energetic eddies in the subtropical gyre, but obviously fails in higher latitudes (e.g. the Labrador Sea). Therefore the effect of eddies on tracers has to be parameterized. The eddy permitting models include the widely used parameterization after GENT AND MCWILLIAMS (1990). The strength of the parameterized eddy-mixing is given by the thickness diffusivity coefficient. In eddy permitting models a moderate value of $200 \text{ m}^2 \text{ s}^{-1}$ is usually adopted (BÖNING ET AL. (2003), BEISMANN AND REDLER (2003)). This value is also used in the previously mentioned experiments of this study.

In order to assess the effect of eddy parameterization, we rerun these experiments using a thickness diffusivity coefficient of $2000 \text{ m}^2 \text{ s}^{-1}$ which is a common value in non-eddy resolving models. In contrast to the low "eddy-mixing" case, the freshwater signal due to an open boundary in the high "eddy-mixing" case reaches now the interior Labrador Sea. Higher eddy-mixing enhances the communication between the boundary currents and the interior of the Labrador Sea with strong consequences for the formation of Labrador Sea Water. A comparison between observations and the results of the eddy permitting experiments clearly reveals that a combination of an open boundary and an adequate representation of the eddies is needed to simulate observed water mass properties.

A problem of using a high thickness diffusion coefficient in the whole model domain are drastic changes in the large circulation (e.g. a very broad Gulf Stream), clearly undesirable in eddy permitting models. The results emphasize the need for a laterally varying parameterization of sub-grid eddy mixing, especially in eddy permitting models.

The role of numerical diapycnal mixing

A simple channel model ($1/12^\circ$) is used to simulate the restratification process after deep convection and to assess the role of diapycnal mixing. The channel is initialized with an analytical temperature field corresponding to an idealized section through the Labrador Sea after deep convection, i.e. a homogeneous patch of dense convective water is placed at one side of the channel in a stratified environment. A series of experiments are discussed differing in the horizontal diffusivity coefficient, whereby a higher coefficient increases the effective diapycnal mixing.

All experiments show the same restratification mechanism as described by JONES AND MARSHALL (1997). A zonal current ("rim current") arises along the front separating the stratified water from the well mixed patch. Subsequently the rim current becomes unstable and the resulting geostrophic eddies disperse the dense patch over the whole domain. The same process can be also described as a transformation of available potential energy (APE). In an purely adiabatic ocean the entire APE is transformed into eddy potential energy and into eddy kinetic energy, where it is finally lost.

The remarkable result in the experiments is the difference in the loss of potential energy (PE) after the restratification phase. The loss of PE is controlled by the amount of diapycnal mixing, i.e. lower diapycnal mixing leads to an increased PE loss. As a consequence hereof, the eddy kinetic energy is increased in case of lower diapycnal mixing. The different PE loss has strong consequences for the stratification of the water column and thus to the preconditioning for the subsequent winter, i.e. with higher diapycnal mixing the water column becomes less stratified.

The lateral mixing of two channel experiments corresponds to two different setups of the basin-scale FLAME $1/12^\circ$ -models, and help to explain their strong differences in the mean March mixed layer depths of ~ 1400 m. A simple 1-dimensional mixed layer model is used to study the effect of diapycnal mixing on the convection depth in the following winter in the corresponding channel experiments. Taking the basinwide averaged density profiles after one year of both channel experiments and applying a cooling at the surface of 200 W/m^2 , we obtain a noticeable difference of ~ 200 m. This difference in the mixed layer depth is reached after only one convective cycle and the effect may accumulate in the following years.

It is supposed that the diapycnal mixing in OGCMs is much higher than suggested by observational estimates. The connection between numerical diapycnal mixing and mixed layer depth may help to explain the large differences in general ocean circulation models.

An improved eddy resolving model

An improved eddy resolving model is designed based on the previously obtained results: 1) the northern open boundary condition successfully used in the eddy permitting model is implemented to improve the advective part of the freshwater budget, and thereby to prevent a salinification of the subpolar North Atlantic; 2)

the numerical diapycnal mixing is minimized by using isopycnic diffusion together with only a small horizontal background diffusion.

The improved model is capable to simulate the characteristics of the subpolar gyre in good agreement with observations. The area of deep convection is concentrated on the Canadian side of the interior Labrador Sea and is constrained by the West Greenland Current, Labrador Current, separated eddies at Cape Desolation, and an anticyclonic recirculation. The maximum mixed layer depths are between 1600 m and 1800 m, using the same forcing as in DYNAMO GROUP (1997). The Labrador Sea Water encompasses a density range between 27.76 and 27.81 $kg\ m^{-3}$, which is still slightly denser than typically used in observational studies (27.74 and 27.80), but significantly improved compared to earlier eddy resolving FLAME-models (27.81 - 27.84). The annual Labrador Sea Water formation rate is ~ 6 Sv, which is in the range of observational estimates of 2 - 12 Sv (SMETHIE AND FINE (2001), RHEIN ET AL. (2002)).

Two noticeable differences between observations and the model have to be mentioned: (1) the model overestimates the salinities in the warm and salty parts of the West Greenland Current and Labrador Current; 2) the anticyclonic recirculation in the Labrador Sea extends northeastward only to about 57°N, 52°W before it turns into the Irminger Sea, whereas observations suggest that it may reach 59°N, 55°W.

Possible causes for the slight differences compared to observations are that the model is not coupled to an realistic ice model nor uses evaporation, precipitation, and river runoff data for the formulation of freshwater fluxes. Furthermore freshwater fluxes from the Baffin Bay are ignored due to a closed boundary in the Davis Strait at 66°N. However, the localization of deep convection and the water mass properties of Labrador Sea Water are remarkably improved compared to previous model solutions, so that the model can be used with more confidence to assess mechanisms of deep convection and its variability.

Mesoscale variability

The heat which is needed to balance the annual heat surface heat loss over the Labrador Sea, is supplied to the region by the boundary currents that flow cyclonically around the convection interior (GASCARD AND CLARKE, 1983). Several studies, based on simple process models, highlight that the exchange between the boundary currents and the interior is regulated by lateral eddy fluxes (e.g. JONES AND MARSHALL (1997), KATSMAN ET AL. (2004), SPALL (2004)).

The dominant eddy kinetic energy (EKE) signal in the Labrador Sea is found in the vicinity of Cape Desolation (e.g. STAMMER AND WUNSCH (1999)). This EKE maximum is located in the region where one part of the West Greenland Current branches off the continental slope following roughly the 3000 m isobath. The model provides annual mean EKE values of more than 600 $cm^2\ s^{-2}$ which is in agreement with observational estimates from satellite data of 600 to 800 $cm^2\ s^{-2}$ (BRANDT ET AL., 2004). The simulated EKE in the boundary currents around the Labrador

Sea is characterized by a pronounced seasonal cycle. The highest eddy activity occurs in winter with an increase of $\sim 25\%$ in the area of Cape Desolation. In spring the EKE remains high in the Labrador Current and around the region of deep convection, which might be an indication for the restratification process. The summer is, in general, characterized by the lowest eddy-activity.

An inspection of the energy transfer terms suggests that conversion of eddy available potential energy into EKE (baroclinic instability) occurs approximately around the region of deep convection, with a pronounced maximum at Cape Desolation. Conversion of mean kinetic energy into EKE (barotropic instability) is concentrated in a narrow region at Cape Desolation. EDEN AND BÖNING (2002) demonstrate the connection between the West Greenland Current transport and the EKE maximum at Cape Desolation, which are both characterized by the same seasonal cycle. The dominant EKE maximum at Cape Desolation is obviously not a direct consequence of deep convection but rather triggered by the local bathymetry, which explain an increase of barotropic (EDEN AND BÖNING, 2002) and baroclinic (BRACCO AND PEDLOSKY, 2004) instabilities in this region.

Associated with the EKE maximum at Cape Desolation is the generation of well stratified "Cape Desolation eddies". Their water mass structure originates from both parts of the West Greenland Current: the fresh and cold Arctic Water on the shelf and the warm and salty Irminger Water at depths between ~ 100 and 1400 m. As a consequence of their stratification, the Cape Desolation eddies suppress deep convection along their main pathway, which follows roughly the 3000 m isobath. A second type of eddies is found, which are predominantly cyclonic. These "rim current eddies" are formed during the convection process and contain newly formed Labrador Sea Water in the upper ~ 600 m. They can be found predominantly in the period March to June and in the interior of the Labrador Sea only. Both types of eddies are also found in observational studies (LILLY ET AL. (2003), STEFFEN AND D'ASARO (2004)). The observed radii of rim current eddies (1 to 10 km) might explain the limited number and larger extent of rim current eddies found in the model (horizontal grid resolution of ~ 5 km). Furthermore, some eddies of ambiguous type are found. All types of eddies appear to be involved in the restratification process.

In contrast to the "classical view" of a homogeneous eddy-induced restratification around the convective patch, the eddy density fluxes at 1000 m in the model are clearly dominated by the Cape Desolation eddies. It is supposed that the lateral eddy fluxes regulate the exchange between boundary currents and the interior. Accordingly, the strongest eddy fluxes in the model occur in or nearby the fluctuating "deep" Labrador Current, which branches off the Greenland coast and follows roughly the 3000 m isobath. Because of the almost disappearing distinction between boundary currents and interior, a quantification of the role of eddies for the restratification and heat budget of the Labrador Sea is difficult.

A comparison between the eddy resolving and the eddy permitting model reveals the importance of resolved eddies for a restratification on observed timescales. Irrespective of the strength of the parameterized eddy-mixing, the eddy permitting

model shows large volumes of unstratified Labrador Sea Water in late summer. This points to a possible weakness of the GENT AND MCWILLIAMS (1990) parameterization as implemented in the model, because of the tapering in case of strong isopycnal slopes. A Lagrangian drifter analysis (P. Brandt, pers. comm.) gives further evidence for the importance of eddies in the restratification and its timescale.

Interannual variability

To explore the mechanism of interannual convection variability some idealized response experiments are performed. The anomalous forcing in these experiments corresponds to persistent high or low NAO situations. This forcing was chosen since the NAO is the most important driver of interannual variability in the North Atlantic Ocean (DICKSON ET AL., 1996).

A positive NAO-phase leads to higher EKE in the Labrador Sea. The EKE increases as a combined effect of deeper convection (rim current eddies) and higher generation of Cape Desolation eddies, primarily as a consequence of a stronger boundary current transport. An enhanced heat loss to the atmosphere is related to stronger Labrador Sea Water formation, but stronger heat loss to the atmosphere in positive NAO-phases is also associated with increased wind stress. Increased wind stress on the other hand, leads to significantly lower formation of Labrador Sea Water due to the stronger generation of Cape Desolation eddies. This might provide a possible explanation for the observed disagreement in specific years between strong heat loss and missing strong convection activity in the Labrador Sea.

A further wind induced mechanism of interannual convection variability is unveiled in a hindcast model simulation of the "WOCE" period 1998-1997. In specific years, like 1989, the wind stress blows parallel to the coast west of Greenland and causes an anomalous Ekman transport of relatively fresh and cold shelf water off the coast towards the interior. This low buoyant water stratifies the water column on the Greenland side of the Labrador Sea. In such cases deep convection occurs only on the Labrador side.

Caveats and outlook

Although the model seems to be resolving a significant part of the mesoscale eddy spectrum in the Labrador Sea, there are observational hints that even smaller scale features may play an important role as; e.g., small scale rim current eddies with a scale of 1 to 10 km are clearly unresolved by our model. Thus modeling the Labrador Sea may demand even higher resolution.

This study does not include the impacts of variability of surface freshwater fluxes or freshwater export from the Arctic (Davis Strait, Fram Strait) on convection and water mass characteristics, these sources also need to be considered in further studies.

The improved eddy resolving model can now be used for a hindcast of the anthropogenic CO₂ uptake and transport of the North Atlantic over the last century to assess the observational estimates by SABINE ET AL. (2004). However, such a hindcast simulation will still challenge present computer resources.

Bibliography

- ARAKAWA, A. and V. R. LAMB, 1977: Computational design of the basic dynamical processes of the UCLA General Circulation Model. *Methods in Comput. Phys.*, p. 173–265.
- BARNIER, B., L. SIEFRIDT and P. MARCHESIELLO, 1995: Thermal forcing for a global ocean circulation model using a three-year climatology of ECMWF analyses. *J. Mar. Systems*, **6**, p. 363–380.
- BECKMANN, A. and R. DÖSCHER, 1997: A method for improved representation of dense water spreading over topography in geopotential-coordinate models. *J. Phys. Oceanogr.*, **27**, p. 581–591.
- BEISMANN, J.-O. and R. REDLER, 2003: Model simulations of CFC uptake in North Atlantic Deep Water: Effects of parameterizations and grid resolution. *J. Geophys. Res.*, **108**, p. 3159–3176.
- BLANKE, B. and S. RAYNAUD, 1997: Kinematics of the Pacific Equatorial Undercurrent: An Eulerian and Lagrangian approach from GCM results. *J. Phys. Oceanogr.*, **27**, p. 1038–1053.
- BÖNING, C. W. and R. BUDICH, 1992: Eddy dynamics in a primitive equation model: sensitivity to horizontal resolution and friction. *J. Phys. Oceanogr.*, **22**, p. 361–381.
- BÖNING, C. W., W. R. HOLLAND, F. O. BRYAN, G. DANABASOGLU and J. C. MCWILLIAMS, 1995: An overlooked problem in model simulations of the thermohaline circulation and heat transport in the Atlantic Ocean. *J. Climate*, **8**, p. 515–523.
- BÖNING, C. W., M. RHEIN, J. DENG and C. DOROW, 2003: Modeling CFC inventories and formation rates of Labrador Sea Water. *Geophys. Res. Letters*, **30**, p. doi:10.1029/2002GL014855.
- BOYER, T. P. and S. LEVITUS, 1997: Objective analyses of temperature and salinity for the world ocean on a 1/4 degree grid. Technical Report, NOAA Atlas NESDIS 11, U.S. Gov. Printing Office, Washington, D.C.
- BRACCO, A. and J. PEDLOSKY, 2004: Vortex generation by topography in locally unstable baroclinic flows. *J. Phys. Oceanogr.*, **33**, p. 207–219.

- BRANDT, P., F. A. SCHOTT, A. FUNK and C. S. MARTINS, 2004: Seasonal to interannual variability of the eddy field in the Labrador Sea from Satellite Altimetry. *J. Geophys. Res.*, **109**, p. doi:10.1029/2002JC001551.
- BRYAN, F. O., 1987: Parameter sensitivity of primitive equation ocean general circulation models. *J. Phys. Oceanogr.*, **17**, p. 970–985.
- BRYAN, K., 1969: A numerical method for the study of the circulation of the world ocean. *J. Comput. Phys.*, **3**, p. 347–376.
- CANUTO, V. M., A. HOWARD, P. HOGAN, Y. CHENG, M. S. DUBOVIKOV and L. M. MONTENEGRO, 2004: Modeling ocean deep convection. *Ocean Model.*, **7**, p. 75–95.
- CLARKE, R. A., 1984: Transport through the Cape Farewell-Flemish Cap section. *Rapp. P.-v. Reun. Cons. Int. Explor. Mer*, **185**, p. 120–130.
- CLARKE, R. A. and J.-C. GASCARD, 1983: The formation of Labrador Sea Water. Part I: Large-scale processes. *J. Phys. Oceanogr.*, **13**, p. 1764–1778.
- COX, M. D., 1985: An eddy resolving numerical model of the ventilated thermocline. *J. Phys. Oceanogr.*, **15**, p. 1312–1324.
- COX, M. D., 1987: Isopycnal diffusion in a z-coordinate model. *Ocean Model.*, **74**, p. 1–5.
- CUMMINS, P. F., G. HOLLOWAY and A. E. GARGETT, 1990: Sensitivity of the GFDL ocean general circulation model to a parameterization of vertical diffusion. *J. Phys. Oceanogr.*, **20**, p. 817–830.
- CUNY, J., P. B. RHINES and P. P. N. ABD S. BACON, 2002: Labrador Sea boundary currents and the fate of the Irminger Sea Water. *J. Phys. Oceanogr.*, **32**, p. 627–647.
- CUNY, J., P. B. RHINES, F. SCHOTT and J. LAZIER, 2004: Convection above the Labrador continental shelf. *J. Phys. Oceanogr.*, p. in press.
- DENGG, J., C. W. BÖNING, U. ERNST, R. REDLER and A. BECKMANN, 1999: Effects of an improved model representation of overflow water on the Subpolar North Atlantic. *International WOCE Newsletter*, **37**, p. 10–15.
- DICKSON, R. R. and J. BROWN, 1994: The production of North Atlantic Deep Waters: sources, rates and pathways. *J. Geophys. Res.*, **99**, p. 12319–12341.
- DICKSON, R. R., J. LAZIER, J. MEINCKE, P. RHINES and J. SWIFT, 1996: Long-term changes in the convective activity of the North Atlantic. *Prog. Oceanogr.*, **38**, p. 241–295.
- DICKSON, R. R., I. YASHAYEV, J. MEINCKE, B. TURRELL, S. DYE and J. HOLFORT, 2002: Rapid freshening of the North Atlantic Ocean over the past four decades. *Nature*, **416**, p. 832–837.

- DYNAMO GROUP, 1997: DYNAMO. Dynamics of North Atlantic Models: Simulation and assimilation with high resolution models. Technical Report 294, Institut für Meereskunde, Kiel, Germany.
- DYNAMO GROUP, 1997: Dynamo Scientific Report. No. 3, Kiel.
- EDEN, C. and C. BÖNING, 2002: Sources of eddy kinetic energy in the Labrador Sea. *J. Phys. Oceanogr.*, **32**, p. 3346–3363.
- EDEN, C. and C. WILLEBRAND, 2001: Mechanism of interannual to decadal variability of the North Atlantic circulation. *J. Climate*, **14**, p. 2266–2280.
- ETOPO5, 1988: Digital relief of the surface of the Earth. 88-mgg-02, National Geophysical Data Center, Boulder, Col.
- FAHRBACH, E., J. MEINCKE, S. OESTERHUS, G. ROHARDT, U. SCHAUER, V. TVERBERG and J. VERDUIN, 2001: Direct measurements of volume transports through Fram Strait. *Polar Research*, **20**, p. 217–224.
- FLAME GROUP, 1998: FLAME – Nitty Gritty Details. Technical Report, AWI Bremerhaven, in prep.
- FLATAU, M. K., L. TALLEY and P. P. NIILER, 2003: The North Atlantic Oscillation, surface currents and SST changes in the Subpolar North Atlantic. *J. Climate*, **16**, p. 2355–2369.
- FRATANTONI, D. M., 2001: North Atlantic surface circulation during the 1990's observed with satellite-tracked drifters. *J. Geophys. Res.*, **106**, p. 22067–22093.
- GASCARD, J. C. and R. A. CLARKE, 1983: The formation of Labrador Sea Water. Part II: Mesoscale and small-scale processes. *J. Phys. Oceanogr.*, **20**, p. 150–155.
- GENT, P. R. and J. C. MCWILLIAMS, 1990: Isopycnal mixing in ocean circulation models. *J. Phys. Oceanogr.*, **20**, p. 150–155.
- GOURETSKI, V. and K. JANCKE, 1998: A new world ocean climatology: Objective analysis on neutral surfaces. Technical report, no. 3, WHP Special Analysis Centre, Hamburg.
- GRIFFIES, S. M., R. C. PACANOWSKI and R. W. HALLBERG, 2000: Spurious diapycnal mixing associated with advection in a z-coordinate ocean model. *Mon. Weather Rev.*, **128**, p. 538–564.
- HAINES, T. W. N., R. K. J. and Y. JIA, 2003: Chlorofluorocarbon Constraints on North Atlantic Ventilation. *J. Phys. Oceanogr.*, **33**, p. 1798–1814.
- HANEY, R. L., 1971: Surface thermal boundary conditions for ocean circulation models. *J. Phys. Oceanogr.*, **1**, p. 241–248.
- HANSEN, B. and S. OESTERHUS, 2000: North Atlantic-Nordic Seas exchanges. *Progress in Ocean.*, **45**, p. 109–208.

- HOUGHTON, R. W. and M. H. VISBECK, 2000: Quasi-decadal salinity fluctuations in the Labrador Sea. *J. Phys. Oceanogr.*, **32**, p. 687–701.
- HURRELL, J. W., 1995: Decadal trends in the north Atlantic Oscillation: Regional temperatures and precipitation. *Science*, **269**, p. 676–679.
- IPCC, 2001: The scientific basis. Contribution of Working Group I to the third assessment report of the intergovernmental panel on climate change. Technical Report.
- JAKOBSEN, P. K., M. H. RIBERGAARD, D. QUADFASEL, T. SCHMITH and C. W. HUGHES, 2003: The near surface circulation in the northern North Atlantic as inferred from Lagrangian drifters: variability from the meso-scale to interannual. *J. Geophys. Res.*, **108**.
- JONES, H. and J. MARSHALL, 1997: Restratification after deep convection. *J. Phys. Oceanogr.*, **27**, p. 2276–2287.
- KALNAY ET AL., E., 1996: The NCEP/NCAR 40-years reanalysis project. *Bull. Am. Meteorol. Soc.*, **77**, p. 437–471.
- KÄSE, R. H., A. BIASTOCH and D. B. STAMMER, 2001: On the mid-depth circulation in the Labrador and Irminger Seas. *Geophys. Res. Letters*, **28**, p. 3433–3436.
- KATSMAN, C. A., M. A. SPALL and R. S. PICKART, 2004: Boundary current eddies and their role in the restratification of the Labrador Sea. *J. Phys. Oceanogr.*, **34**, p. 1967–1983.
- KHATIWALA, S. and M. VISBECK, 2000: An estimate of eddy-induced circulation in the Labrador Sea. **27**, p. 2277–2280.
- KILLWORTH, P. D., 1996: Time interpolation of forcing fields in ocean models. *J. Phys. Oceanogr.*, **26**, p. 136–143.
- KRAUS, E. B. and J. S. TURNER, 1967: A one-dimensional model of the seasonal thermocline. II. The general theory and its consequences. *Tellus*, **19**, p. 98–106.
- LABSEAGROUP, 1998: The Labrador Sea deep convection experiment. *Bull. Amer. Met. Soc.*, **79**, p. 2033–2058.
- LAVENDER, K. L., R. E. DAVIS and B. OWENS, 2000: Mid-depths recirculation observed in the interior Labrador and Irminger Seas by direct velocity measurements. *Nature*, **407**, p. 66–69.
- LAVENDER, K. L., R. E. DAVIS and B. OWENS, 2002: Observations of open-ocean deep convection in the Labrador Sea from subsurface floats. *J. Phys. Oceanogr.*, **32**, p. 511–526.
- LAZIER, J. R. N., R. HENDRY, A. CLARKE, I. YASHAYAEV and P. RHINES, 2002: Convection and restratification in the Labrador Sea, 1990–2000. *Deep-Sea Res.*, **49**, p. 1819–1835.

- LAZIER, J. R. N. and D. G. WRIGHT, 1993: Annual velocity variations in the Labrador Current. *J. Phys. Oceanogr.*, **32**, p. 659–678.
- LEGG, S., J. MCWILLIAMS and J. GAO, 1998: Localization of deep ocean convection by a mesoscale eddy. *J. Phys. Oceanogr.*, **28**, p. 944–970.
- LEVITUS, S. and T. P. BOYER, 1994: World Ocean Atlas 1994. Volume 4: Temperature. NOAA Atlas NESDIS 4, NOAA, Washington D.C.
- LILLY, J. M., P. R. RHINES, F. SCHOTT, K. LAVENDER, J. R. LAZIER, U. SEND and E. D’ASARO, 2003: Observations of the Labrador Sea eddy field. *Progress Oceanog.*, **59**, p. 57–176.
- LILLY, J. M., P. R. RHINES, M. VISBECK, R. DAVIS, J. R. LAZIER, F. SCHOTT and D. FARMER, 1999: Observing deep convection in the Labrador Sea during winter 1994–1995. *J. Phys. Oceanogr.*, **29**, p. 2065–2098.
- LORENZ, E. N., 1955: Available potential energy and the maintenance of the general circulation. *Tellus*, **2**, p. 157–167.
- MARSHALL, J. and F. SCHOTT, 1999: Open-Ocean convection: observations, theory and models. *Rev. Geophys.*, **37**, p. 1–64.
- MEDOC-GROUP, 1970: Observations of formation of deep water in the Mediterranean Sea. *Nature*, **227**, p. 1037–1040.
- MÜLLER, P. and J. WILLEBRAND, 1989: Equations for oceanic motions. In: *Landolt–Börnstein, Group V, Oceanography, Volume 3b*, J. Sündermann, Ed., Springer Verlag, Berlin, p. 1–14.
- ORLANSKI, I., 1976: A simple boundary condition for unbounded hyperbolic flows. *J. Comput. Phys.*, **21**, p. 251–269.
- OSCHLIES, A., 2002: Improved representation of upper-ocean dynamics and mixed layer depths in a model of the North Atlantic on switching from eddy-permitting to eddy-resolving resolution. *J. Phys. Oceanogr.*, **32**, p. 2277–2298.
- PACANOWSKI, R. C., 1995: MOM 2 Documentation, User’s Guide and Reference Manual. Technical Report 3, GFDL Ocean Group.
- PAIVA, A. M., E. P. CHASSIGNET and R. BLECK, 1999: Turbulent behavior of a fine mesh ($1/12^\circ$) numerical simulation of the North Atlantic. *Journal of Marine Systems*, **21**, p. 307–320.
- PICKART, R. S., D. J. TORRES and R. A. CLARKE, 2002: Hydrography of the Labrador Sea during active convection. *J. Phys. Oceanogr.*, **32**, p. 428–456.
- RAHMSTORF, S., 1993: A fast and complete convection scheme for ocean models. unpublished manuscript.

- REDI, M. H., 1982: Oceanic isopycnal mixing by coordinate rotation. *J. Phys. Oceanogr.*, **12**, p. 1154–1158.
- REDLER, R., K. KETELSEN, J. DENG and C. BÖNING, 1998: A high-resolution numerical model for the circulation of the Atlantic ocean. In: *Proceedings of the Fourth European SGI/CRAY MPP Workshop*, H. Lederer and F. Hertweck, Hg., Max-Planck-Institut für Plasmaphysik, p. 95 – 108.
- RHEIN, M., J. FISCHER, W. M. SMETHIE, D. SMYTHE-WRIGHT, R. F. WEISS, C. MERTENS, D. H. MIN, U. FLEISCHMANN and A. PUTZKA, 2002: Labrador Sea Water: Pathways, CFC-inventory and formation rates. *J. Phys. Oceanogr.*, **32**, p. 648–665.
- ROBERTS, M. J., R. MARSH, A. L. NEW and R. A. WOOD, 1996: An inter-comparison of a Bryan-Cox type ocean model and an isopycnic ocean model. Part I: The subpolar gyre and high-latitude processes. *J. Phys. Oceanogr.*, **26**, p. 1495–1527.
- SABINE, C. L., R. A. FEELY, N. GRUBER, R. M. KEY, K. LEE, J. L. BULLISTER, R. WANNINKHOF, C. S. WONG, D. W. R. WALLACE, B. TILBROOK, F. J. MILLERO, T.-H. PENG, A. KOZYR, T. ONO and A. F. RIOS, 2004: The sink of anthropogenic CO₂. *Science*, **305**, p. 367–370.
- SAUNDERS, P. M., 1990: Cold outflow from the Faroe Bank Channel. *J. Phys. Oceanogr.*, **20**, p. 29–43.
- SAUNDERS, P. M., 1994: The flux of overflow water through the Charlie-Gibbs Fracture Zone. *J. Geophys. Res.*, **99**, p. 12343–12355.
- SCHOTT, F., L. STRAMMA, R. ZANTOPP, M. DENGLER, J. FISCHER, M. WILBAUX and A. CLARKE, 2004: Circulation and Deep Water export at the western exit of the subpolar North Atlantic. *J. Phys. Oceanogr.*, **in press**.
- SMETHIE, W. M. and R. A. FINE, 2001: Rates of North Atlantic Deep Water formation calculated from chlorofluorocarbon inventories. *Deep-Sea Res.*, **48**, p. 189–215.
- SMITH, R., M. MALTRUD, F. BRYAN and M. HECHT, 2000: Numerical simulation of the North Atlantic Ocean at 1/10°. *J. Phys. Oceanogr.*, **30**, p. 1532–1561.
- SPALL, M. A., 2004: Boundary currents and water mass transformation in marginal seas. *J. Phys. Oceanogr.*, **34**, p. 1197–1213.
- STAMMER, D. and C. WUNSCH, 1999: Temporal changes in eddy kinetic energy of the oceans. *Deep-Sea Res. II*, **46**, p. 77–108.
- STEFFEN, E. L. and E. A. D’ASARO, 2004: Meso- and submesoscale structure of a convecting field. *J. Phys. Oceanogr.*, **34**, p. 44–60.
- STEVENS, D. P., 1991: The open boundary condition in the United Kingdom Fine-Resolution Arctic Model. *J. Phys. Oceanogr.*, **21**, p. 1494–1499.

- STRAMMA, L., D. KIEKE, M. RHEIN, F. SCHOTT, I. YASHAYAEV and K. P. KOLTERMANN, 2004: Deep water changes at the western boundary of the sub-polar North Atlantic during 1996 to 20001. *Deep-Sea Res.*, **51**, p. 1031–1056.
- SY, A., M. RHEIN, J. R. N. LAZIER, K. P. KOLTERMANN, J. MEINCKE, A. PUTZKA and M. BERSCH, 1997: Surprisingly rapid spreading of newly formed intermediate waters across the North Atlantic Ocean. *Nature*, **386**, p. 675–679.
- TREGUIER, A. M., B. BARNIER, A. DE MIRANDA, J. MOLINES, N. GRIMA, M. IMBARD, G. MADEC, C. MESSEGER, T. REYNAUD and S. MICHEL, 2001: An eddy-permitting model of the Atlantic Circulation: evaluating open boundary conditions. *J. Geophys. Res.*, **106**, p. 22115–22129.
- TREGUIER, A. M., S. THEETTEN, E. CHASSIGNET, T. PENDUFF, R. SMITH, L. TALLEY, C. BOENING and J.-O. BEISMANN, 2004: Salinity distribution and circulation of the North Atlantic subpolar gyre. *submitted to JPO*.
- VISBECK, M., T. H. J. MARSHALL and M. SPALL, 1997: Specification of eddy transfer coefficients in coarse-resolution oceanic circulation models. *J. Phys. Oceanogr.*, **27**.

Danksagung

Bedanken möchte ich mich ganz herzlich bei allen, die mich während meiner Promotionszeit unterstützt haben. Besonders danken möchte ich meinem Doktorvater Prof. Dr. Claus W. Böning für die Vergabe und Betreuung dieser Arbeit.

Ausserdem bin ich C. Eden und H. Dietze für ihre Anregungen und Hilfe zu besonderem Dank verpflichtet. Weiterhin danke ich U. Schweckendiek, J. Dengg, A. Biastoch und allen weiteren Mitgliedern der Abteilung Theorie und Modellierung.

Herzlichen Dank an Rena und Hanna.

Erklärung

Hiermit erkläre ich, daß diese Arbeit meine eigene Arbeit ist, die ich, abgesehen von den Beiträgen meiner akademischen Lehrer, selbständig und nur unter Verwendung der angegebenen Hilfsmittel verfaßt habe. Sie hat weder ganz noch in Teilen einer Prüfungskommission vorgelegen.

Kiel, den 15. Dezember 2004.

Lars Czeschel

Lebenslauf

Persönliche Daten

Lars Czeschel
Jägersberg 19a
24103 Kiel

Tel.: 0431 / 5579876
E-Mail: lczeschel@ifm-geomar.de

Geb. am 15.06.1974 in Flensburg
deutsche Staatsangehörigkeit

Werdegang

Juni 1993	Abitur, Gymnasium Satrup
Januar 2001	Diplom in Phys. Ozeanographie, Universität Kiel
seit Juni 2001	Leibniz-Institut für Meereswissenschaften (IFM-Geomar), Doktorarbeit betreut von Prof. Dr. C. W. Böning

Kiel, den 15. Dezember 2004.